Politecnico di Torino

Master of Science in Biomedical Engineering

Design and characterization of a microfluidic device resembling exocrine pancreas

Supervisors

Prof. Gianluca Ciardelli

Prof. Chiara Tonda Turo

Prof. Matteo Cocuzza

Dr. Simone Luigi Marasso

Dr. Viola Sgarminato

Candidate

Marta Grassetti

A.Y. 2022/2023
July 2023

Sommario

Abstract

Pancreatic ductal adenocarcinoma (PDAC) is a highly lethal tumor affecting the exocrine pancreas. Its poor survival rate is attributed to late-stage symptom onset, invasive metastasis, and limited therapeutic options. To address these challenges, *in vitro* models that replicate the pancreatic tissue microenvironment are crucial for therapy development and to predict drug efficacy. Organ-on-chip technology offers a powerful approach to achieving these goals.

In this thesis project, a microfluidic device is developed to model the cellular composition of the pancreatic acino-ductal unit. The device comprises a multilayer structure using Polydimethylsiloxane (PDMS), with three layers, two of them separated by a membrane. In particular, the bottom layer is loaded with human foreskin fibroblasts (HFF-1) embedded in a type I collagen hydrogel to mimic the stromal component, while the top layer reproduces the healthy or cancer epithelial component, using human pancreatic ductal epithelial cells (HPDE). An additional reservoir layer provides nutrients supply during the incubation time. The nanofibrous membrane, made of polycaprolactone and gelatin (PCL/Gel), enables the crosstalk between PDAC and stromal components, which is recognized as a key player in cancer progression.

The fabrication process involved replica molding for the PDMS layers and SU-8 photolithography or 3d printing for the molds, whereas solution electrospinning was used to produce the membrane.

Surface and morphological characterization of the molds and microfluidic device were performed using optical microscopy and fluidic characterization was conducted through insertion and diffusivity tests. *In vitro* studies allowed to evaluate cell proliferative capability and cellular response using various pancreatic tissue-specific cell lines seeded in the top layer, such as Human Pancreatic Duct Epithelial Cells in wild-type form that show non-mutated gene (HPDE-WT) to mimic healthy microenvironment, and Human Pancreatic Duct Epithelial Cells with oncogene KRAS mutation (HPDE-KRAS) or MIA-PaCa-2 cells for the pathological condition. Viability assays and fluorescence imaging confirmed the cellular functionality and the physiological morphological structure of cells in the different layers of the device.

Overall, these studies demonstrated the successful optimization and characterization of this microfluidic device for modeling the pancreatic acino-ductal unit and studying the interaction between PDAC and stromal components. The system provides valuable insights into the tumor microenvironment and holds potential for drug development and understanding cellular crosstalk in PDAC.

1 Introduction

1.1 The clinical issue: Pancreatic Ductal Adenocarcinoma (PDAC)

Pancreatic Ductal Adenocarcinoma (PDAC) is an aggressive malignancy originating from the epithelial cells lining the pancreatic ducts. It is associated with a dismal prognosis, characterized by a significantly low five-year survival rate. According to data from the American Cancer Society, the five-year survival rate for PDAC is estimated to be approximately 10% (1). The aggressive nature of PDAC is attributed to its rapid tumor progression, early metastatic dissemination, and intrinsic resistance to standard treatment modalities.

PDAC demonstrates an alarming growth rate, infiltrating adjacent tissues and organs with remarkable efficiency. This aggressive behavior is facilitated by the cancer cells' ability to induce angiogenesis, stimulating the formation of new blood vessels that sustain their nutritional and oxygen demands. Moreover, PDAC exhibits an early propensity for metastasis, with cancer cells disseminating through hematogenous and lymphatic routes. The metastatic dissemination often occurs before clinical detection, leading to advanced-stage diagnoses and limited treatment options.

Resistance to therapeutic interventions is another hallmark of PDAC. The tumor cells undergo genetic alterations and acquire mutational profiles that confer survival advantages and resistance to chemotherapy and radiation therapy (1). This resistance poses significant challenges in achieving favorable treatment outcomes and underscores the need for novel therapeutic strategies targeting the unique characteristics of PDAC.

The complexities surrounding PDAC's aggressive behavior necessitate comprehensive scientific investigations to unravel its underlying molecular mechanisms. Elucidating the genetic and biological features of PDAC is crucial for identifying potential therapeutic targets and developing innovative treatment approaches that can improve patient prognosis.

1.2 Pancreas tissue overview

The pancreas, an essential organ in the human body, exhibits a distinct anatomical structure and plays a vital role in digestion and hormone regulation. Situated in the upper abdomen, posterior to the stomach, the pancreas is positioned near neighboring structures such as the duodenum, spleen, and liver. It consists of different regions, including the head, body, and tail, which are arranged horizontally across the abdomen (fig.1.2.1). The pancreas is composed of two main types of tissues: exocrine and endocrine. The exocrine component comprises the majority of the pancreatic tissue and is responsible for producing digestive enzymes that are released into the duodenum through a complex network of ducts. On the other hand, the endocrine tissue consists of specialized clusters called pancreatic islets or islets of Langerhans, which secrete hormones involved in regulating blood glucose levels, such as insulin and glucagon (2).

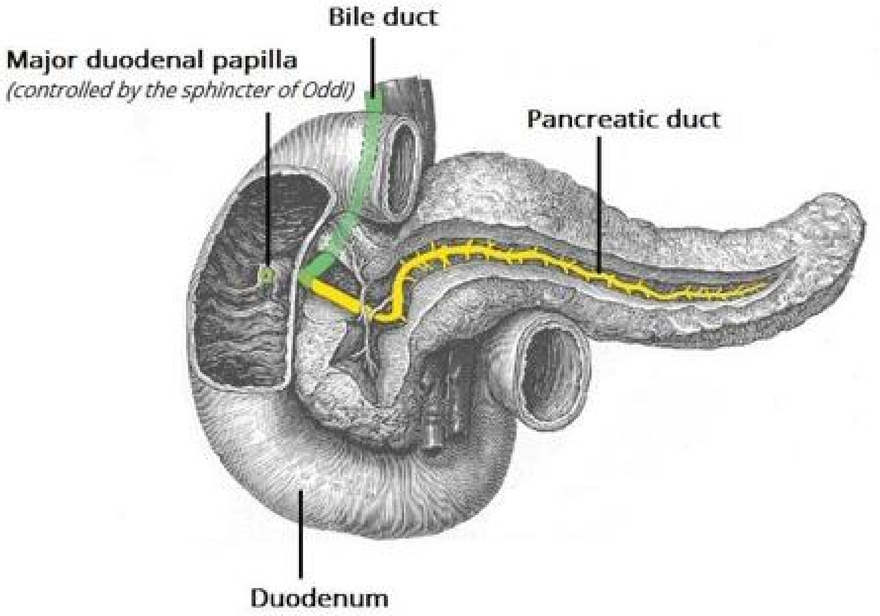

Figure 1.2.1 Pancreas anatomy and its position (3)

1.2.1 Exocrine pancreas

The pancreas is a complex organ with a dual secretory function, consisting of both exocrine and endocrine glandular formations. Microscopically, each lobule of the pancreas comprises numerous exocrine cells and a smaller population of endocrine cells.

The exocrine component of the pancreas constitutes approximately 80-85% of the organ and plays a crucial role in producing and releasing pancreatic juice into the duodenum to facilitate complete digestion (Figure 1.2.1). The exocrine pancreas consists of two primary types of cells: acinar cells and ductal cells (figure 1.2.2).

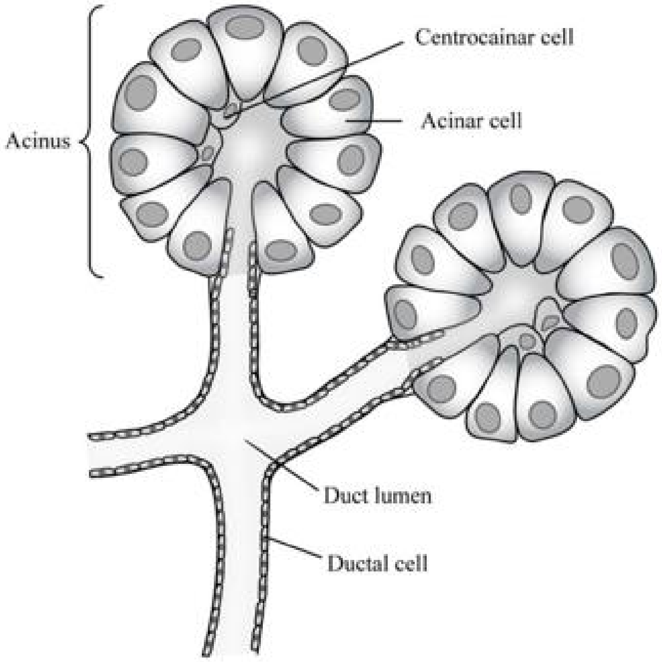

Figure 1.2.2 Acinar cell and ductal cell (4)

Acinar cells, which have a pyramidal shape, make up the parenchymal cells of the pancreas. These cells are arranged in a convoluted manner, often interconnected in a tubular-acinar network within the lobules. The apexes of the acinar cells form a small central lumen, representing the terminal portion of the secretory ducts known as the acino-ductal unit. Acinar cells possess a well-developed Golgi apparatus and abundant rough endoplasmic reticulum, which are responsible for exocrine secretion (5).

Ductal cells, on the other hand, are smaller than acinar cells and have a single nucleus (Figure 1.2.2). These cuboidal cells form a single layer lining the interlobular and normal ducts. Duct cells are responsible for secreting water and bicarbonate, which are essential for transporting enzyme proteins into the duodenum. The secretion of ductal cells is regulated by the vagal nerves and secretin.

The secretions from the acini drain into a highly branched duct system that eventually joins the common bile duct, flowing into the ampulla of Vater. The ampulla of Vater opens into the duodenum at the greater duodenal papilla. Additionally, there is an accessory duct, called Santorini, located in the upper portion of the pancreas head. It branches off from the main duct and leads to the minor duodenal papilla (figure1.2.3) (5).

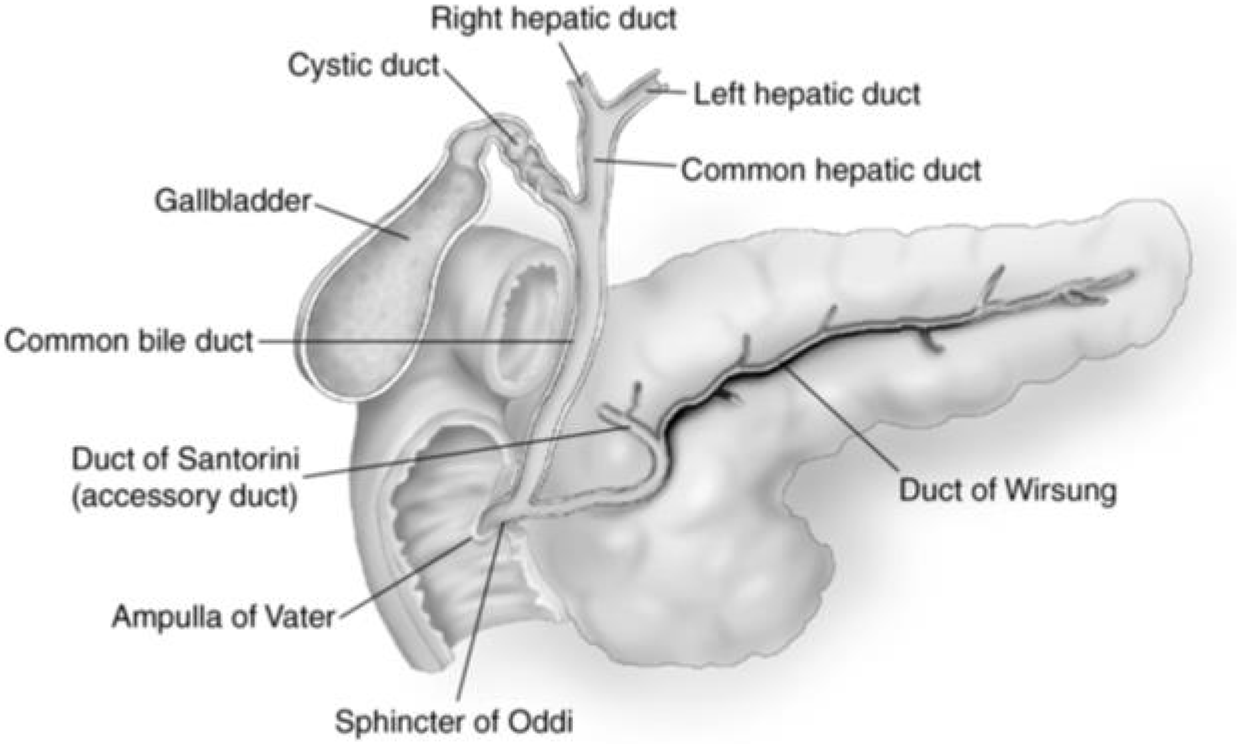

Figure 1.2.3 Pancreas structure (6)

Studying the three-dimensional organization of the exocrine pancreas is crucial for understanding the changes that occur during pancreatic diseases.

1.2.2 Endocrine pancreas

The endocrine component, which accounts for about 2% of the pancreas, consists of pancreatic Langerhans' islets. These islets are dispersed throughout the exocrine part, mainly in the tail region, and are separated from the rest of the tissue by reticular fibers.

Pancreatic islets are spherical clusters of polygonal endocrine cells. The islet cells are connected to each other and surrounded by fenestrated capillaries for rapid hormone release into the bloodstream.

There are four main types of cells in the pancreatic islets (5)(figure 1.2.4):

- *Beta cells* (B cells) secrete insulin and constitute about 75% of the islet cells.
- *Alpha cells* (A cells) secrete glucagon and make up 15% of the islet cells.
- *Delta cells* (D cells) secrete somatostatin and constitute 5% of the islet cells.

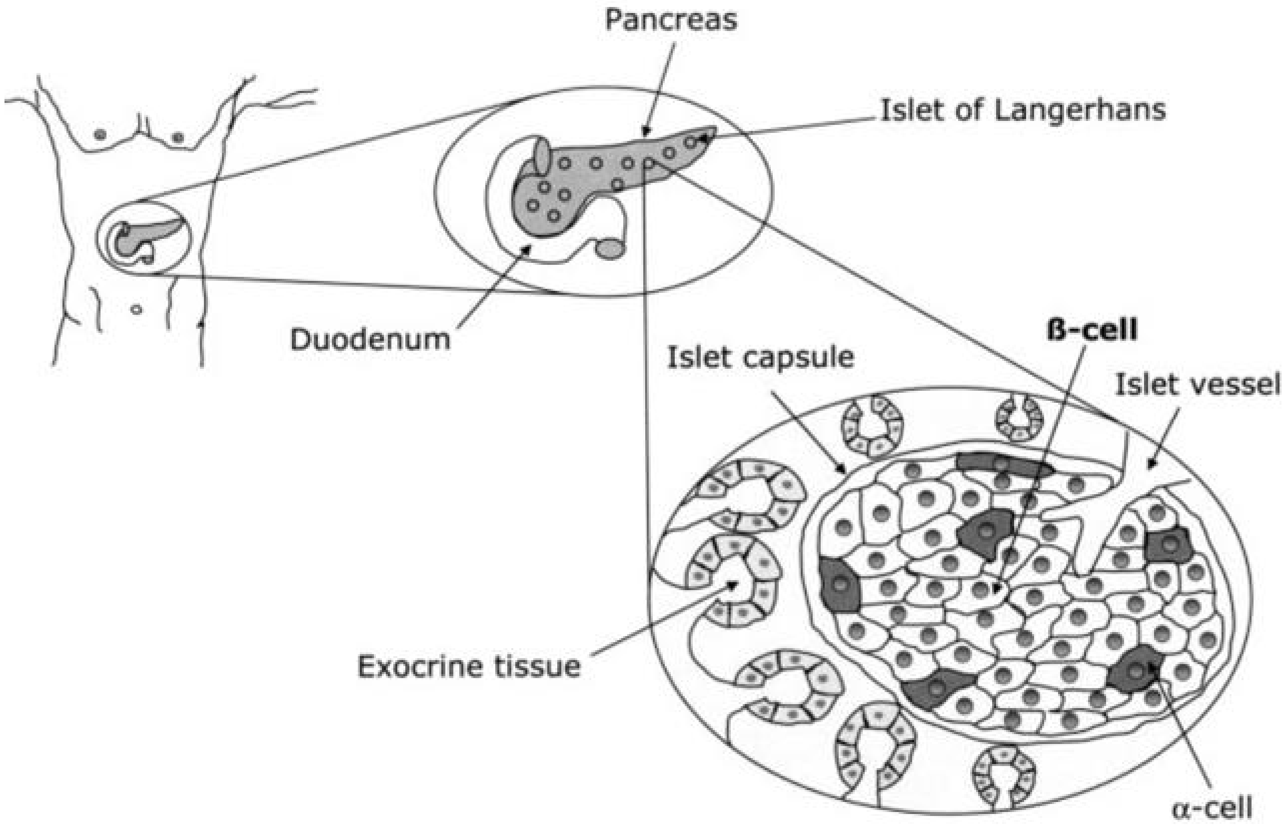

Figure 1.2.4 Pancreatic Islets and main cells (7)

These endocrine cells play a crucial role in regulating glucose, lipid, and protein metabolism.

One distinguishing feature of the pancreas on histology slides is the clear demarcation of the pancreatic islets from the acinar cells. Additionally, the intercalated ducts of the pancreas start within the acini, unlike other glands where they continue from the acini.

1.3 Pathogenesis of PDAC

Pancreatic cancers can arise from both endocrine and exocrine cells, and they exhibit distinct histological features. Endocrine tumors are relatively rare but have a better prognosis compared to pancreatic adenocarcinoma, the most common form of pancreatic cancer. Endocrine tumors, derived from pancreatic islet cells, can produce excessive levels of hormones, leading to noticeable symptoms such as hypoglycemia or skin rash. Exocrine tumors, particularly pancreatic ductal adenocarcinoma (PDAC), account for the majority of pancreatic malignancies. PDACs are aggressive, frequently metastasize to other organs, and often diagnosed at advanced stages. These cancers possess cytoprotective mechanisms that promote drug resistance, contributing to their poor response to anti-cancer therapies.

The development of PDACs is preceded by the formation of precancerous lesions called pancreatic intraepithelial neoplasias (PanINs) and intraductal papillary mucinous neoplasms (IPMNs). IPMNs are characterized by papillary structures protruding into the pancreatic duct, while mucinous tumors secrete mucin, giving them a distinctive appearance. Although less invasive than adenocarcinomas at the time of diagnosis, mucinous tumors still pose a risk of developing into cancer.

Whole exome-sequencing studies have provided insights into the molecular heterogeneity of pancreatic ductal adenocarcinoma (PDAC). The disease is characterized by four common genetic alterations:

oncogenic KRAS mutation, and the inactivation of tumor suppressors CDKN2A, TP53, and SMAD4. However, there are numerous additional genes that are mutated in subsets of tumors, albeit at a low frequency (≤10%), and many of these mutations do not occur in a recurrent manner. Despite their infrequent occurrence, these mutations converge on a limited number of pathways and cellular processes, including KRAS, TGF-β, WNT, NOTCH, and Hedgehog signaling, as well as S-phase entry, axonal guidance, chromatin remodeling, DNA repair, and RNA processing (8).

The presence of activating KRAS mutations is a defining genetic characteristic of PDAC progression, found in approximately 92% of PDAC cases. KRAS is a small GTPase that regulates various cellular processes, including cell proliferation, differentiation, survival, and migration. Normally, KRAS cycles between an active state (bound to GTP) and an inactive state (bound to GDP), regulated by guanine nucleotide exchange factors (GEFs) and GTPase-activating proteins (GAPs). In cancer, mutations occur in KRAS or related family members (HRAS and NRAS), impairing their ability to hydrolyze GTP and resulting in constitutive activation of downstream effector pathways (8).

Activating KRAS mutations are the earliest genetic alterations in the development of almost all PDACs. They are present in over 90% of low-grade precursor lesions called pancreatic intraepithelial neoplasia (PanIN). However, additional inactivation of tumor suppressor genes (CDK2NA, TP53, and SMAD4) is required for malignant tumor progression. While oncogenic

KRAS promotes the initiation of PDAC development, its role in tumor maintenance is less clear.

Tumor suppressor genes (TSGs) play a crucial role in restricting cell proliferation and are functionally lost in pancreatic ductal adenocarcinoma (PDAC). The three most commonly altered TSGs in PDAC are CDKN2A, TP53, and SMAD4/DPC4, and their inactivation occurs sequentially after the appearance of oncogenic KRAS mutations. CDKN2A is frequently altered in PDAC, with approximately 95% of tumors showing functional loss. The inactivation of CDKN2A is crucial for disease pathogenesis, as it bypasses the senescence response induced by oncogenic KRAS. TP53, another major TSG, is inactivated in up to 75% of PDAC tumors through missense mutations and loss of heterozygosity. Mutant p53 loses its DNA-binding ability, resulting in the inability to induce cell cycle arrest or apoptosis in response to cellular stress. Additionally, mutant p53 may contribute to the metastatic nature of PDAC by promoting the expression of genes involved in motility and invasiveness. Other TSGs with low-frequency inactivation in PDAC include STK11/LKB1, which regulates cell polarity and metabolism, and caretaker genes such as BRCA1, BRCA2, hMLH1, and hMSH2, which maintain genome integrity. These alterations in TSGs constitute a major driving force behind PDAC development and highlight the complexity of genetic alterations in the disease (8).

1.4 PDAC - Stroma crosstalk

Pancreatic ductal adenocarcinoma (PDAC) is characterized by an intense interaction between cancer cells and the surrounding stroma, leading to a complex crosstalk that influences tumor progression and treatment response. The tumor microenvironment in PDAC is composed of various cellular and non-cellular components. Malignant cancer cells are surrounded by a dense stroma consisting of fibroblasts, immune cells, endothelial cells, and extracellular matrix (ECM) proteins. This stromal compartment plays a critical role in supporting tumor growth and metastasis (9)(figure 1.4.1).

Fibroblasts within the PDAC stroma, also known as cancer-associated fibroblasts (CAFs), are a key component of the tumor microenvironment. They exhibit activated characteristics and secrete various factors that contribute to tumor progression. CAFs promote cancer cell survival, proliferation, and invasion through the release of growth factors, cytokines, and ECM remodeling enzymes (10).

Inflammatory and *immune cells*, such as tumor-associated macrophages (TAMs), lymphocytes, and myeloid-derived suppressor cells (MDSCs), also play crucial roles in the PDAC microenvironment. TAMs can exhibit pro-tumorigenic or anti-tumorigenic properties depending on their polarization state, influencing cancer cell behavior and immune responses. Lymphocytes, including cytotoxic T cells and natural killer (NK) cells, can infiltrate PDAC tumors, but their functional impairment and low numbers often limit effective immune responses.

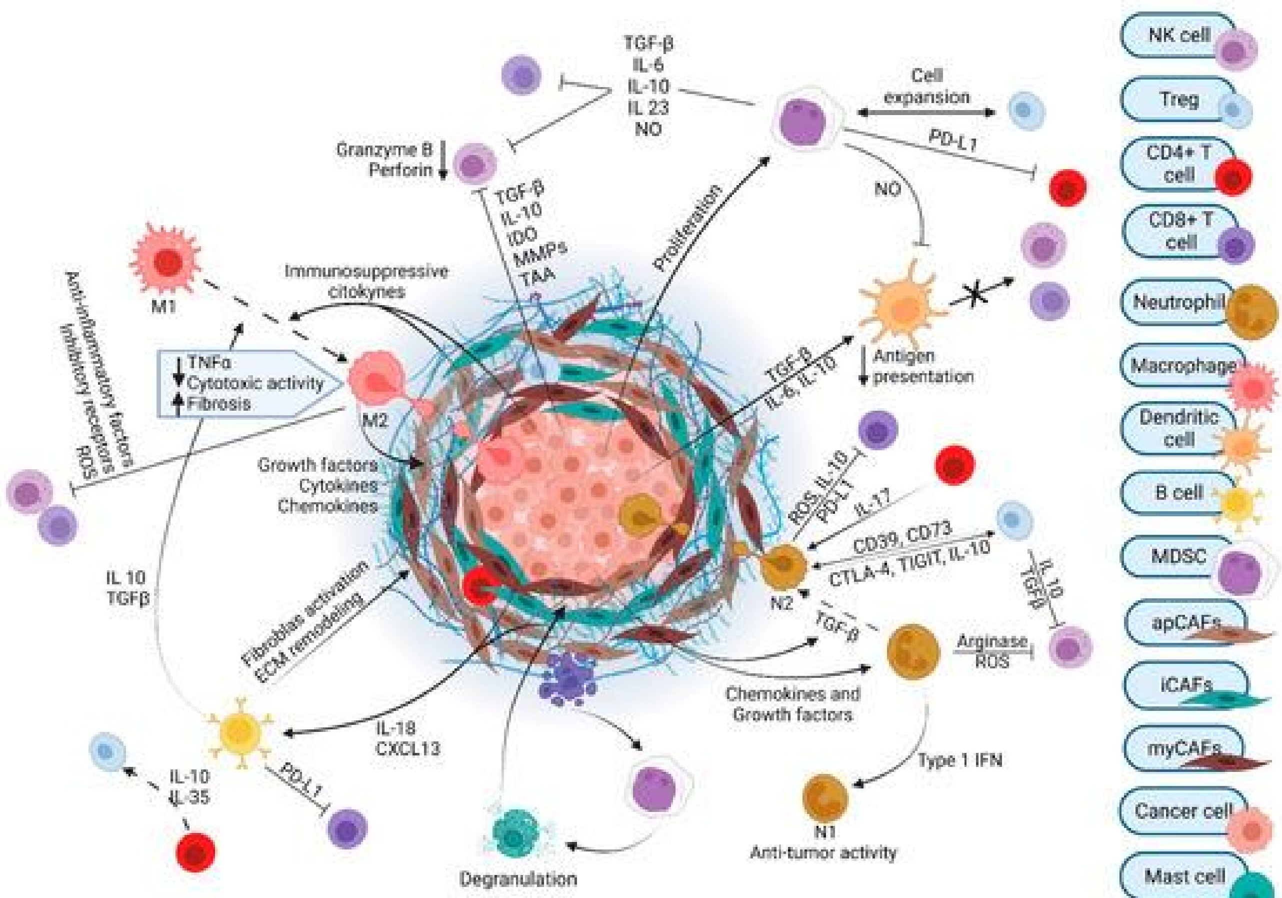

Figure 1.4.1 Tumor microenvironment of PDAC (11).

Furthermore, the PDAC stroma is rich in ECM proteins, such as collagen, fibronectin, and hyaluronic acid. These ECM components contribute to tumor stiffness, promote cancer cell survival, and facilitate tumor cell migration and invasion (12).

The crosstalk between PDAC cells and the stroma involves the exchange of various signaling molecules and interactions mediated by cell surface receptors. Cancer cells secrete growth factors (e.g., VEGF, bFGF, EGFR-ligand) that promote angiogenesis, stimulate the recruitment of immune cells, and induce the activation of stromal cells, including CAFs and TAMs. Conversely, stromal cells produce factors, such as TGF-β, interleukins, and chemokines, that can influence cancer cell behavior and alter the immune landscape within the tumor microenvironment (13) (14).

Understanding the intricate PDAC-stroma crosstalk is crucial for developing effective therapeutic strategies. Targeting components of the stroma or disrupting specific signaling pathways involved in this crosstalk holds promise for improving treatment outcomes in PDAC patients.

1.5 The pancreatic stellate cells

The pancreatic stellate cells (PSCs) play a significant role in the development and progression of pancreatic ductal adenocarcinoma (PDAC). PSCs are quiescent cells residing in the normal pancreas, but they become activated and acquire myofibroblast-like properties during pancreatic injury and cancer. Activated PSCs contribute to the desmoplastic reaction observed in PDAC, characterized by excessive deposition of extracellular matrix (ECM) proteins and fibrosis within the tumor microenvironment. These cells secrete various ECM proteins, such as collagen, fibronectin, and laminin, which contribute to the stiffness of the tumor and create a supportive niche for cancer cells (15) (14)

PSCs also play a crucial role in promoting tumor growth and progression through the secretion of growth factors and cytokines. They produce transforming growth factor-beta (TGF-β), platelet-derived growth factor (PDGF), and hepatocyte growth factor (HGF), among others, which can stimulate cancer cell proliferation, angiogenesis, and invasion.
Moreover, PSCs have been implicated in immune modulation within the PDAC microenvironment. They can interact with immune cells and promote an immunosuppressive environment through the production of immunosuppressive factors like interleukin-6 (IL-6) and indoleamine 2,3-dioxygenase (IDO), thereby impairing antitumor immune responses (16) (17).

Targeting PSCs and their interaction with the tumor microenvironment has emerged as a potential therapeutic strategy for PDAC (18). Indeed, inhibiting PSC activation or targeting specific signaling pathways involved in PSC-cancer cell crosstalk may offer novel approaches for improving treatment outcomes in PDAC patients.

1.6 Tissue Engineering and PDAC in vitro models

Tissue engineering has played a crucial role in developing in vitro models to study pancreatic ductal adenocarcinoma (PDAC) and understand its pathogenesis. These models aim to recapitulate the complex tumor microenvironment and provide a platform for studying tumor biology and evaluating therapeutic strategies.

One approach in tissue engineering is the use of three-dimensional (3D) cell culture systems, such as *organoids* and *spheroids*, which better mimic the architecture and cellular interactions observed in tumors. PDAC organoids, derived from patient-derived tumor cells or genetically engineered cell lines, can be cultured in a 3D matrix to create a more physiologically relevant model (19).

In addition to organoids, the incorporation of stromal components is important for studying the interaction between cancer cells and the tumor microenvironment. Co-culture systems that include pancreatic stellate cells (PSCs), immune cells, and endothelial cells have been developed to mimic the stromal component of PDAC (20).

Furthermore, bioengineered scaffolds can be utilized to recreate the extracellular matrix (ECM) composition and physical properties found in PDAC. These scaffolds provide a supportive structure for tumor cell growth and allow the investigation of cell-ECM interactions and invasion (21).

To enhance the physiological relevance of in vitro models, microfluidic devices have been developed to mimic the dynamic flow of nutrients, oxygen, and waste products within the tumor microenvironment. These systems permit to test the drug responses and to study the tumor evolution mechanisms, such as the metastatic processes, under more realistic conditions. Therefore, they represent valuable tools for studying PDAC biology, drug screening, and personalized medicine approaches.

1.7 Animal models

Animal models have been widely used in tissue engineering research to evaluate the efficacy and safety of engineered tissues and study their integration with the host organism. These models provide valuable insights into the in vivo behavior of tissue-engineered constructs and their potential for clinical translation. One commonly utilized animal model in tissue engineering is the rodent model, particularly mice and rats, due to their small size, short reproductive cycle, and well-characterized genetic background. These models allow for the assessment of tissue-engineered constructs in terms of biocompatibility, functionality, and host immune response (22). Large animal models, such as pigs, sheep, and non-human primates, offer advantages in terms of anatomical and physiological similarities to humans. These models provide a more clinically relevant platform for evaluating tissue-engineered constructs, especially for applications involving larger tissue defects or complex anatomical sites. For studying specific tissue types, animal models with tissue-specific characteristics and disease models can be employed (23) (22).

In addition to naturally occurring disease models, genetically modified animal models can be created to mimic human diseases and assess the therapeutic potential of tissue-engineered interventions. These models allow researchers to investigate the underlying mechanisms of disease progression and test the effectiveness of tissue-engineered treatments.

Furthermore, the advancement of imaging technologies, such as magnetic resonance imaging (MRI), computed tomography (CT), and positron emission tomography (PET), has greatly facilitated the non-invasive monitoring of tissue-engineered constructs in animal models (24). These imaging techniques enable the assessment of construct integration, vascularization, and cell viability over time.

Animal models in tissue engineering research provide critical preclinical data necessary for the translation of tissue-engineered therapies to clinical applications. They offer a comprehensive understanding of the in vivo behavior of engineered tissues, allowing researchers to optimize their design and functionality before moving forward with human trials.

1.7 Two-dimensional (2D) models

Two-dimensional (2D) models have been extensively employed in tissue engineering research to investigate cell behavior, cellular interactions, and the effects of various factors on cell response. These models provide valuable insights into cell culture techniques, cell behavior, and initial screening of biomaterials and therapeutics.

In 2D models, cells are cultured on flat surfaces, such as tissue culture plates or glass slides, creating a simplified environment that allows for controlled experimentation. These models offer advantages in terms of ease of use, cost-effectiveness, and the ability to study specific cellular processes in a controlled manner. One widely used 2D model in tissue engineering is the monolayer culture, where cells are grown as a single layer on a substrate. This model allows for the investigation of cell adhesion, proliferation, migration, and differentiation in a simplified manner (25). Monolayer cultures have been instrumental in understanding cellular processes and signaling pathways, as well as drug screening and toxicity testing.

Transwell systems, also known as cell culture inserts, are another type of 2D model commonly used in tissue engineering that can be compatible with a microfluidic device. These systems consist of a permeable membrane that separates two compartments, allowing for the study of cell migration, invasion, and interaction between different cell types. Transwell models have been employed to investigate the behavior of cancer cells, immune cell trafficking, and drug permeability (26).

Micropatterned substrates are emerging as a powerful tool in 2D tissue engineering models. These substrates contain precise patterns and features that guide cell adhesion, shape, and organization, mimicking the in vivo tissue microarchitecture. Micropatterning techniques have been utilized to study cell alignment, cell-cell interactions, and the influence of substrate topography on cell behavior (27). Furthermore, advancements in microfluidic technology have enabled the development of 2D tissue engineering models with perfusable microchannels. These models replicate physiological flow conditions, allowing for the study of cell behavior under fluid shear stress and the investigation of vascularization and drug transport in a controlled microenvironment (28).

The advantages of 2D cultures include easy and cost-effective maintenance and the ability to perform functional tests. However, there are several disadvantages associated with adherent cultures. Firstly, 2D cultured cells do not replicate the natural structures of tissues or tumors, leading to a lack of cell-cell and cell-extracellular environment interactions. These interactions are crucial for various cellular functions, including differentiation, proliferation, gene and protein expression, responsiveness to stimuli, and drug metabolism (25). The transfer of cells to 2D conditions alters their morphology, cell division mode, and diverse phenotypes. This can impact cellular function, structure organization, secretion, and cell signaling. Adherent cells also lose polarity, affecting their response to phenomena like apoptosis. Additionally, 2D culture allows cells unlimited access to medium ingredients, unlike the variable availability of nutrients and oxygen in the natural tumor mass. The 2D system can alter gene expression, splicing, topology, and biochemistry of cells (25). Moreover, adherent cultures typically consist of monocultures, limiting the study to one cell type and lacking the tumor microenvironment required by cancer-initiating cells *in vivo*. Overall, these limitations emphasize the need for alternative culture models that better resemble the *in vivo* conditions.

1.8 Three-dimensional (3D) models

Three-dimensional (3D) models have revolutionized tissue engineering and have become invaluable tools for studying tissue development, disease modeling, and drug testing. These models aim to mimic the complex three-dimensional architecture and cellular interactions found in native tissues, providing a more physiologically relevant environment for research.

In tissue engineering, 3D models offer several advantages over traditional two-dimensional (2D) models. They allow for the spatial organization of cells, the formation of tissue-like structures, and the recreation of key microenvironmental cues (25). These models can better replicate the native tissue microarchitecture, cell-cell interactions, and cell-matrix interactions, leading to improved understanding and more accurate predictions of the *in vivo* responses.

In the context of pancreatic ductal adenocarcinoma (PDAC), 3D models have emerged as powerful tools for studying tumor progression, drug response, and therapeutic interventions. Indeed, PDAC is known for its complex tumor microenvironment, characterized by interactions between cancer cells, stromal cells, and extracellular matrix components. 3D models provide a means to recreate this intricate microenvironment and investigate the crosstalk between different cell types, contributing to a deeper understanding of PDAC biology (29).

Spheroid models, where cells are cultured as three-dimensional aggregates, have been widely used in PDAC research (figure 1.8.1). These models enable the recapitulation of tumor-like features, including cell-cell interactions, nutrient gradients, and hypoxic regions. Spheroids provide a more representative platform for drug testing and evaluation of therapeutic efficacy, offering insights into the response of PDAC tumors to different treatment modalities (30) (25).

Organoid models, derived from patient tissues or cell lines, have also shown promise in PDAC research (figure 1.8.1). These models involve the culture of cells in a 3D matrix, allowing for the formation of miniaturized organs that resemble the histological and genetic characteristics of the original tissue. PDAC organoids provide a powerful platform for studying disease mechanisms, testing drug sensitivity, and potentially guiding personalized treatment approaches (25) (30).

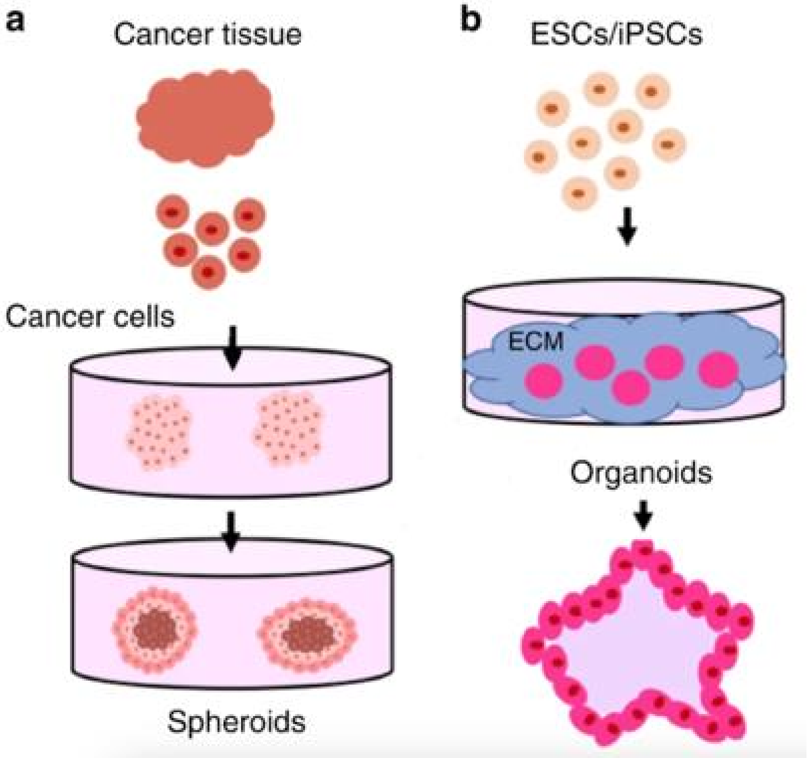

Figure 1.8.1 Spheroids and organoids compared (31).

Moreover, advances in bioprinting technologies have facilitated the fabrication of complex 3D structures by depositing cells and biomaterials layer by layer. Bioprinting allows for precise control over cell distribution, organization, and tissue architecture, enabling the creation of highly customized and functional tissue models (30). Bioprinted PDAC models have been utilized to study tumor invasion, drug screening, and personalized medicine approaches, paving the way for more effective therapeutic strategies.

The use of 3D models in tissue engineering, particularly in the context of PDAC, has opened new avenues for research and therapeutic development. These models provide a more realistic representation of the tumor microenvironment, allowing for the investigation of complex cellular interactions, drug testing, and the development of personalized medicine approaches, ultimately leading to improved outcomes for patients with PDAC.

1.9 Microfluidic Systems

Microfluidic systems have emerged as powerful tools in tissue engineering, offering precise control over fluid flow, cell microenvironments, and tissue formation within miniaturized devices. These systems integrate microscale channels, chambers, and valves to create dynamic and customizable environments for cell culture and tissue development. They enable the replication of physiological conditions, such as perfusion, shear stress, and nutrient gradients, which are crucial for maintaining cell viability and function (32).

In the context of pancreatic ductal adenocarcinoma (PDAC), microfluidic devices have been employed to investigate various aspects of tumor biology and therapeutic interventions. These devices allow for the precise manipulation of the tumor microenvironment and the study of complex cellular interactions involved in PDAC progression. They provide a platform for examining tumor cell migration, invasion, and response to anti-cancer drugs, enabling the development of more effective treatment strategies (33).

The microfluidic systems have been largely adopted to model PDAC microenvironment, as these organ-on-a-chips allow to recreate the physiological conditions and cellular interactions observed in the pancreas, providing a more accurate representation of PDAC progression. By integrating pancreatic cells, stromal cells, and extracellular matrix components within microfluidic devices, researchers can mimic the tumor microenvironment and study its influence on tumor development and response to therapy (34).

Pancreas-on-a-chip models offer a platform to study various aspects of pancreatic function, disease progression, and therapeutic interventions. These models enable the investigation of pancreatic islet function, insulin secretion, and glucose metabolism, providing insights into diabetes mellitus and potential treatments (35).

Furthermore, microfluidic devices have been utilized for the development of diagnostic tools. These devices can capture and analyze circulating tumor cells (CTCs) or tumor-derived extracellular vesicles (EVs) from patient blood samples. By leveraging the unique properties of PDAC-derived CTCs or EVs, such as surface markers or genetic signatures, microfluidic-based diagnostic platforms offer the potential for early cancer detection, *real-time* monitoring of disease progression, and assessment of treatment response (36).

Microfluidic systems have revolutionized tissue engineering and are playing a significant role in PDAC research because these devices offer precise control over the cellular microenvironment, enabling the creation of organ-on-a-chip models that closely resemble in vivo conditions.

Overall, pancreas-on-a-chip technology provides a valuable tool for studying pancreatic function, disease mechanisms, and drug testing in a controlled and reproducible manner. These models offer the opportunity to better understand pancreatic diseases, including PDAC, and accelerate the development of innovative therapeutic strategies (37).

1.10 Fabrication techniques

In this thesis work, various techniques have been employed to fabricate the microfluidic chips used for indirect co-culture. The microfluidic chips consist of three layers: a bottom layer, a top layer, and a reservoir layer. The fabrication process involved different techniques for each layer. SU-8 lithography was used for the bottom layer, while 3D printing technology was utilized for the top and reservoir layers. These techniques served as the foundation for replica molding, which involved creating PDMS replicas.

Lithographic techniques play a crucial role in nanofabrication and are categorized as top-down approaches. These techniques involve transferring a pattern onto a substrate covered with a photosensitive material called resist. The lithography process consists of several steps, including resist coating, substrate irradiation, development to remove excess resist, and substrate etching. The choice of energy source and development method depends on the type of resist and the specific lithography technique used. There are two types of resists: *negative resist* and *positive resist* (figure 1.10.1). Negative resist is sensitive to irradiation and is removed during development, while positive resist becomes stronger with irradiation due to cross-linking. Physical mask methods or mask lithography involve using masks for substrate irradiation, while software methods or direct write methods involve directly drawing the pattern on the substrate (38).

One notable lithography technique is *soft lithography*, which is a subset of lithography techniques that utilizes elastomeric materials, typically polydimethylsiloxane (PDMS), to create microstructures. It is a bottom-up approach and is known for its simplicity, low-cost, and versatility. Soft lithography involves creating a master mold, usually using photolithography techniques, on a substrate such as a silica wafer.

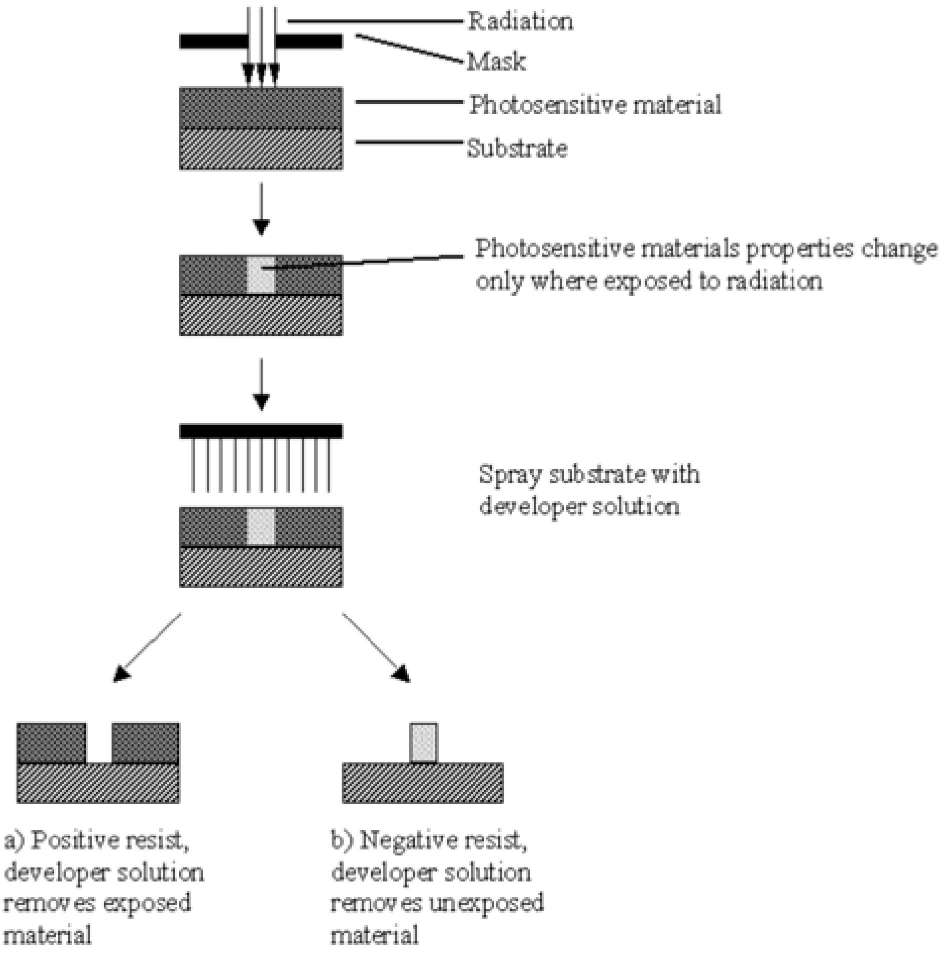

Figure 1.10.1 Positive (a) and negative (b) resist compared (38).

The master mold is then used to replicate the desired microstructures in PDMS. PDMS replicas can be created by pouring PDMS onto the master mold and allowing it to cure, resulting in a flexible and transparent replica with the desired microscale features. Soft lithography is widely used in various fields, including microfluidics, tissue engineering, and biosensors, due to its ability to produce complex and customizable microstructures (39). These techniques demonstrate the versatile nature of lithography and its application in microfluidic chip fabrication, allowing for precise control over the design and functionality of the devices.

3D printing, also known as additive manufacturing, is a process of creating three-dimensional objects by layering materials based on a digital model. There are various 3D printing techniques available, each with its own advantages and applications. One popular 3D printing technique is PolyJet. PolyJet is a type of 3D printing technology that uses inkjet printing principles to deposit and cure layers of liquid photopolymer materials. The process involves jetting ultra-thin layers of liquid resin onto a build platform. These layers are then cured or hardened using UV light to create solid structures (40). PolyJet printers can produce high-resolution, detailed, and multi-material objects. One of the key features of PolyJet technology is its ability to print objects with varying material properties in a single print job. By using multiple print heads that can jet different types of materials simultaneously, PolyJet printers can produce models with different colors, textures, and even varying levels of flexibility or rigidity. This capability makes PolyJet ideal for applications where complex and realistic prototypes or models are required. PolyJet is widely used in various industries, including product design, engineering, healthcare, and education (40). It enables the rapid prototyping of functional parts, the creation of realistic anatomical models for surgical planning, and the production of intricate and detailed architectural models, among many other applications. This technique has been used for printing top and reservoir layers but also for the bottom layer in a second time evaluation.

2 Aim of the work

The aim of this thesis project is the optimization of the device in terms of microfluidics. The device is composed of three layers in PDMS, as shown in figure 2.1. From left to right, we have the reservoir layer, top layer, and bottom layer with the interposition of a PCL/gelatin membrane.

However, the previous version of the device had several issues related to the internal flow and the insertion of the membrane.

Figure 2.1 Device disassembled. From left: reservoir layer, top layer and bottom layer with membrane.

Bottom layer: It consists of three channels: in the central one, fibroblasts and collagen will be seeded (orange channel depicted in figure 2.2), and two outer channels where the culture medium will be inserted to support the growth and provide nutrients to the cells in the central channel, resembling the physiological crosslinking of the pancreas (depicted with a blue dye).

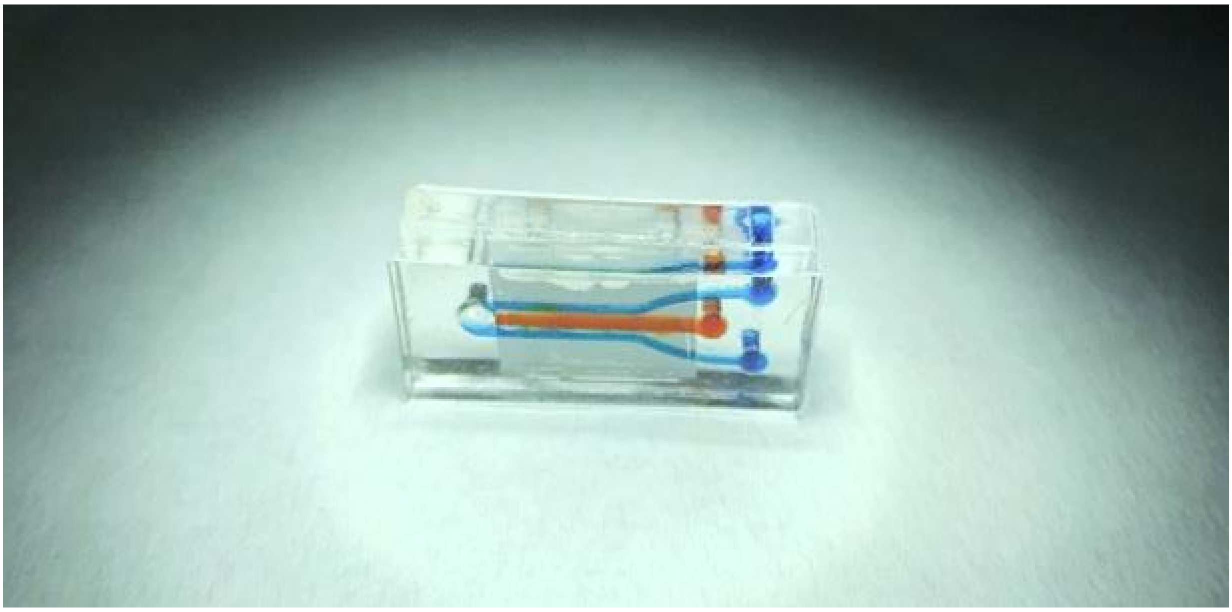

Figure 2.2 Device assembled. External channels in blue and the central channel in orange dye.

Top layer: As shown in figure 2.1, this device has four inlets for the introduction of fluids through a 200um pipette. Two inlets, shown in blue color in figure 2.2 and 2.3, are intended for filling the external channels of the bottom layer with the culture medium. One inlet, in orange, is for introducing collagen and fibroblasts into the bottom layer under the membrane, and the last one in red is for pancreatic epithelial cells above the membrane. Two additional channels are projected for sampling and renewing the medium, one for the bottom and one for the top on the left of the device.

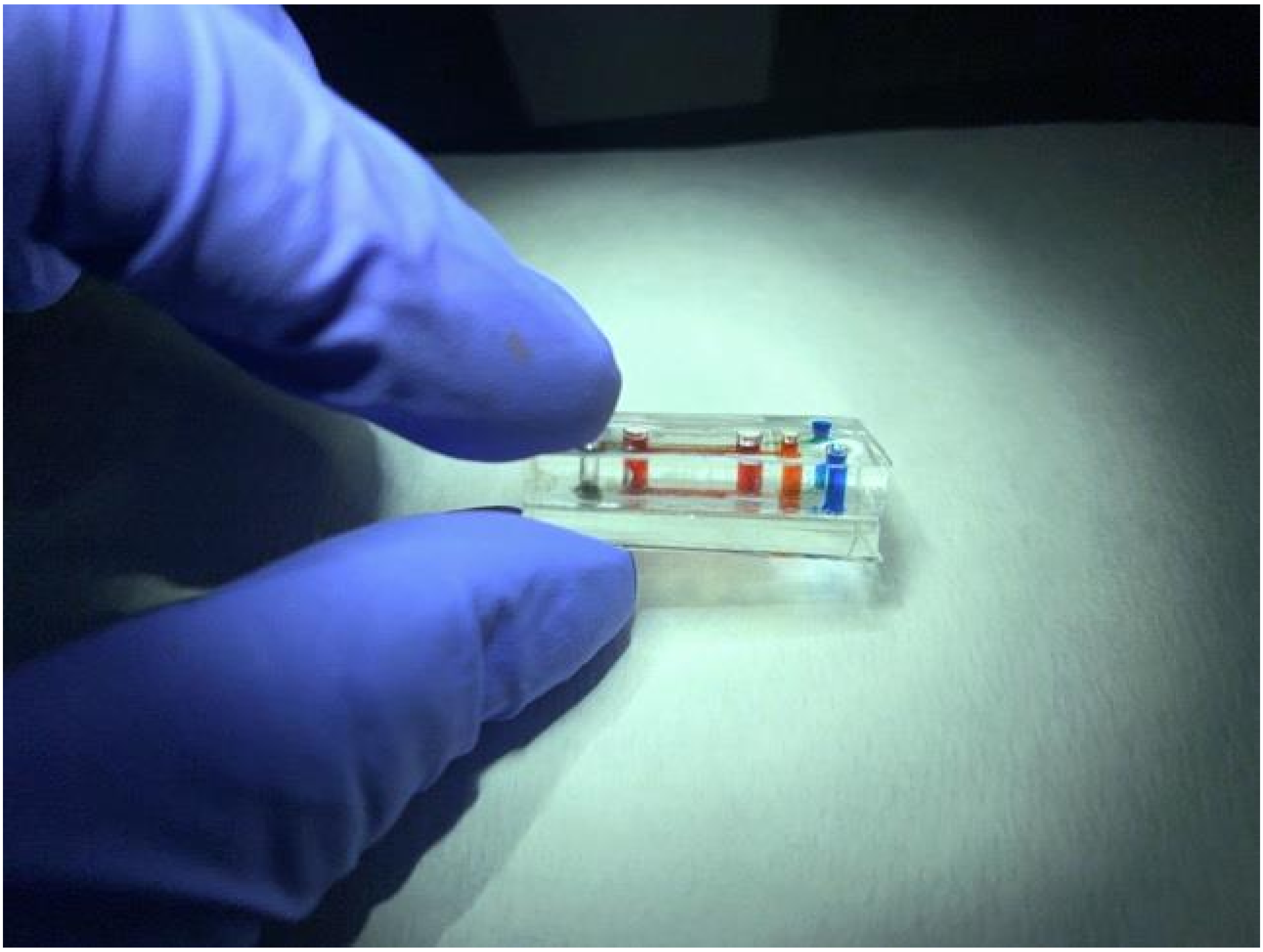

Figure 2.3 Device assembled. External channels in blue and the central channel in orange dye.

Membrane: It is an electrospun nanomembrane made of PCL/gelatin in which fibroblasts and gelatin will be seeded and cultured under the membrane, indicated by the orange dye in figure 2.2, while pancreatic epithelial cells will be seeded above the membrane, shown in red dye, figure 2.3.

Reservoir layer: It is the upper layer of the device and shows two medium reservoirs for the storage of the medium and works as a nutrient supply.

Please note that figure 2.2 does not represent the device of the study case as it presents the theoretical development of the idea of flow separation. This version does not have an interconnection between the external and internal channels and therefore would not be able to mimic the physiological microenvironment of the pancreas. The device used for seeding differs only in the presence of interconnections, which we will call "merlons," between the channels of the bottom layer, thus ensuring nutrient and substance exchange for the fibroblasts in the central channel.

This work aims at optimizing the design and fabrication of the previous fabricated multilayer device, proposed by Beatrice Minervini (41) and Matilde Aronne (42), to facilitate the cell seeding procedure, the monitoring and the fluid dynamics in the assembled configuration of the chip. Indeed, previous tests and characterization were performed to validate the functionality of each layer, in the disassembly configuration.

2.1 Original device issues

The devices designed by Beatrice Minervini (41) and Matilde Aronne (42) presented some issues, including:

Membrane detachment: To achieve biological characterization under the microscope, the membrane needed to be isolated. During the disassembly of the device, specifically when separating the bottom layer from the top layer, the membrane resulted delaminated or broken, preventing its analysis.

Channel filling: The filling of external and internal channels was significantly difficult to perform. In particular, the central channel was obstructed by the membrane which hindered the flow passage. Indeed, the membrane might lack a proper support from the surrounding surfaces, bending and falling into the central channel, acting as an obstacle. Another cause was the capillary effect, where fluid injected into an inlet would rise from the nearest upflow channel without filling the channels of the bottom layer. The presence of air bubbles inside also posed a problem as they prevented homogeneous channel filling or the unilateral filling of only one of the two external channels.

Liquid separation: As mentioned in the "Aim of the work" paragraph, the goal was to confine the collagen/fibroblast solution in the central channel and contain the culture medium separately in the external channels, while allowing communication between the channels for nutrient passage. However, what was obtained from the initial device was fluid leakage from the central channel to the external channels, and vice versa, from the external channels to the internal one.

3 Materials and methods

3.1 Device design

3.1.1 Bottom layer design – *lithography*

The bottom layer design was developed based on the optimized protocols by Beatrice Minervini during her master thesis work (figure 3.1.1) (41) and was produced with *lithography* and projected using *Rhinoceros*. The design incorporates three channels with the following dimensions: the central channel measures 900µm in width, 6.4mm in length, and 200µm in height, while the lateral channels measure 500µm in width, 6.4mm in length, and 200µm in height. To separate the central channel from the lateral ones, two rows of pillars were introduced. Each pillar has a diameter of 100µm and a height of 200µm, with a pitch of 75µm between the pillars.

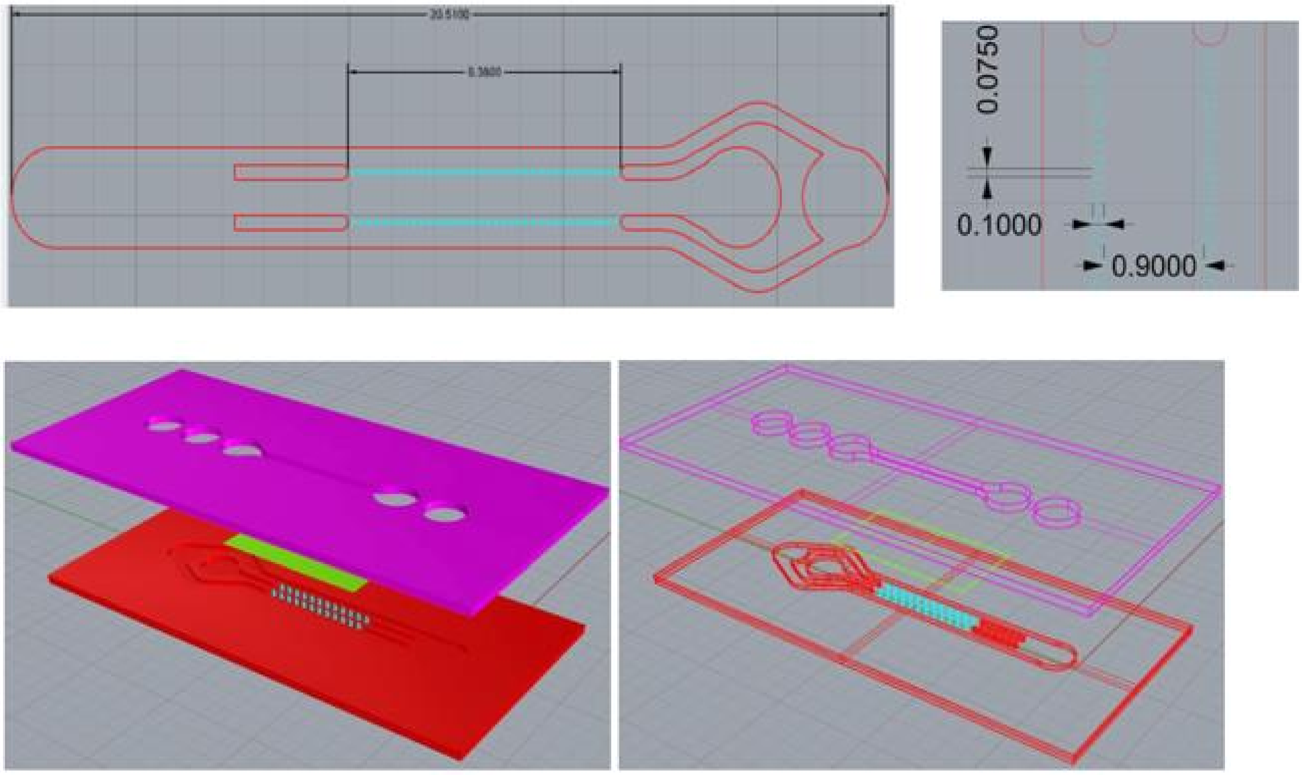

Figure 3.1.1 Original device CAD (41).

Characterization of Bottom layer– *lithography*

A preliminary microfluidic test of the device in Figure 3.1.1 was conducted under a digital microscope by filling the central channel from the second inlet using a 200 µl pipette with water and blue dye (figure 3.1.1c-3.1.2c). As can be seen from the test, the liquid flowed back from the third inlet (inlet of the top layer) and spread throughout the bottom layer, even overflowing from the external channels. The same test was conducted by attempting to fill the external channels (Figure 3.1.3c-3.1.4c).

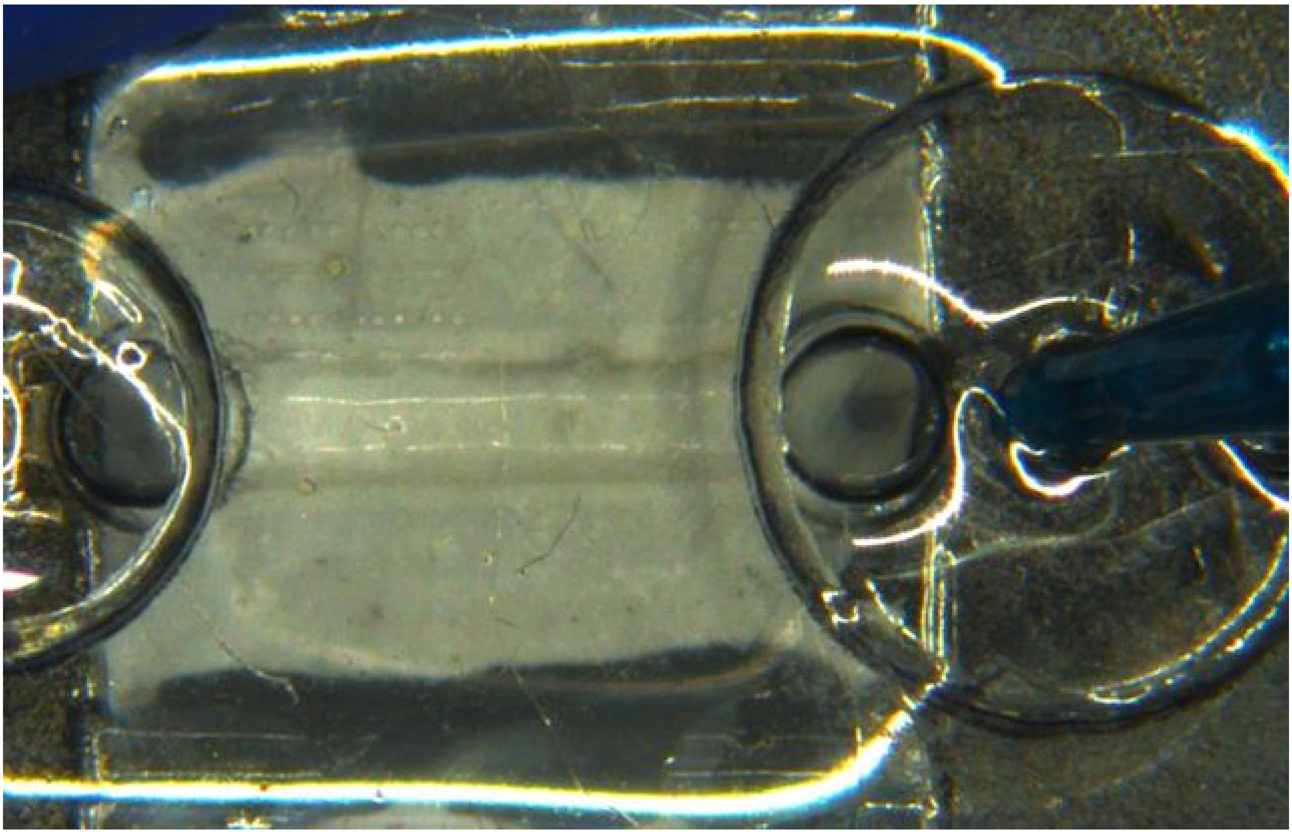

Figure 3.1.1c Start point of a microfluidic test during the filling of the central channel.

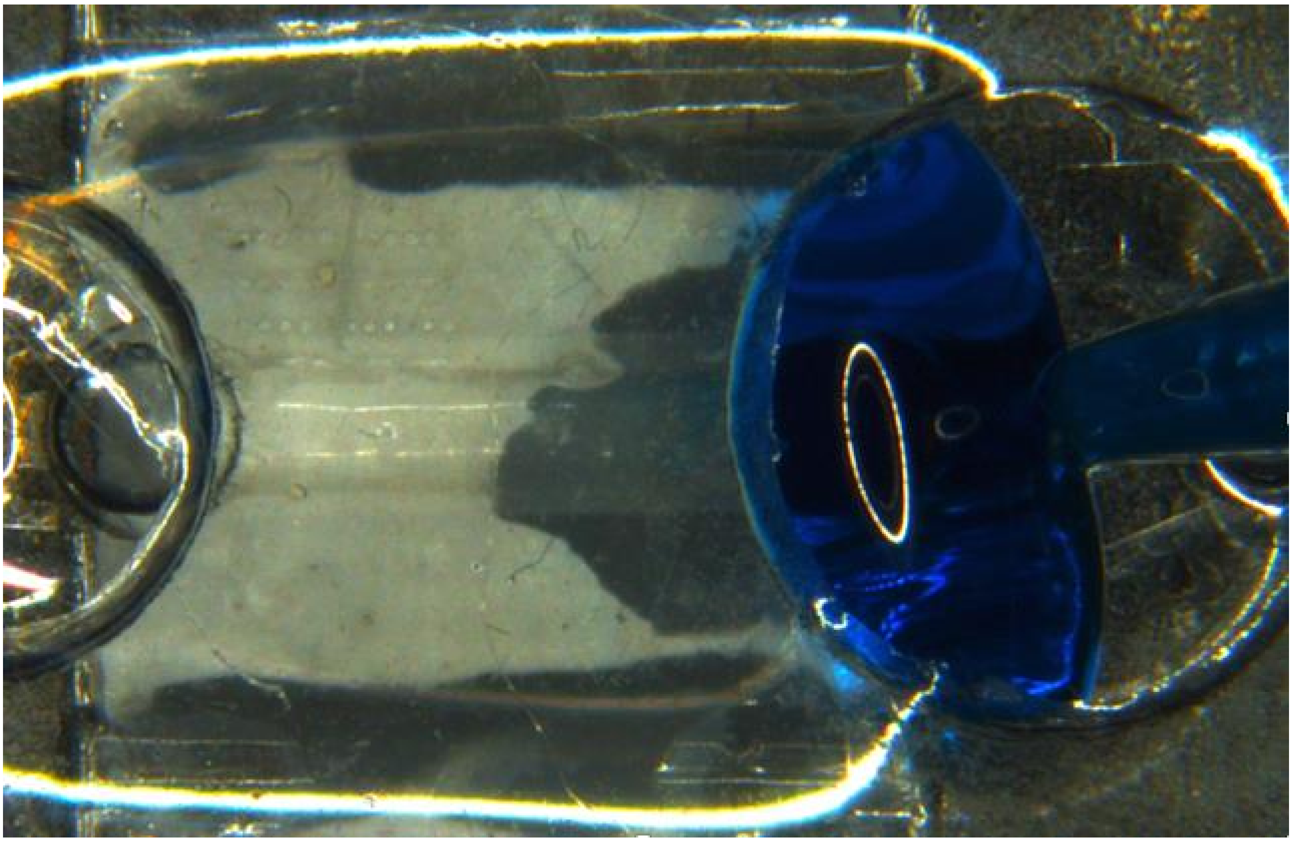

Figure 3.1.2c End point of a microfluidic test during the filling of the central channel.

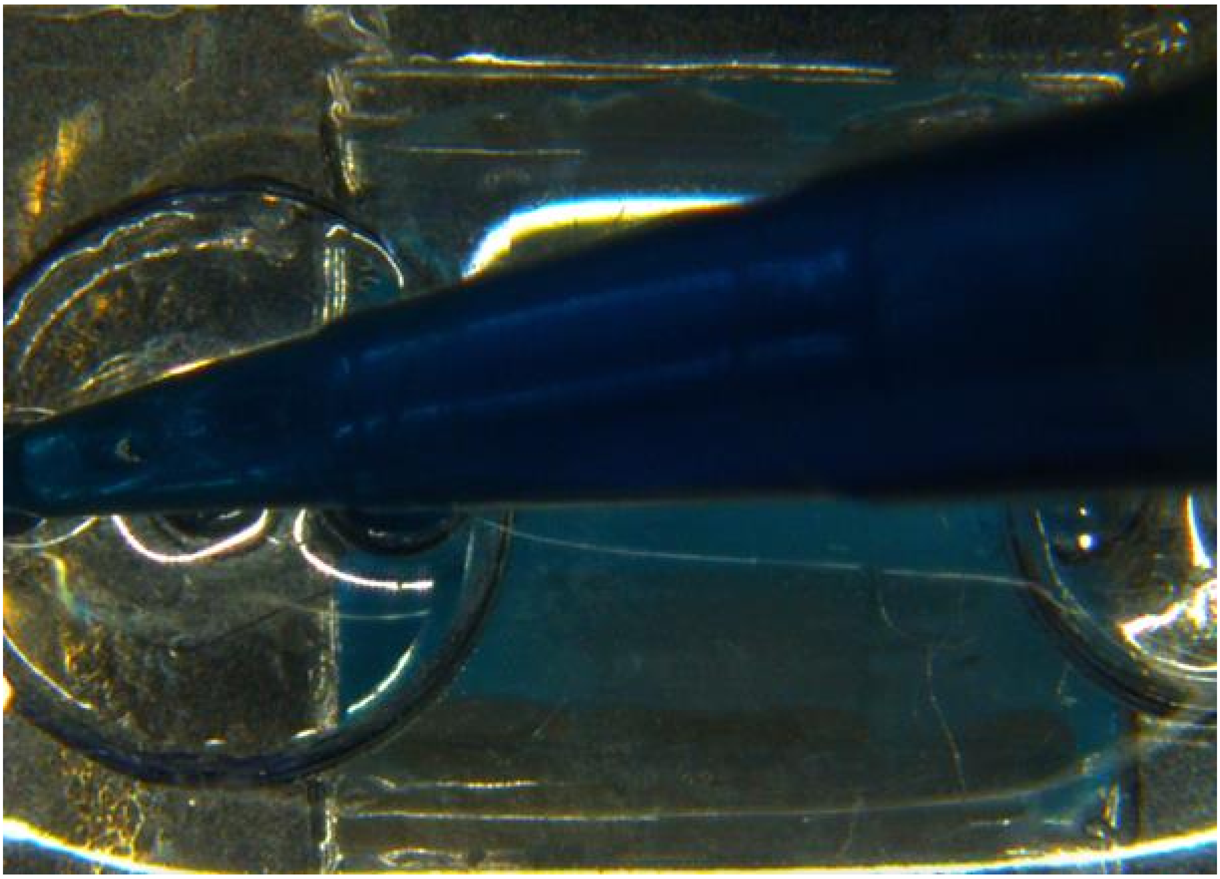

Figure 3.1.3c Start point of a microfluidic test during the filling of external channels.

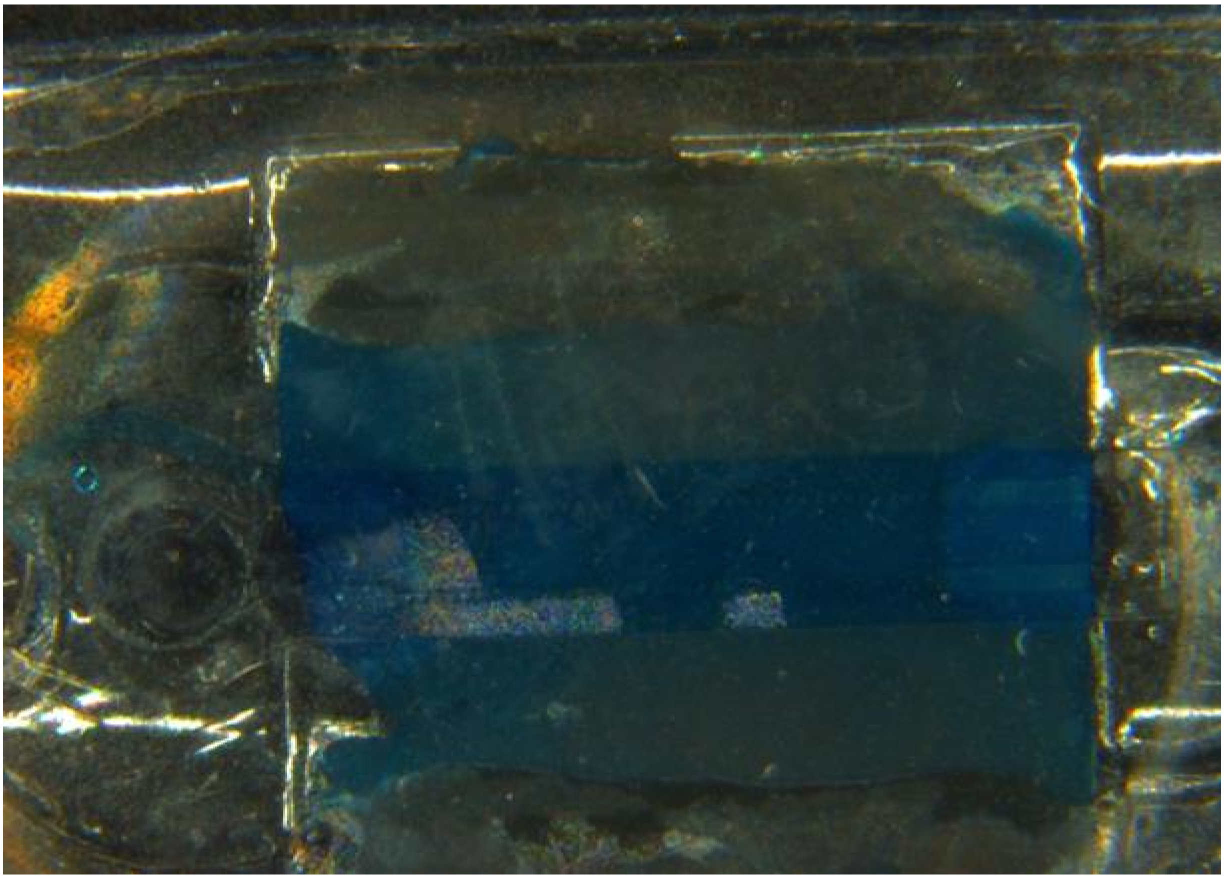

Figure 3.1.3c End point of a microfluidic test during the filling of external channels. Bottom view.

From the bottom view of Figure 3.1.3c, it can be observed that the flow was not confined within the external channels but entered the central one. Furthermore, the filling occurred unilaterally, as we can see that only the upper external arm was completely filled.

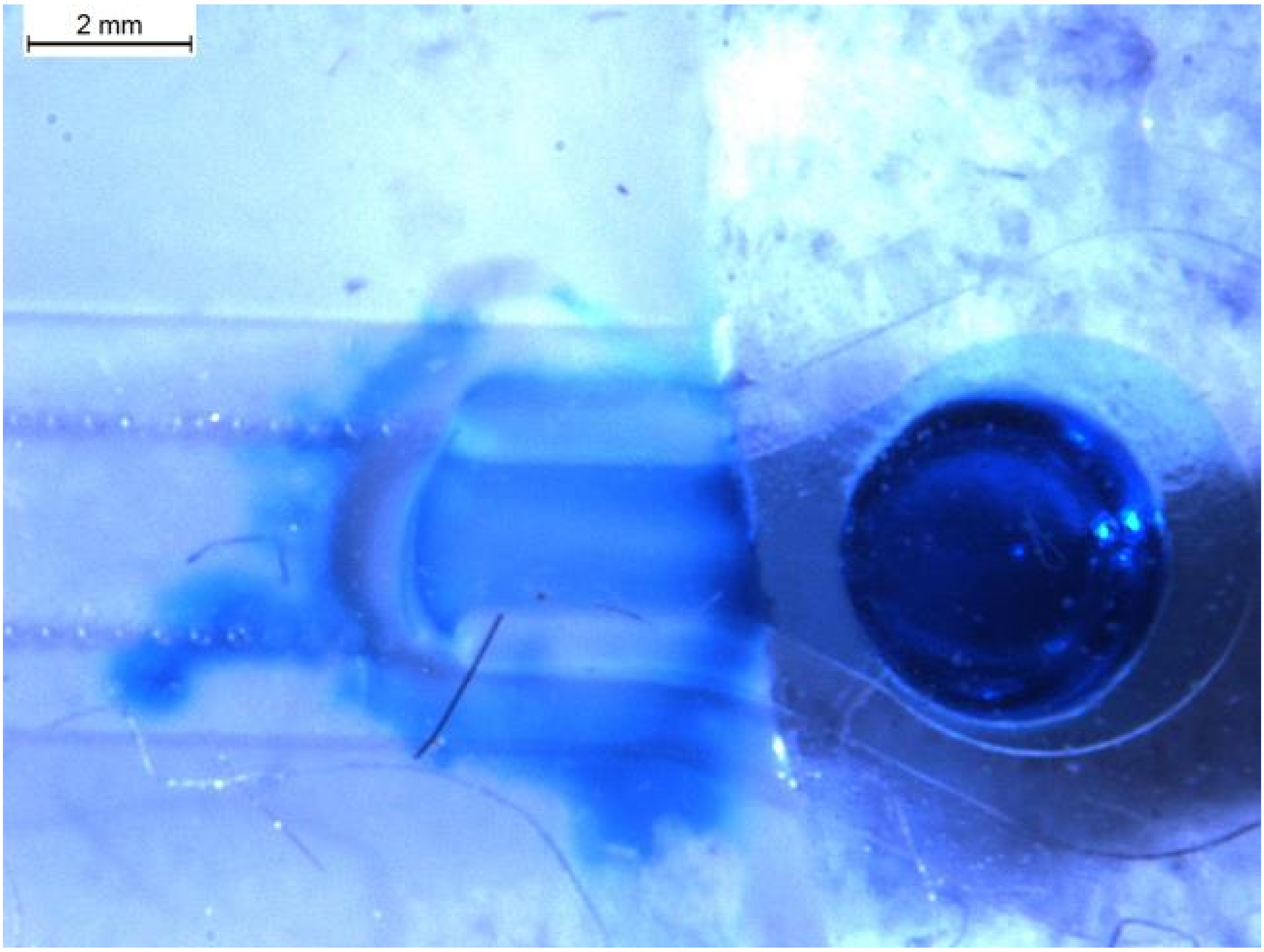

Figure 3.1.4c Result of a microfluidic test. Bottom view.

As seen from the figure above (figure 3.1.4c), the membrane acted as a barrier to the flow of fluid, preventing the central channel from being completely filled. In fact, it appears more saturated and of a dark blue color.

3.1.2 Bottom layer design – *lithography's modification*

The first modification made to the design involved altering the central channel to better confine the fluid within it. The continuous wall of pillars was replaced with an alternating pattern of pillars and slots, promoting a more contained flow (figure 3.1.2). The central channel remained almost unaltered, measuring 950µm in width. The length of the slots is (missing value), the diameter of the pillars was reduced to 50µm, and the distance between the slots and pillars is 30 µm. Due to the precision required, the mold was fabricated using lithography, as illustrated below.

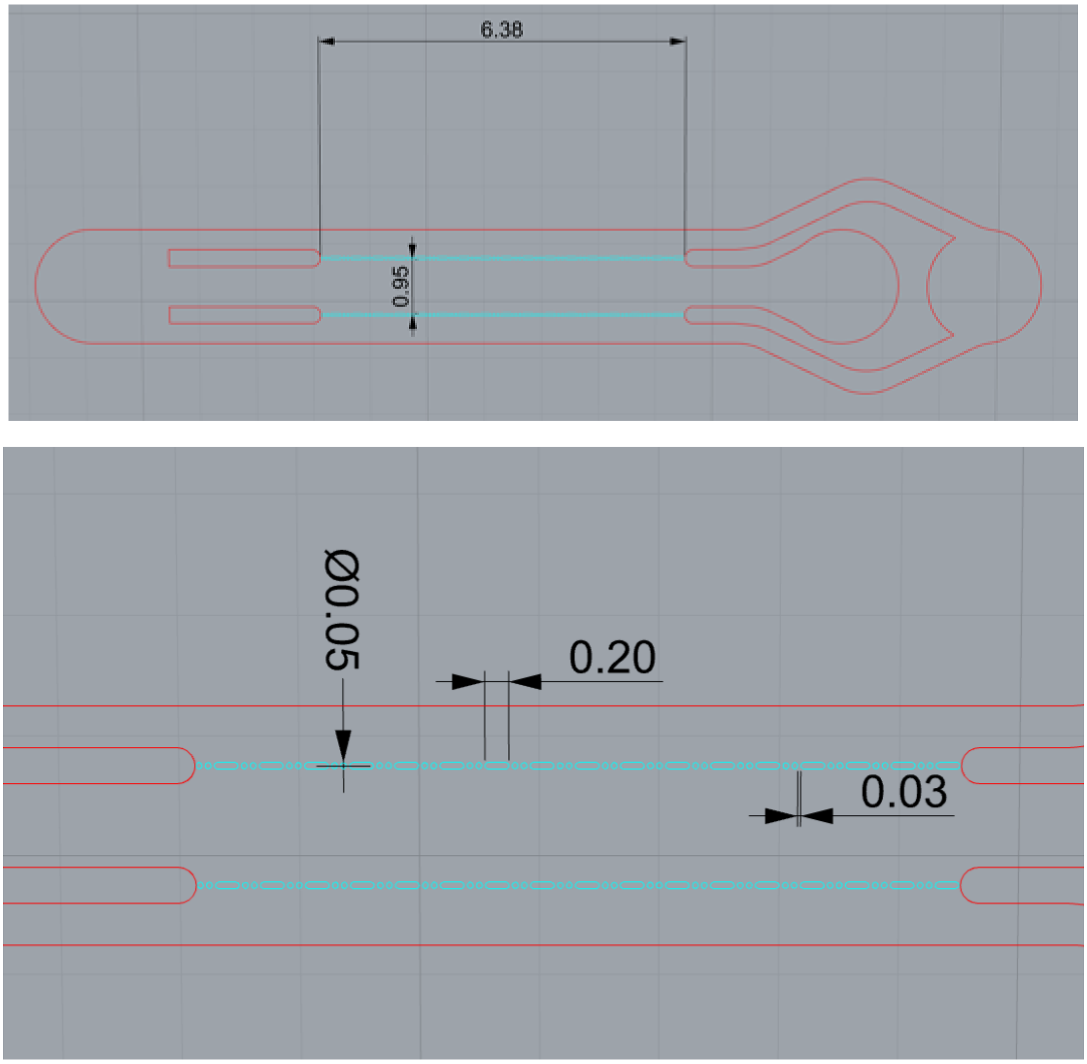

Figure 3.1.2 Slots and pillars device CAD.

Characterization of Bottom layer – *lithography's modification*

As evident from the sectional view (figure 3.1.5c) obtained by digital microscope, the pillars undergo slight deformation during casting and debonding, which did not compromise the results in a first microfluidic test using water and dye (figure 3.1.6c). This test was successfully conducted and passed.

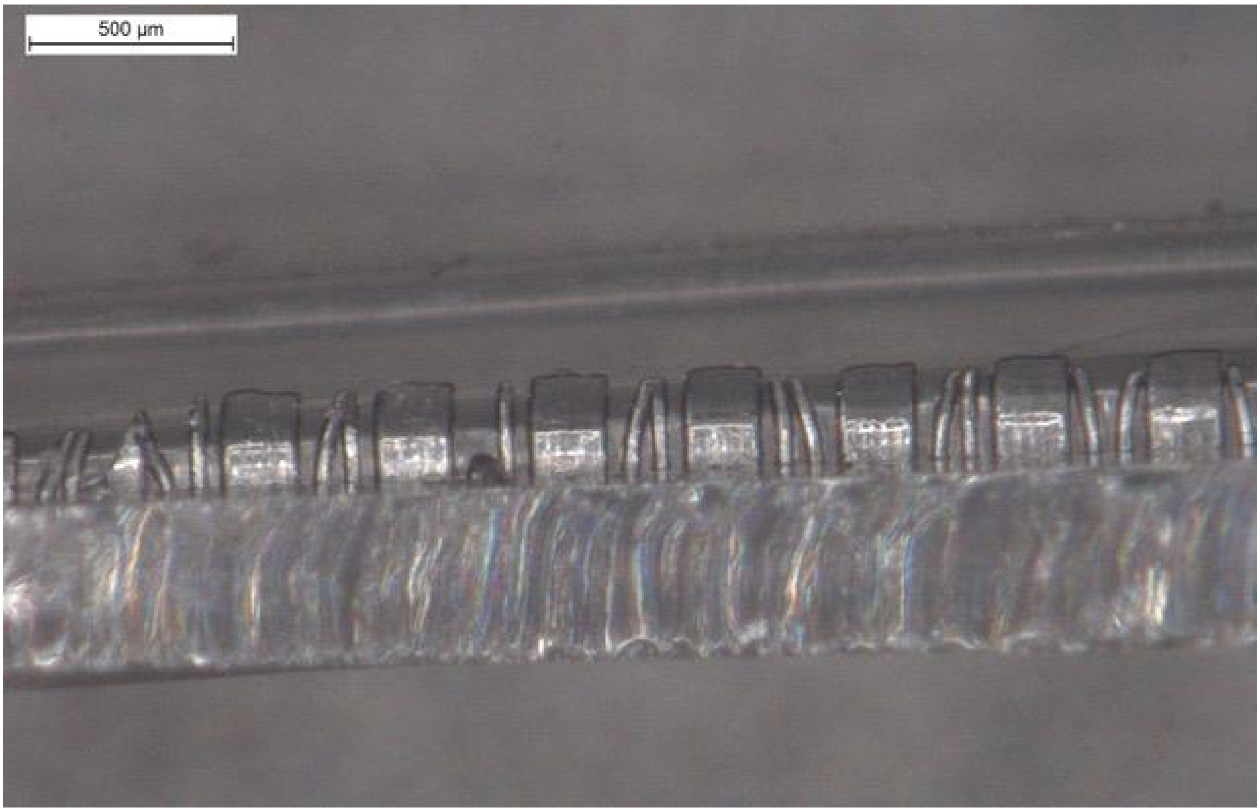

Figure 3.1.5c Sectional view of slots and pillars.

Figure 3.1.6c Microfluidic test for the central channel.

However, when the test was conducted with the assembled device and the membrane inserted, material leakage from the central channel into the outer channels was observed, due to the wettability of the membrane and deformed pillars (Figure 3.1.7c).

Figure 3.1.7c Results of a microfluidic test.

3.1.3 Bottom layer design – 3d printing

Given the long timeframes and limited versatility of lithography, the fabrication of the device proceeded using *3D printing*, allowing for the testing of multiple devices in less time. Firstly, I tested the accuracy of the OBJET30 printer, theoretically at 0.1mm (43), using an initial model that corresponded to the equivalent of the one used in lithography. However, this model had a wall thickness of 0.1mm composed of only slots with 0.2mm in length, without the inclusion of pillars, as it was already known in advance that they would exceed the limits imposed by the printer. All other dimensions of the design remained unchanged. The printing process was unsuccessful because the minimum required accuracy was 0.1mm (43), but the width of the wall was at the limit of accuracy and the distance between the slots was significantly smaller (figure 3.1.3).

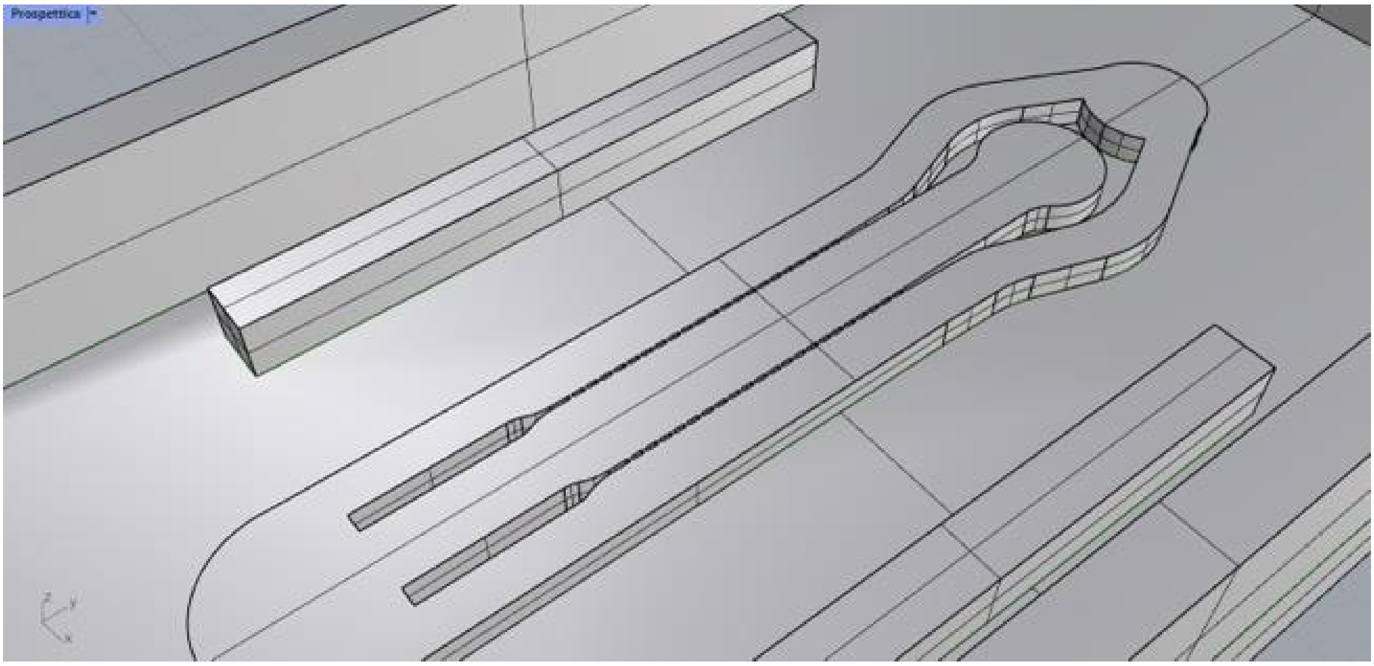

Figure 3.1.3 Pillars and slots walls.

An addition to the design was the incorporation of lateral protrusions. By replicating them in PDMS, their negative imprints formed recesses to accommodate the membrane, fixing it and preventing it from bending or delaminating during bonding and disassembly.

Anyway, unable to use either pillars or slots, the design and its dimensions were changed (figure 3.1.4-3.1.5). The central channel needed to have better containment to properly confine the fluid, so the idea was to use a conductive wall with a height of 0.3mm and merlons of 0.2mm on top of it (figure 3.1.6). The function of the merlons is to ensure the exchange of substances and nutrients between the central and lateral channels, maintaining the role that the pillars had in the initial design. Remember that the mold represents the negative of the replica in PDMS, so the terms "wall" and "merlons" refer to the replica and not the mold.

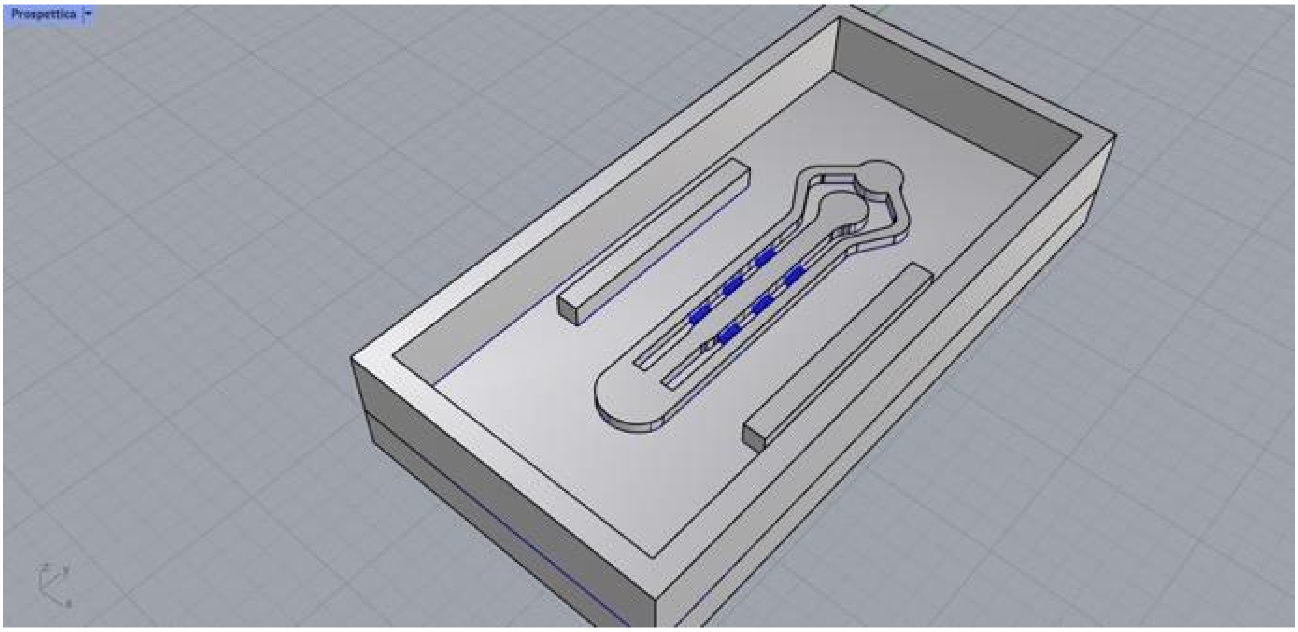

Figure 3.1.4 Overall view of the device with merlons.

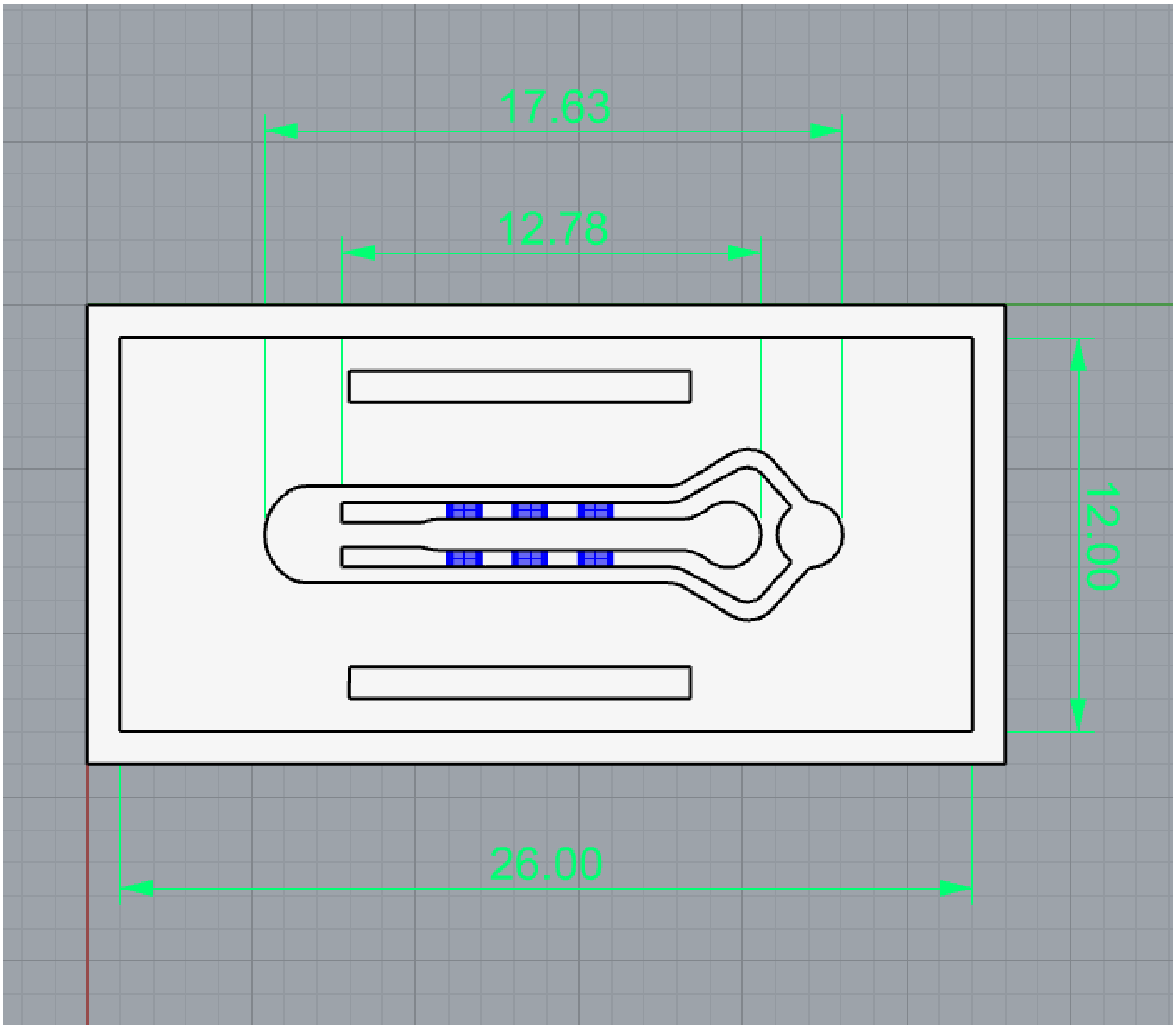

Figure 3.1.5 Device dimensions.

Figure 3.1.6 Section view of merlons.

Characterization of Bottom layer – *3d printing*

In the figure 3.1.8c, we can see the cross-sectional view of the bottom layer, particularly of the central channel and the merlons.

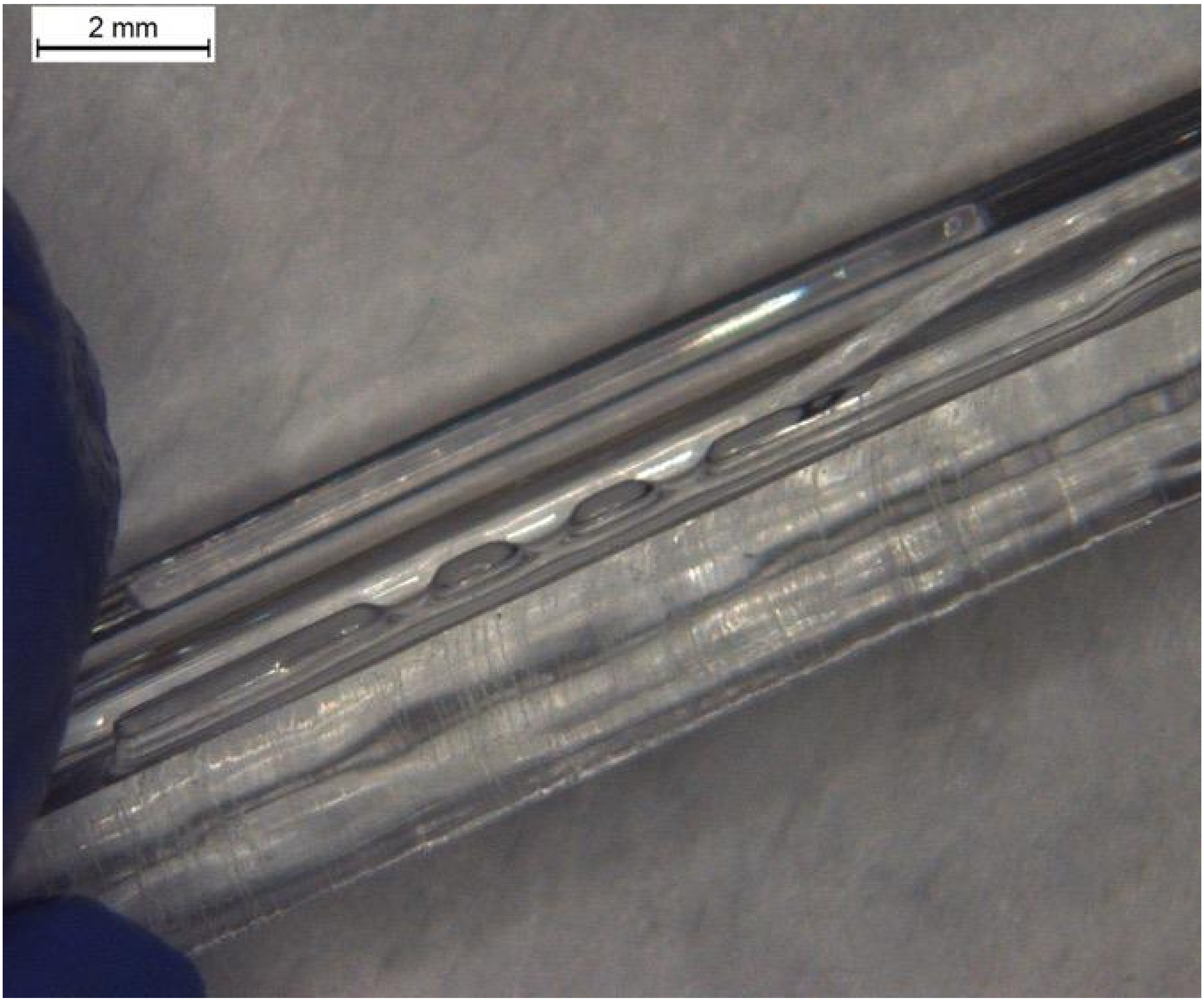

Figure 3.1.8c Section view of merlons.

A microfluidic test was conducted to fill the central channel with water and dye, which was successfully achieved. However, there remained an issue with the external channels (figure 3.1.9c). Specifically, as the fluid filled the external channel, it attempted to rise through the centrally positioned inlets due to capillary action, entering the central channel and flowing back through the inlets. Furthermore, we continue to observe the uneven filling of only one of the lateral channels (figure 3.1.10c).

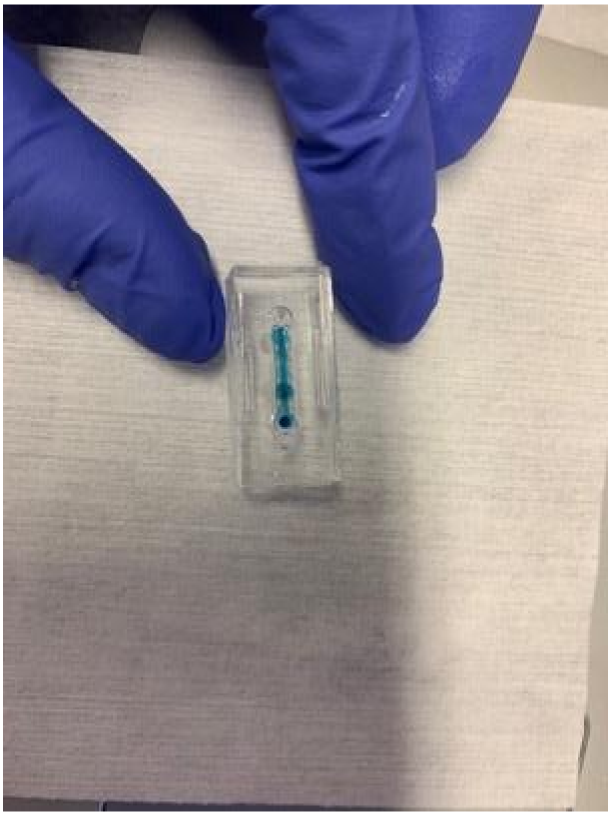

Figure 3.1.9c central channel flow.

Figure 3.1.10c Section view of merlons.

3.1.4 Bottom layer design – 3d printing - 1° modification

The issue related to capillary action primarily concerned the proximity of the inlet channels. To overcome this problem, the outer arms were expanded and widened to avoid interference with the top channel (see Figure 3.1.7).

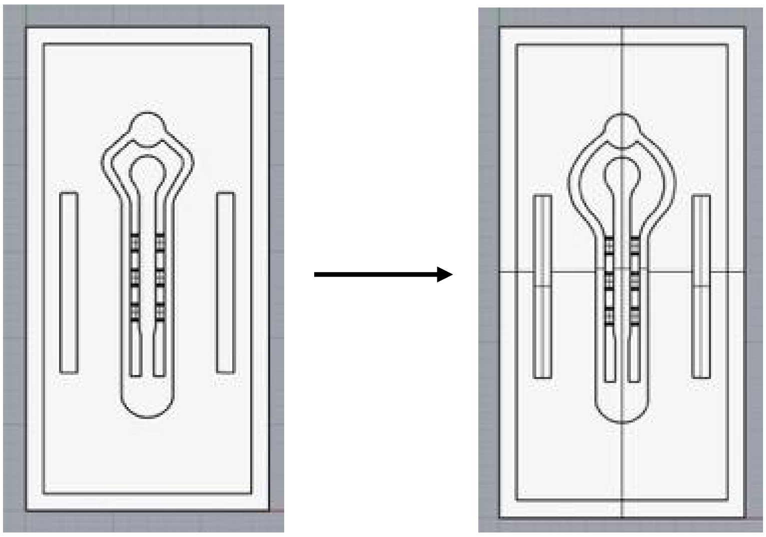

Figure 3.1.7 Changes made to the CAD.

Characterization of Bottom layer - *3d printing - 1° modification*

As seen from a video frame during a microfluidic test, the central channel continued to fill properly, but the issue of non-uniform filling persisted in the external channels (figure3.1.11c and 3.1.12c).

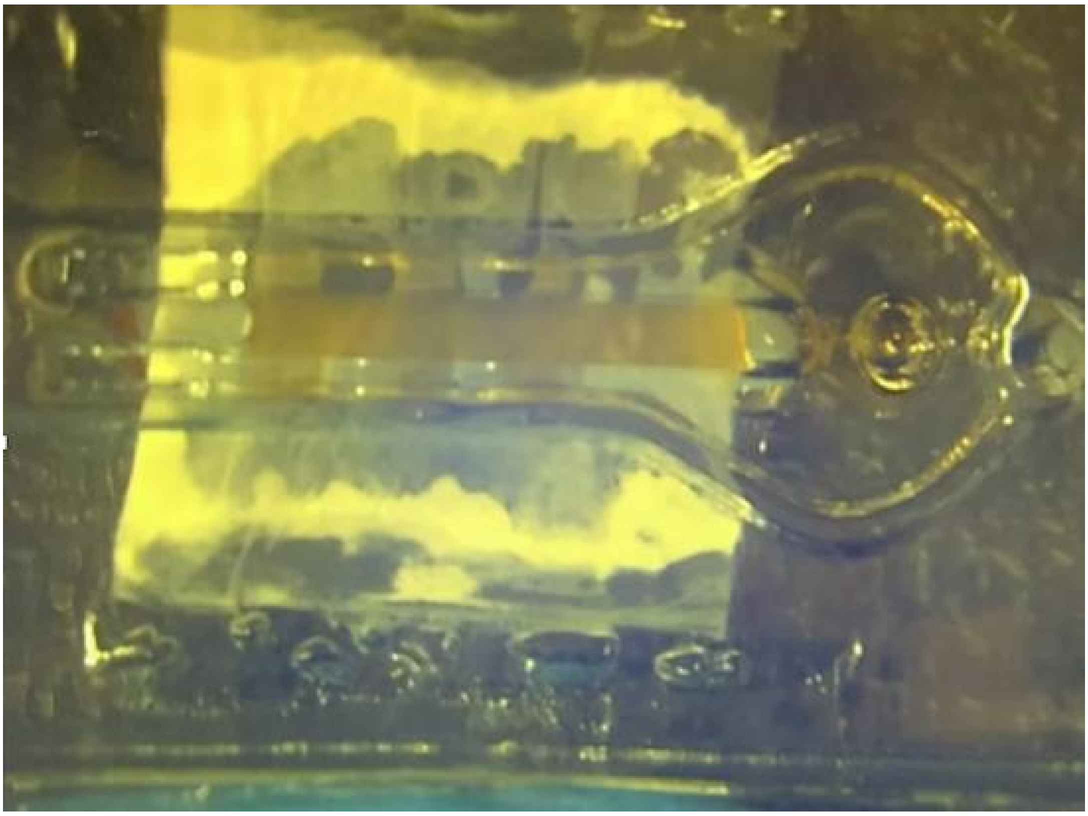

Figure 3.1.11c Central channel flow.

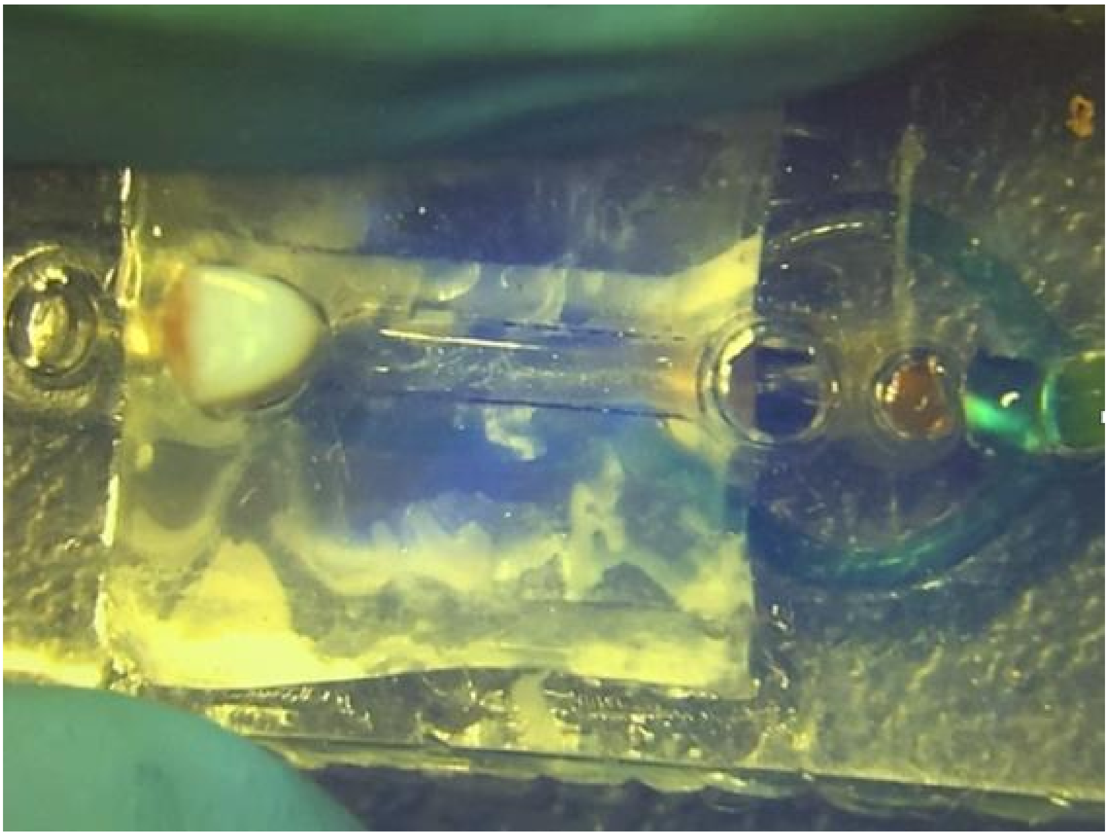

Figure 3.1.12c Unilateral filling external channel.

3.1.5 Bottom layer design – 3d printing - 2° modification

The external channels likely experienced non-uniform filling not only due to the presence of air but also because the flow took a preferential path based on how the pipette tip was inserted into the channel, the applied force, and the tilt of the pipette in the inlet. To address this issue, it was decided to move the bifurcation point further away from the inlet, reducing the susceptibility to these issues and allowing the flow to become more linear along the straight channel, reducing preferential flow paths (figure 3.1.8).

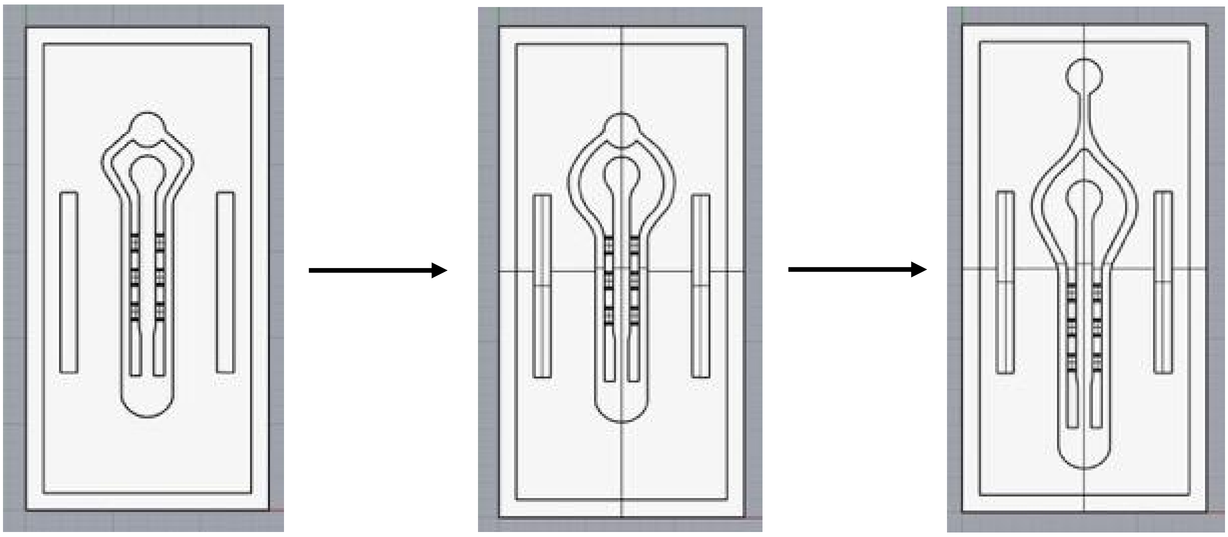

Figure 3.1.8 Changes made to the CAD.

Characterization of Bottom layer - *3d printing - 2° modification*

Like the previous tests, the central channel didn't encounter any filling problems, whereas the outer channels still presented notable challenges.

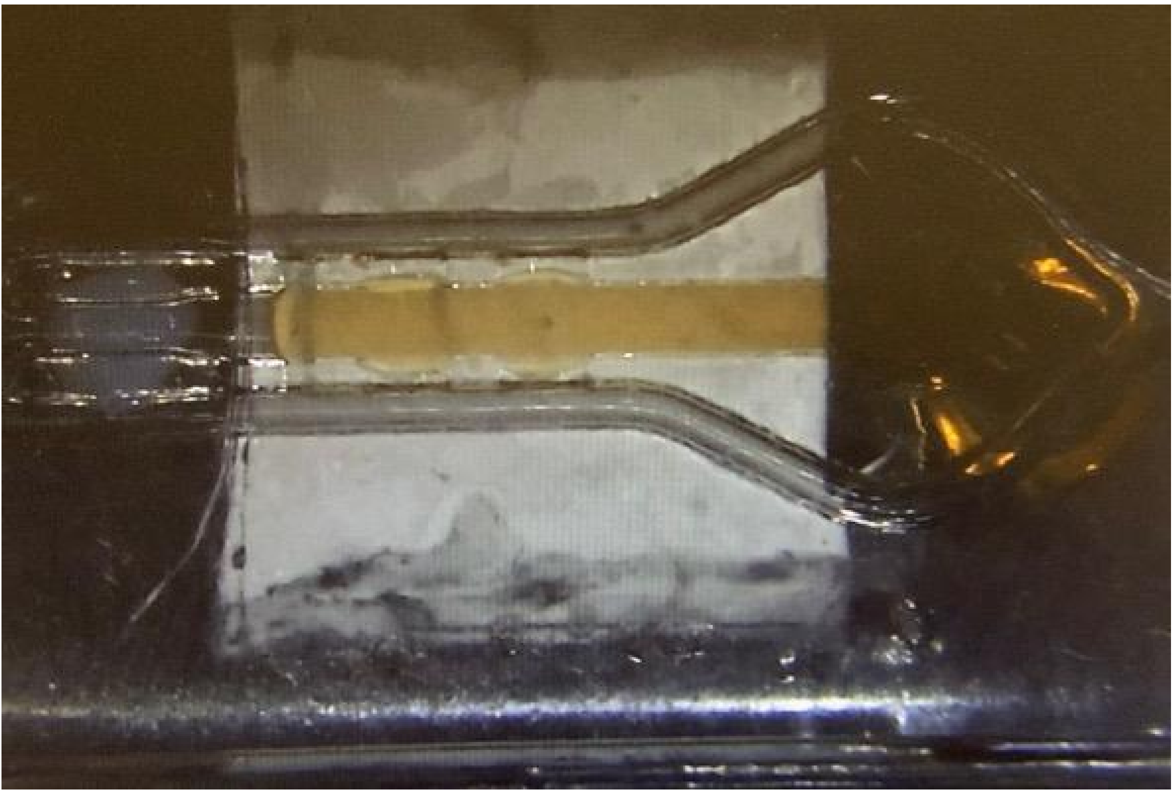

.

Figure 3.1.12c Central channel flow.

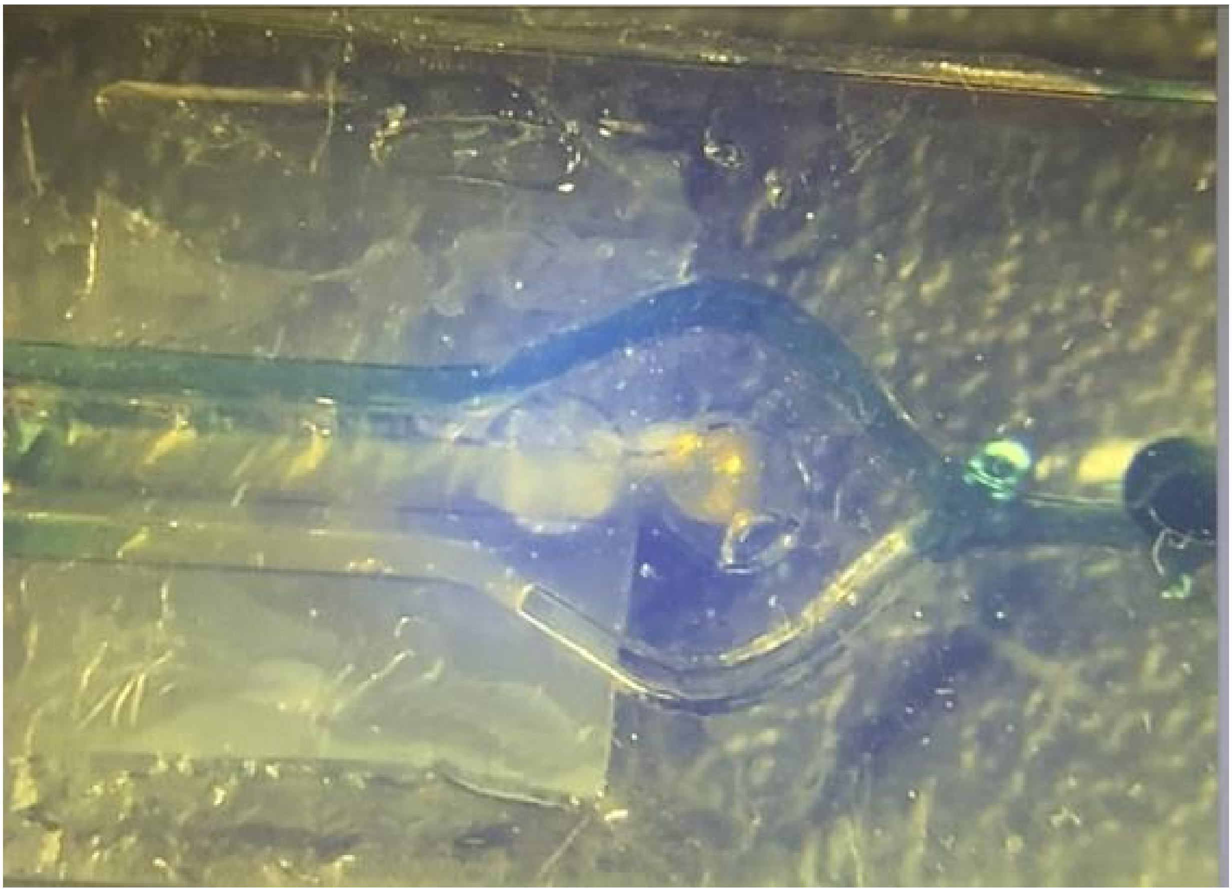

Figure 3.1.13c Central channel flow.

3.1.6 Bottom layer design – 3d printing – Final design

The only and definitive solution, then, is to have separate inlets for the external channels to facilitate the uniform filling of both. Therefore, based on the study conducted by Drifka et al. (44) and the previous thesis work of Matilde Aronne (42), the device with four separate inlets has been optimized. Two inlets were intended for the side channels of the bottom layer, one for the central channel of the bottom layer, and the fourth one for the top layer channel (figure 3.1.9-3.1.10).

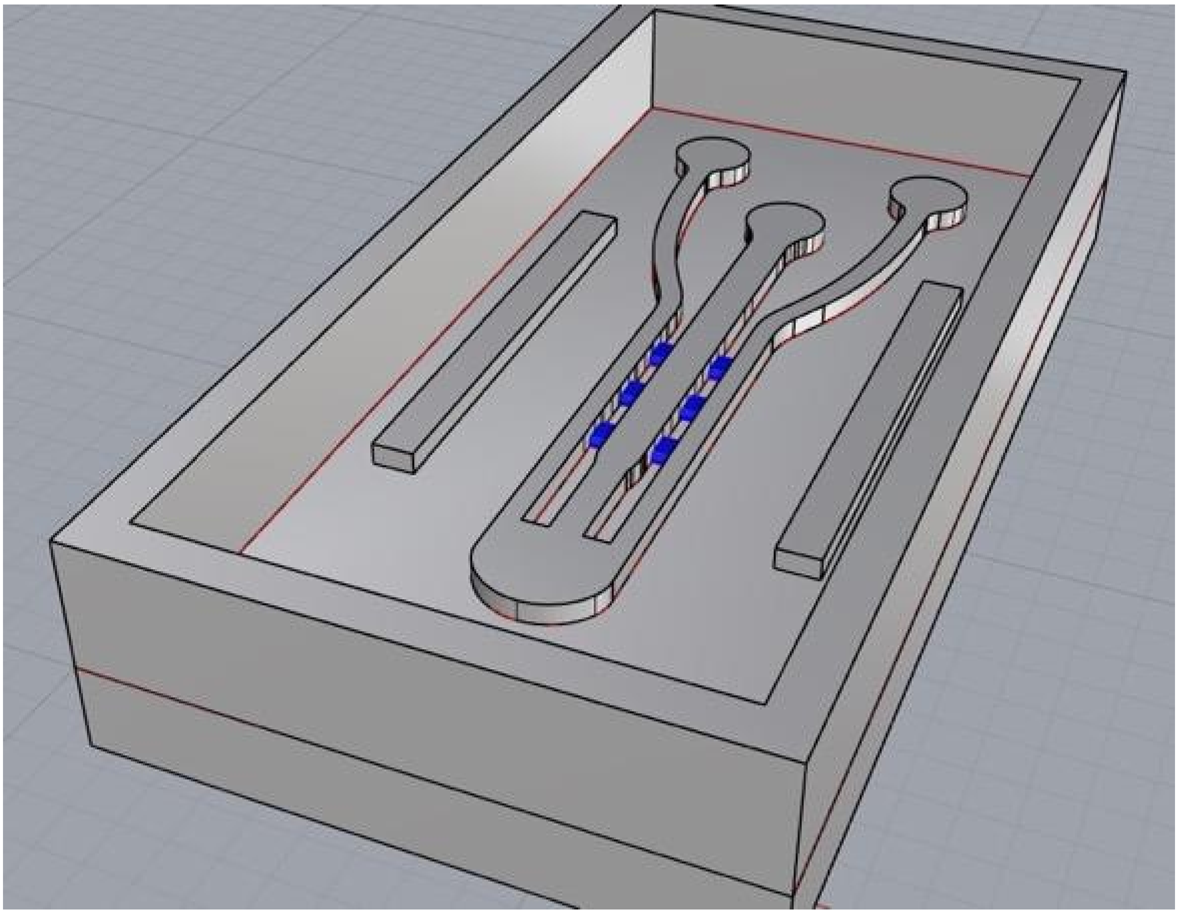

Figure 3.1.9 Overall view of the device in Rhinoceros.

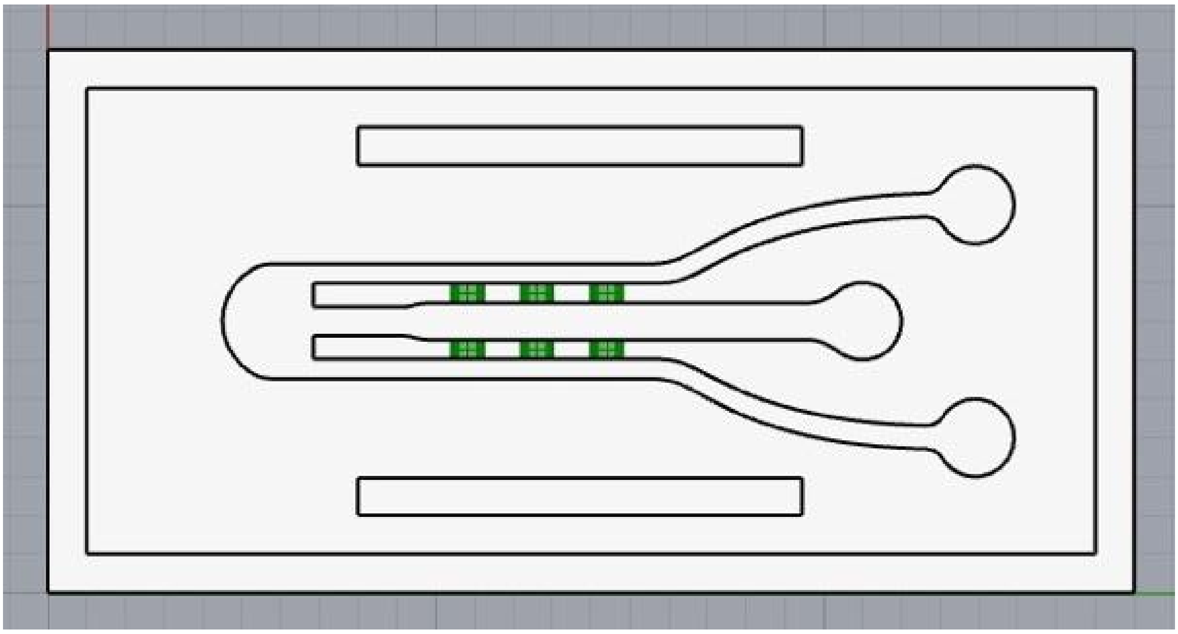

Figure 3.1.10 Upper view of the final device.

The device's dimensions have been optimized to enhance fluidic performance, with particular focus on reducing the size of the merlons (figure 3.1.11-3.1.12).

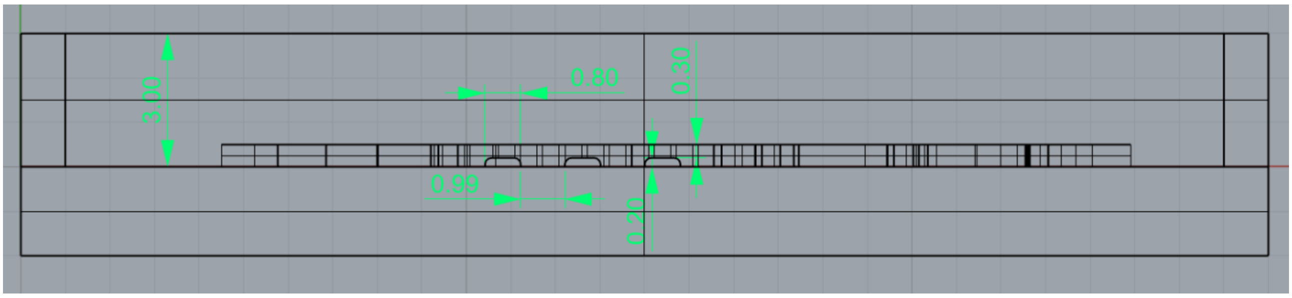

Figure 3.1.11 Lateral view of the final device.

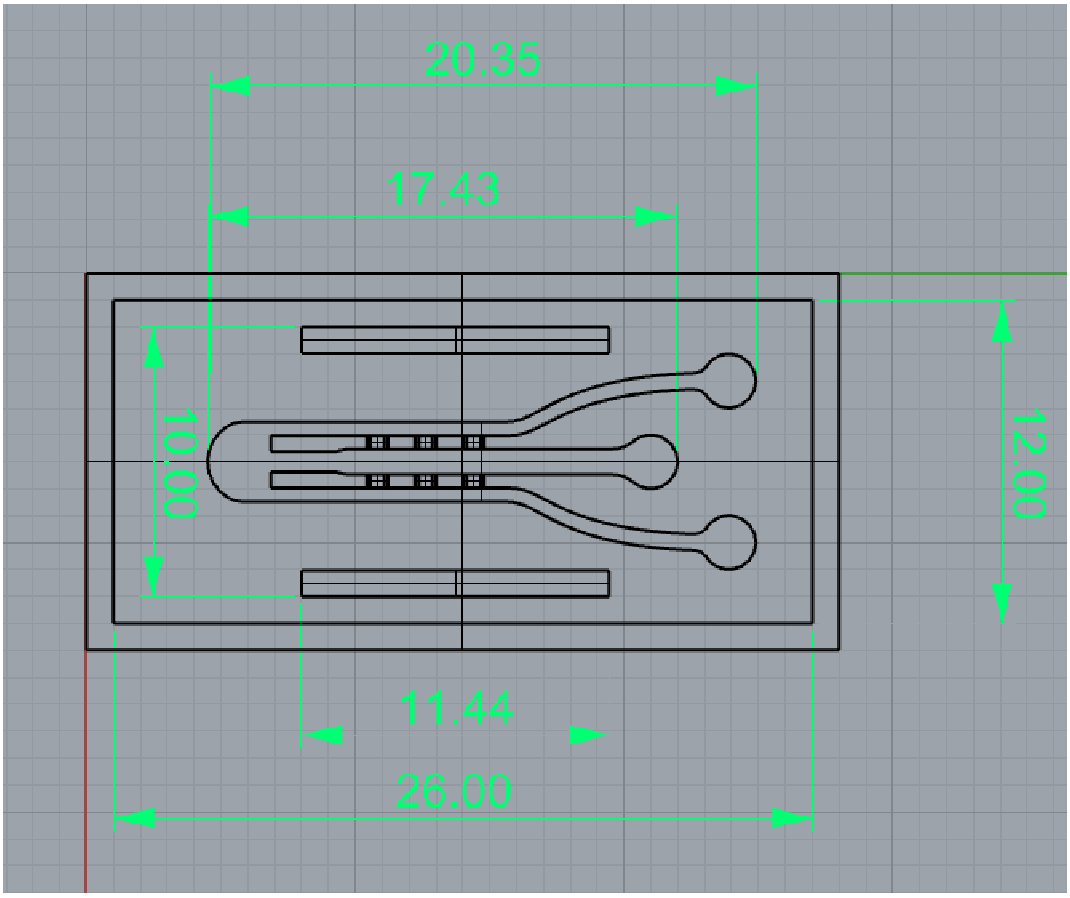

Figure 3.1.12 Upper view of the final device with dimensions.

Characterization of Bottom layer – *3d printing - Final design*

From the final microfluidic tests, we can observe the uniform filling of all the channels, including the central channel (Figure 3.1.14c), the external channels, and the top layer channel (Figure 3.1.15c).

Figure 3.1.14c Central channel flow.

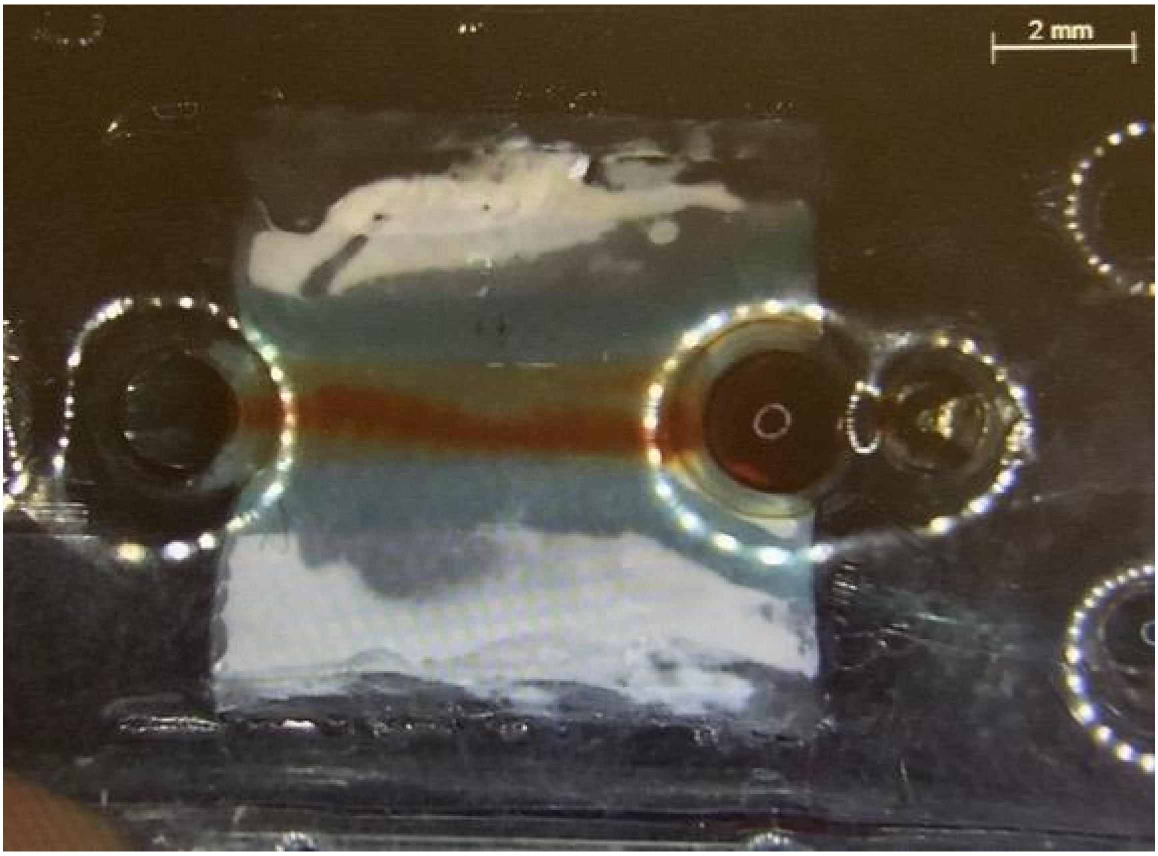

Figure 3.1.15c Filling of the external channels and the channel in the top layer.

From this image below (figure 3.1.16c), we can see that only the external channels with four inlets are adequately filled.

Figure 3.1.16c Testing conducted on various samples of the device after the microfluidic test.

3.1.7 Top layer design

The top layer design was created based on the bottom layer. The design features a channel with the new dimensions, compared to that of Marilde Aronne (42) the canal has been increased in height (figure 3.1.13). This channel corresponds to the central channel of the bottom layer, and they are separated by a polycaprolactone (PCL)/gelatine electrospun membrane. The design includes four inlet holes with a diameter of approximately 2mm and two outlet holes of the same size as the inlet holes. Additionally, there is a rectangular frame surrounding the channel, which serves as the housing for the membrane.

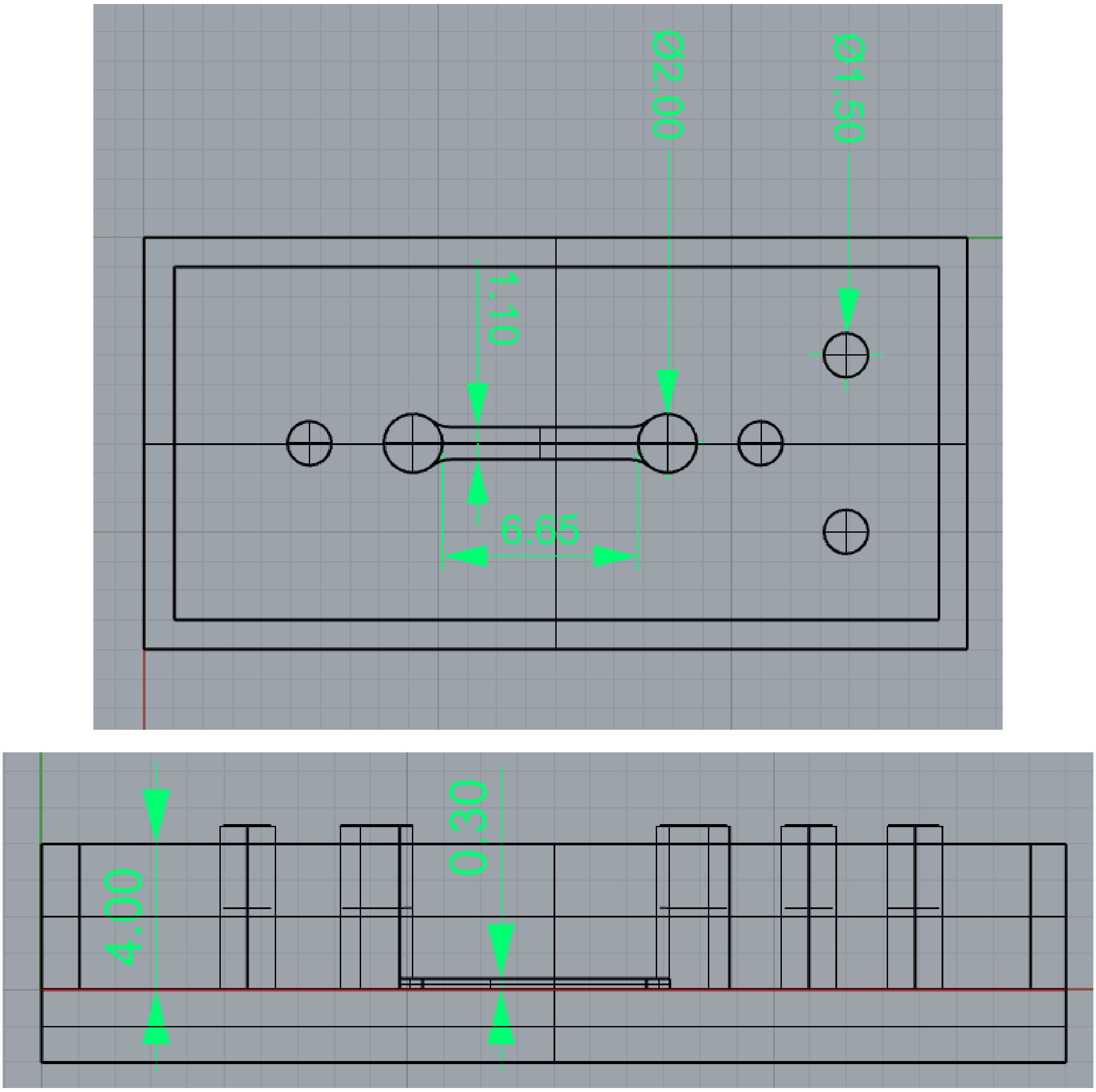

Figure 3.1.13 Upper and lateral view with dimensions – top layer.

3.1.8 Reservoir design

On top of the previously described layers, the pancreas-on-chip model includes an additional layer known as the reservoirs. The purpose of this layer is to serve as storage for the culture media required for the cells seeded in the other layers. The reservoirs layer consists of two holes, one located at the inlets with a diameter of 10 mm, and another at the outlets with a diameter of 6.3 mm. The CAD design of this layer created in Rhinoceros is depicted in figure (figure 3.1.14).

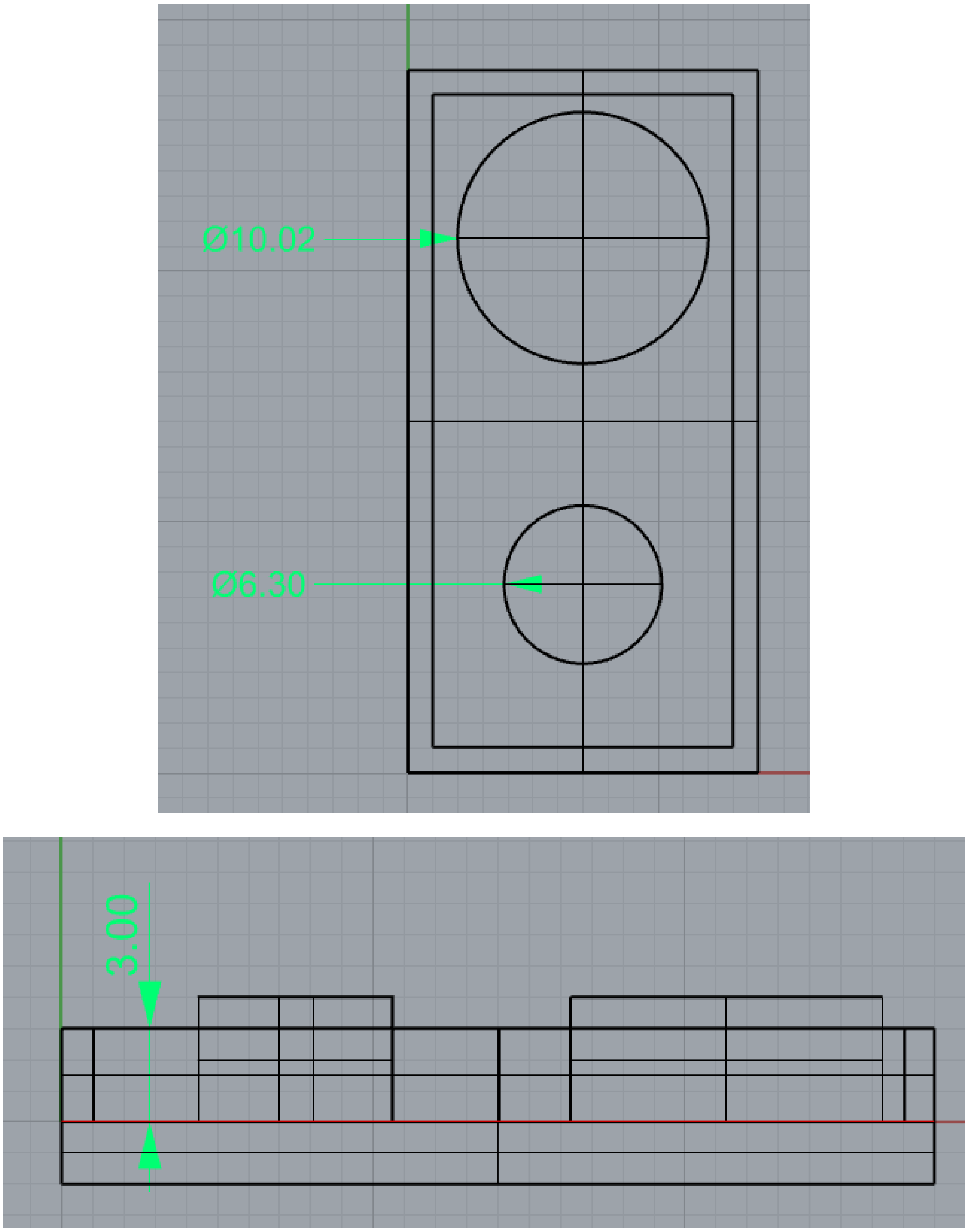

Figure 3.1.14 Upper and lateral view with dimensions – reservoir layer.

3.2 Device fabrication

3.2.1 Replica molding

Replica molding, also known as soft lithography or microcontact printing, is a technique used to create replicas or copies of a master pattern with high fidelity. It is widely used in microfabrication and microfluidics to produce structures and devices with intricate features.

The replica molding process involves the following steps (45):

1. *Master fabrication*: A master pattern is created using a high-resolution technique such as photolithography (figure 3.2.1) or 3d printing (figure 3.2.2) in this study case. The master pattern can be made on a silicon wafer or other suitable substrate.
2. *Preparing the mold*: A liquid polymer, such as polydimethylsiloxane (PDMS), is poured over the master pattern and cured. PDMS is a commonly used material in replica molding due to its flexibility, transparency, and ease of use.
3. *Demolding*: Once the PDMS has cured and solidified, it is carefully peeled off from the master, resulting in a negative replica of the master pattern embedded in the PDMS.
4. *Replica production*: The PDMS mold is then used to create multiple replicas by pouring or casting various materials such as polymers, gels, or even metals into the mold. The material fills the cavities of the mold, replicating the features of the original master pattern.

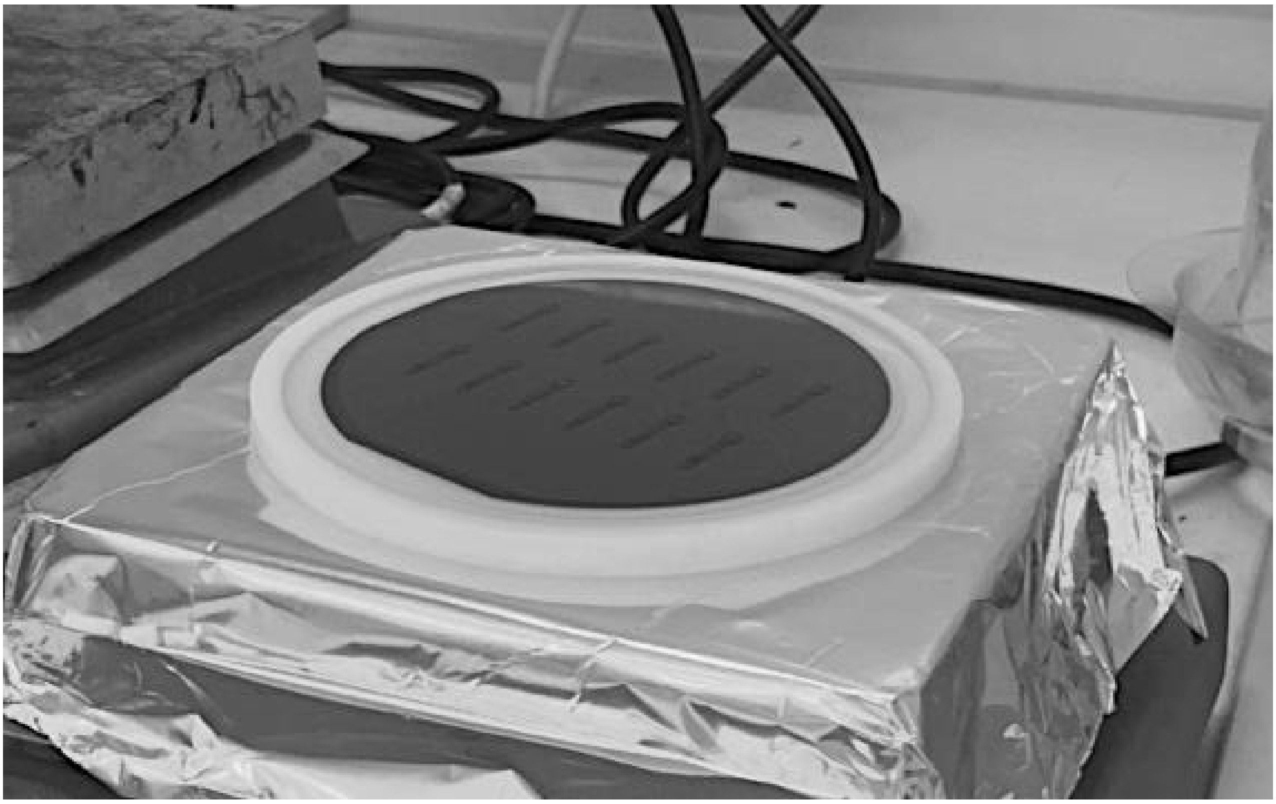

Figure 3.2.1 Mold with PDMS during baking. Wafer mold produced by soft lithography.

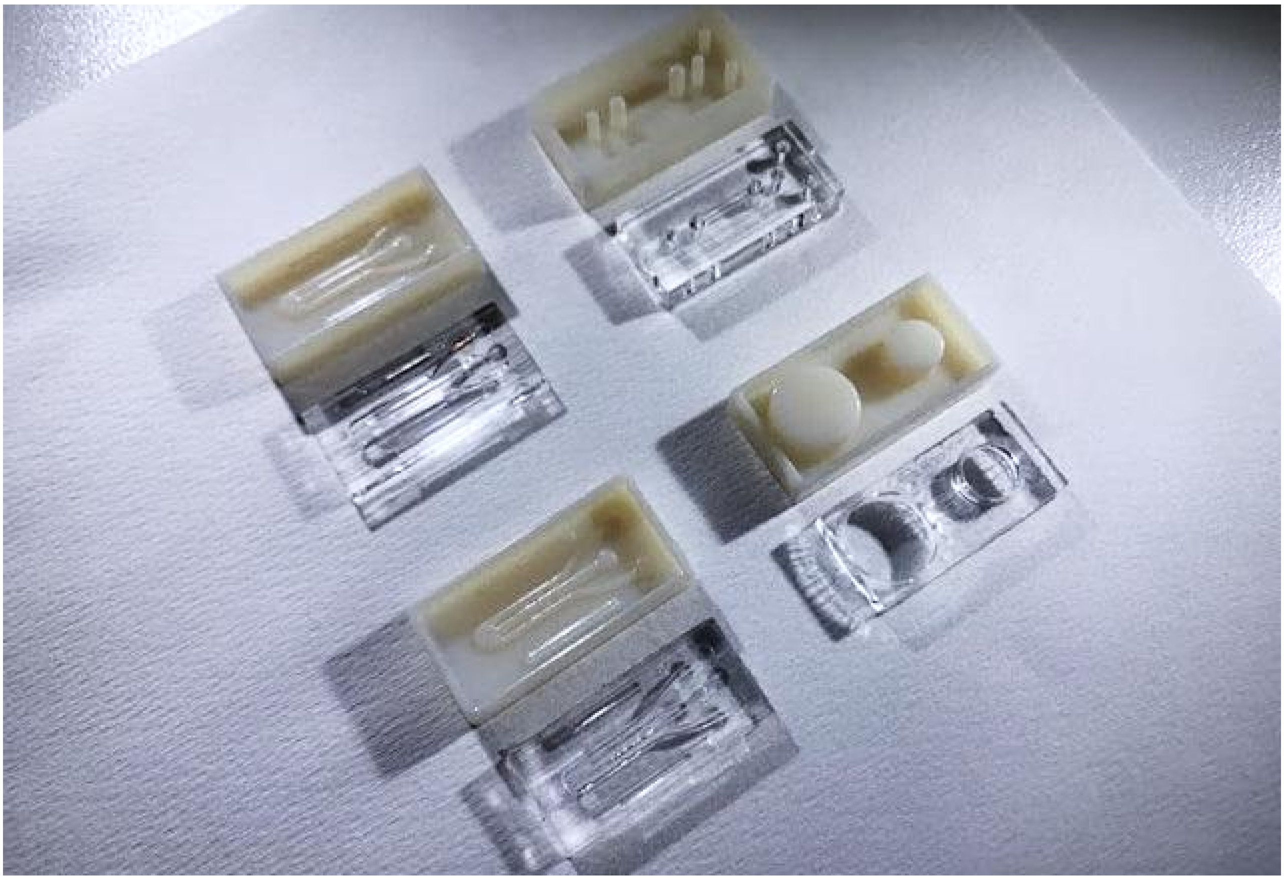

Figure 3.2.2 Molds and replicas of bottom, top and reservoir layers. Molds produced by 3d printing.

Replica molding offers several advantages in microfabrication and microfluidics. It is a cost-effective and efficient technique that enables the production of multiple replicas from a single master, allowing for scalability and mass production. It also allows for the replication of complex and high-resolution patterns with excellent fidelity.

3.2.2 SU-8 photolithography and mask realization

In this work, to produce the mold of bottom layer SU-8 photolithography technique has been used. This technique is divided into two phases, the first phase consists in the mask fabrication and the second is the real production of mold in SU-8. The entire process was done in a ISO clean room under yellow light illumination (Figure 3.2.3) and the optimized protocol developed by Matilde Aronne was followed (42).

Mask realization

In this work, the mask for photolithographic techniques was created using a direct laser writing technique. The LaserWriter used was MICROTECH LASERWRITER LW405 A71 (figure 3.2.3), which utilizes a GaN laser beam at 405nm to pattern a planar geometry on surfaces covered by photoresist.

This low-cost technique offers high performance and excellent resolution, capable of achieving patterns as small as 0.7μm (46).

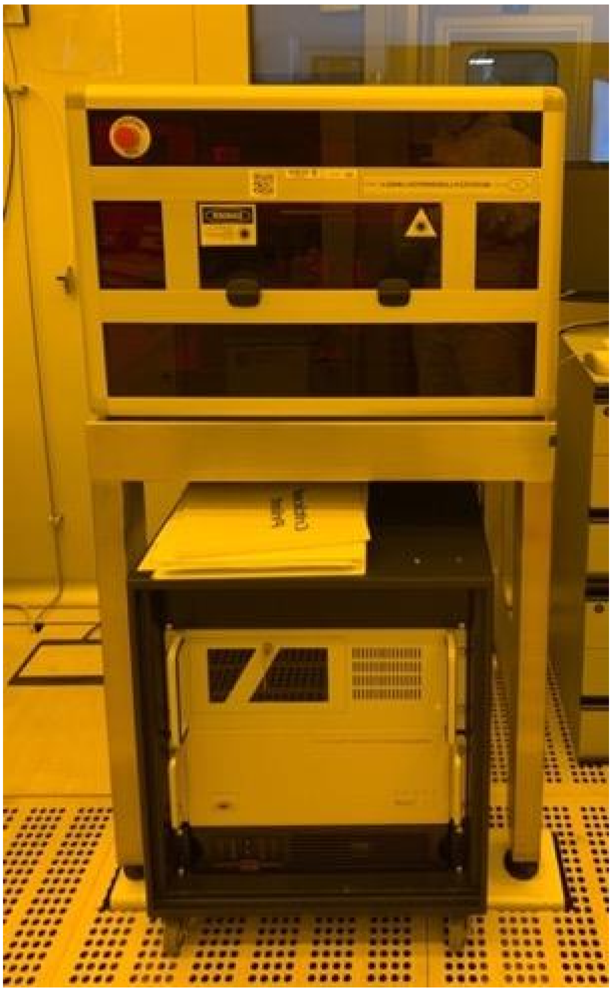

Figure 3.2.3 MICROTECH LASERWRITER LW405 A71 at Chilab.

The LaserWriter consists of several sections (42):

- The *write unit*, housing the GaN laser, substrate microtranslation system, laser interferometer, and electro-optical components. It enables beam adjustment through specific optics for precise pattern writing.
- The *cabinet*, providing protection from clean room air flow to prevent vibrations that may affect the laser beam.

- The *control unit*, responsible for managing the laser beam via various interconnections.

For this study, the mask was created using a chromium/glass support (Cr/SiO2) and patterned using the LaserWriter, following the .CIF CAD design shown in figure 3.2.4 (converted from Rhinoceros CAD using CleWin). The writing process takes approximately 1 hour, after which the mask undergoes development and etching.

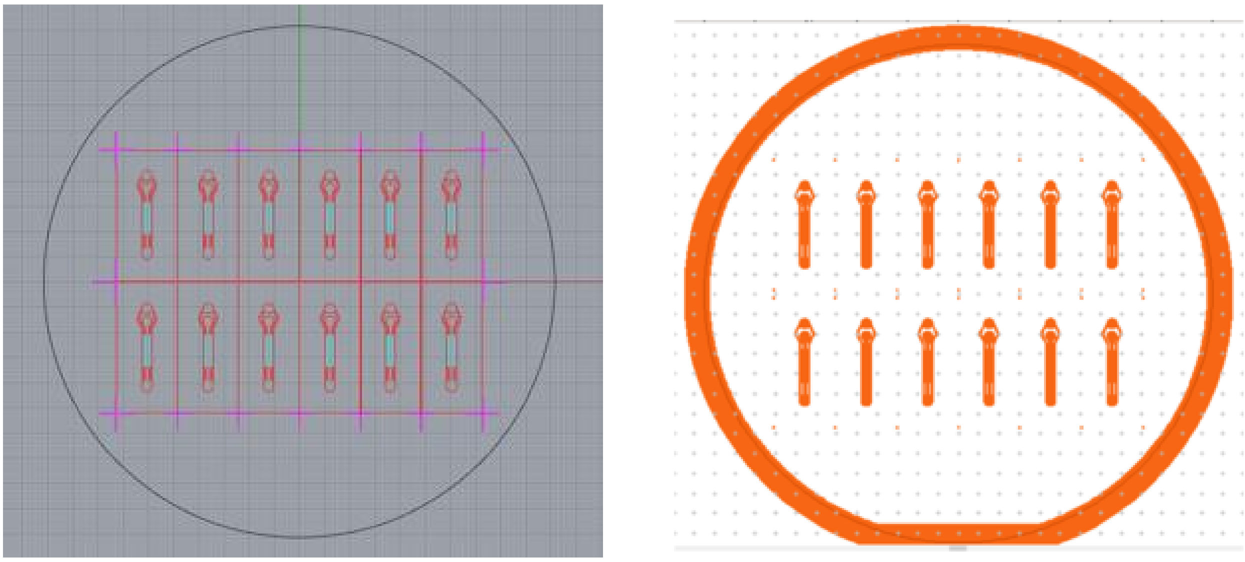

Figure 3.2.4 Mask CAD realized in Rhinoceros (left) and in Clewin (right).

The mask development/etching process involves the following steps (42):

- Mask dipping into a solution of water and AZ 400k Developer by Merck (in a 3:1 ratio) to remove excess resist. The mask is then rinsed in deionized water (DI) and dried with hyperpure nitrogen (figure 3.2.4).

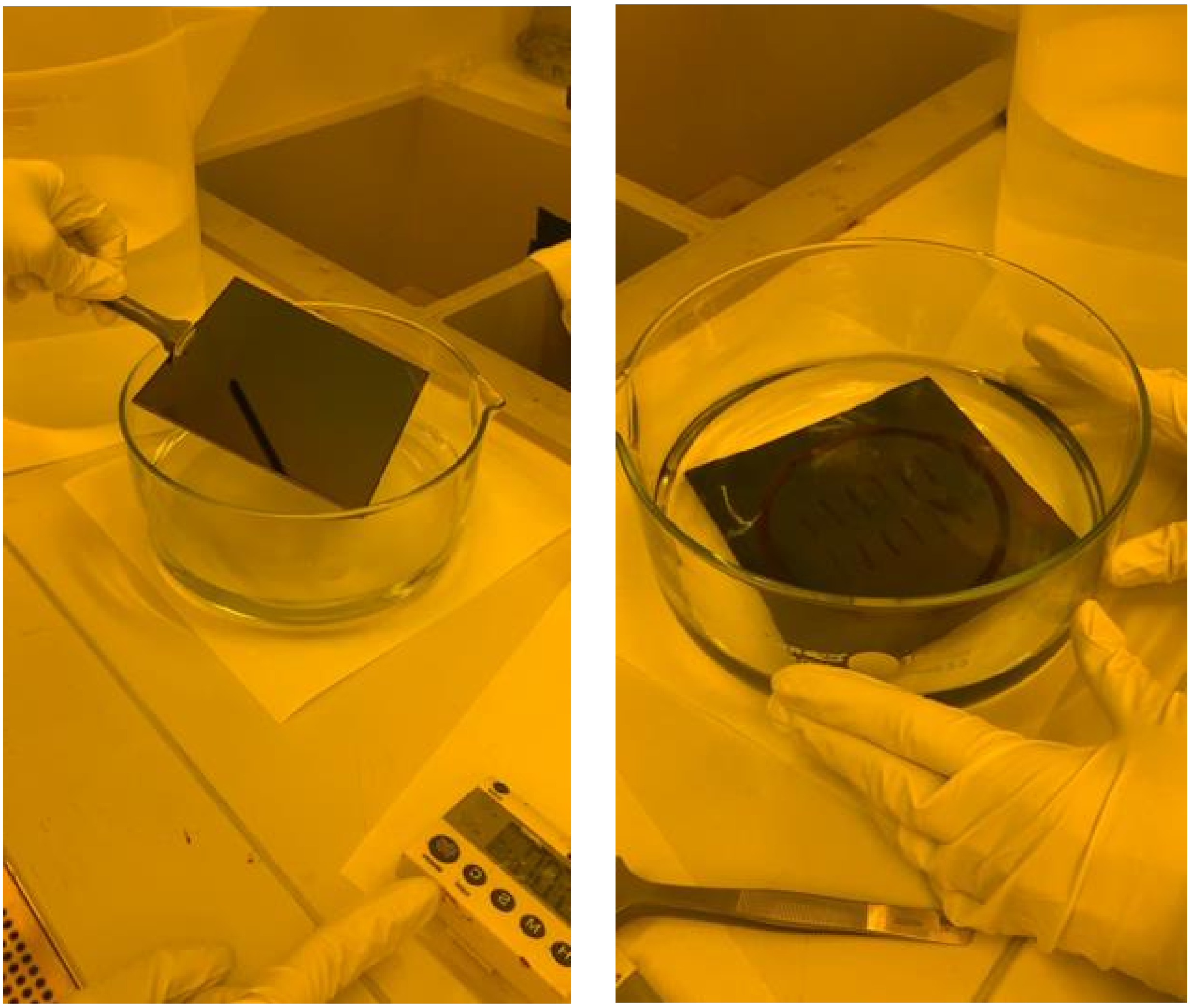

Figure 3.2.4 Before and after developing the mask.

- Chromium etching to remove the exposed chromium layer where the resist was previously removed. The mask is immersed in chromium etchant (Chrome ETCH Nº1, SIGMA-ALDRICH®) until the pattern becomes clearly visible. It is then rinsed with acetone and isopropyl alcohol (IPA), washed in DI, and dried with nitrogen (figure 3.2.5).

- Mask cleaning involves dipping the mask into a pirañha solution for 30 minutes to ensure its cleanliness before use. The solution is composed of 3 parts sulfuric acid (99%) and 1 part hydrogen peroxide (30%). Afterward, the mask is washed in DI and dried with nitrogen (figure 3.2.6).

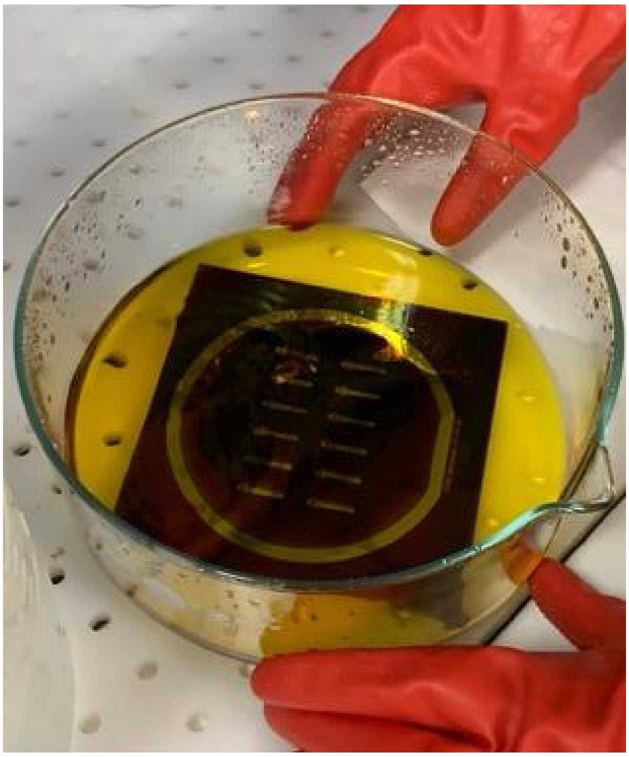

Figure 3.2.5 Chromium etching phase.

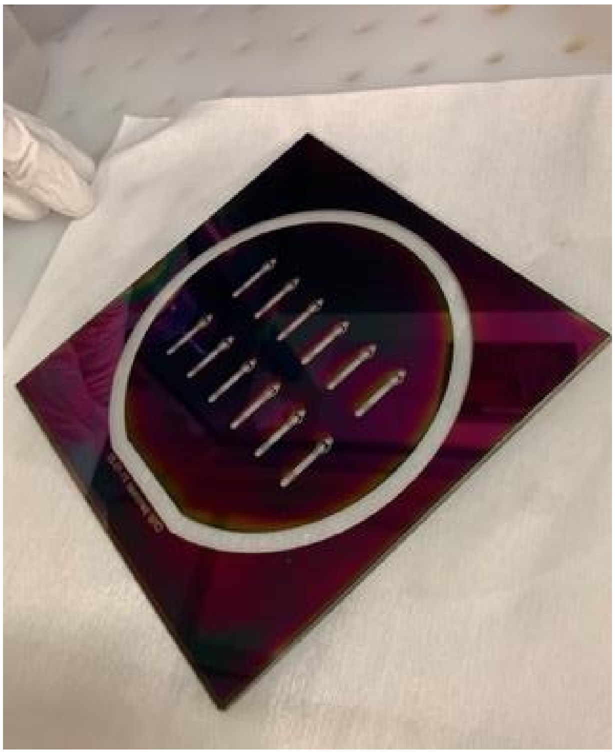

Figure 3.2.6 After cleaning the mask.

SU-8 lithography

The SU-8 photoresist is a negative epoxy-based resist widely used for microfabrication of high aspect-ratio microcomponents in MEMS. Its properties include high sensitivity, resolution, low optical absorption, thermal stability, and chemical resistance, making it suitable for various applications such as microstructure supports, molding, and packaging. However, the specific characteristics of SU-8 depend on processing conditions, such as curing time, temperature, and irradiation dose, which affect the degree of crosslinking and subsequently the physico-chemical properties of the polymer (47). It consists of acid-labile groups and a photoacid generator. Upon irradiation, a strong acid catalyst is generated, which initiates the cross-linking process. Subsequent heating activates cross-linking and regenerates the acid catalyst, significantly increasing the resist's sensitivity. The main components of SU-8 include a Bisphenol A Novolak epoxy oligomer (EPONR SU-8 resin, Shell Chemical, figure 3.2.7) and a photoacid generator (CYRACURER UVI, Union Carbide) that decomposes to form hexafluoroantimonic acid.

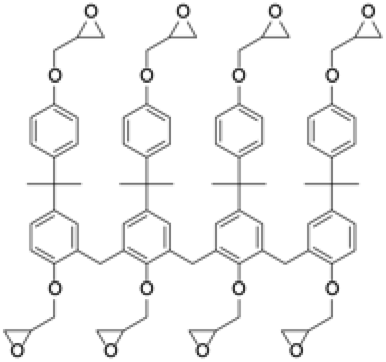

Figure 3.2.7 Chemical structure of the Bisphenol A Novolak epoxy oligomer contained in SU-8 formulations (48).

The acid protonates the epoxides in the oligomer, allowing them to react with neutral epoxides in a series of cross-linking reactions upon application of heat. With each monomer molecule containing eight reactive epoxy sites, a high degree of cross-linking is achieved upon photothermal activation. This leads to lithographic structures with high mechanical and thermal stability after processing (48). In this project, the photolithographic process involved the use of SU-2150 and SU-2100 photoresist by MicroCHEM to create a mold. These two materials have different properties (figure 3.2.8), so different settings will be used during the coating phase. SU-2150 was used to recreate the initial model of Beatrice Minervini's device, while SU-2100 was used to fabricate the modified device as previously described, which featured pillars and slots.

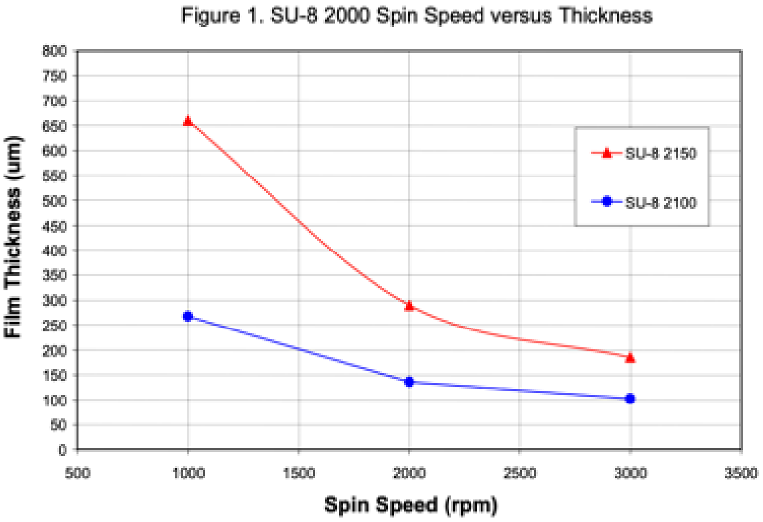

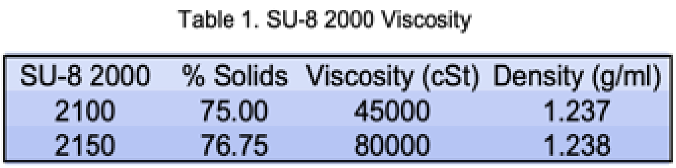

Table 1. SU-8 2000 Viscosity

SU-8 2000	% Solids	Viscosity (cSt)	Density (g/ml)
2100	75.00	45000	1.237
2150	76.75	80000	1.238

Figure 3.2.8 Properties of SU-2150 and SU-2100 (49).

The manufacturing process for the bottom layer mold involved several steps:

1. Substrate pre-treatment: A silicon/silicon oxide wafer was prepared before the process. To promote the adhesion of SU-8, the wafer underwent a heating treatment at 200°C for 15 minutes, followed by O2 plasma treatment. Adhesion promoters such as Omnicoat can also be used during this phase.

2. Coat: A photoresist layer was deposited on the prepared surface using a spin coater (figure 3.2.9). The wafer was centered on the spin coater support, and SU-8 2150 was dispensed at the center. The spin coating process consisted of two steps: first, spinning at 500 rpm for 10 seconds to facilitate SU-8 spreading, and then spinning at 2000 rpm for 60 seconds for the SU-2150 to achieve the desired layer thickness, whereas using the SU-1000 the first phase was reduced to 300 rpm in order to create a uniform coating without air inclusion, and at 2000 rpm for 60 seconds in the second phase,

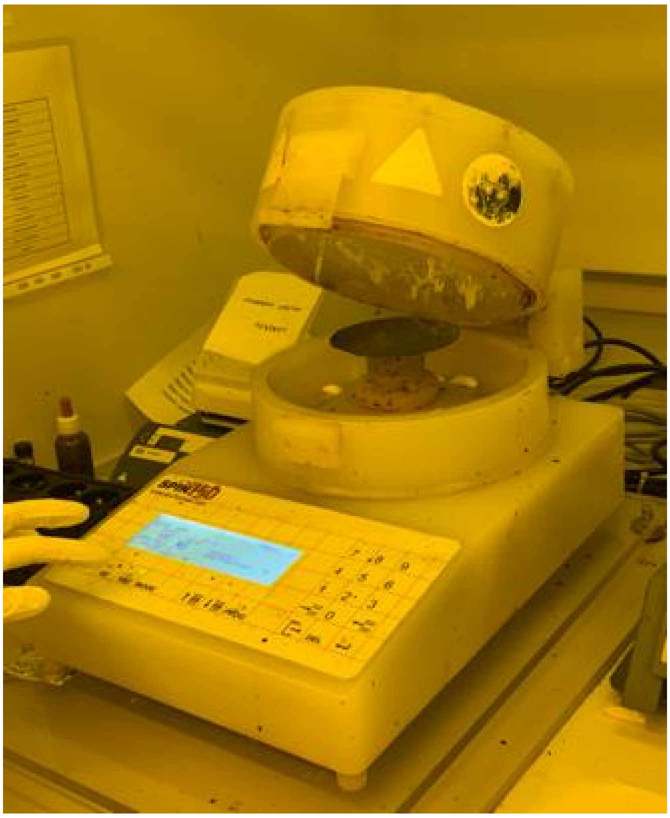

Figure 3.2.9 Spin coater with wafer placed.

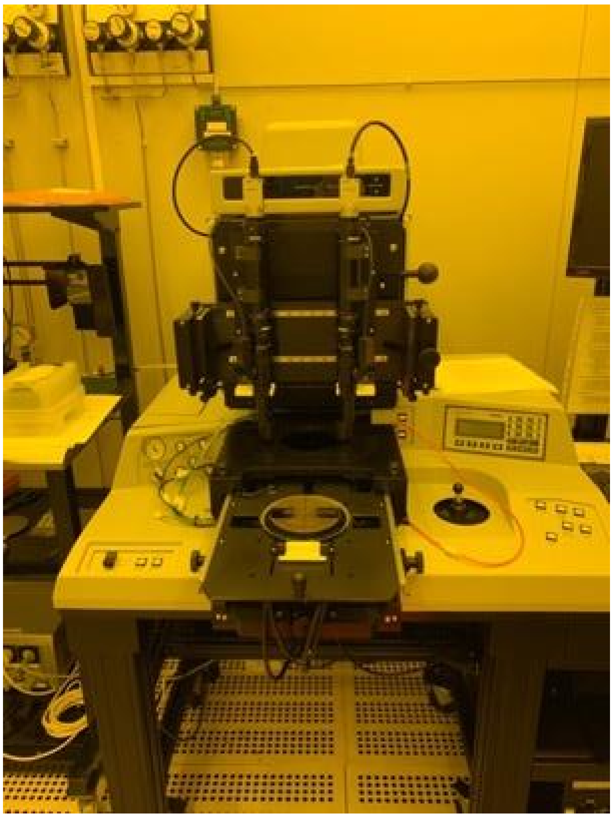

Figure 3.2.10 Mask-aligner at Chilab.

3. Edge bead removal (EBR): In this work, the EBR step was skipped since the wafer edges did not play a role in the process. Typically, 2-Propanol Alcohol (IPA) is used to remove the excess SU-8 from the edges.

4. Soft bake: This step involved a two-temperature protocol to allow solvent evaporation and solidification of SU-8. The coated wafer was first kept at 65°C for 8 minutes, followed by ramping to 95°C and maintaining this temperature for 40 minutes. Soft bake variations can affect the resist layer thickness before UV exposure.

5. Exposure: A UV lamp was used to expose the photoresist, inducing cross-linking in the exposed regions of SU-8. A mask was positioned above the

coated substrate to select the areas to be irradiated. Exposure was performed using a mask aligner (figure 3.2.10) with a filter to remove radiation under 365nm. The exposure time was set to 50 seconds to ensure sufficient energy absorption by SU-8.

6. Post-exposure bake (PEB): The purpose of this step was to provide additional energy to complete the cross-linking process in the exposed photoresist. To control mechanical stress, temperature increase and decrease were carefully managed. The exposed wafer was heated at 65°C for 5 minutes, ramped to 95°C, and kept at this temperature for 20 minutes. Wafer cooling was performed gradually on a hot plate up to 25°C (figure 3.2.11).

***Figure 3.2.11 Post-exposure bake** before the development*

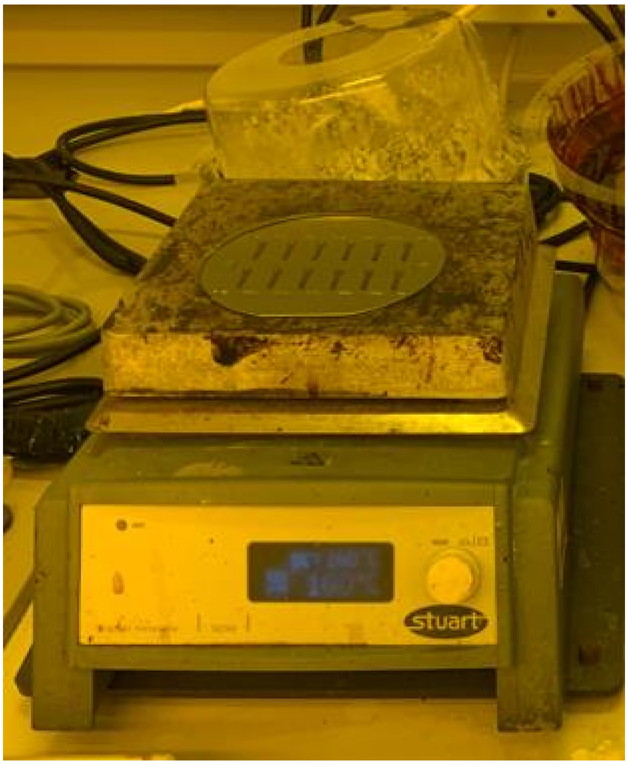

***Figure 3.2.12 Hard bake** after the development*

7. Development: The developed wafer underwent the development process using a SU-8 developer, which diluted the non-cross-linked photoresist, revealing the desired pattern on the wafer. The coated wafer was submerged in the developer and stirred for approximately 20 minutes. It was then rinsed with fresh developer and rinsed with IPA. Finally, the wafer was dried with nitrogen.

8. Hard bake: To eliminate residual mechanical stresses within the SU-8 photoresist, a hard bake step was performed. The developed wafer was heated at 150°C for 5 minutes and then cooled to 25°C on the hot plate (figure 3.2.12).

Prior to using the mold for replica molding, a silanization process was performed on the wafer to create a passivation layer. This layer allowed for easy peeling of PDMS and prevented adhesion to the master. The procedure involved the following steps:

1. Solution preparation: Toluene and trichloromethylsilane were mixed in a Petri dish in a ratio of 1:10. (figure 3.2.13)

2. Rest: The wafer was immersed in the solution and left submerged for 3 hours.

3. Washing and baking: The wafer was washed with IPA and dried with nitrogen (figure 3.2.14). Subsequently, it was baked at 160°C for 15 minutes.

Figure 3.2.13 Toluene and trichloromethylsilane.

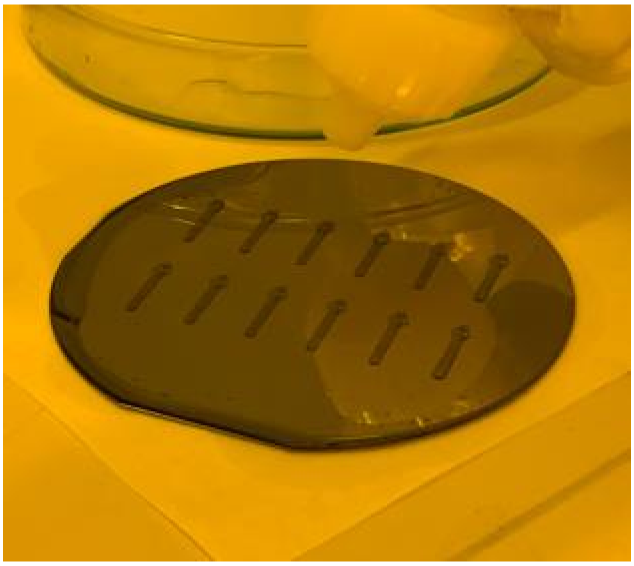

Figure 3.2.14 Drying with nitrogen.

3.2.3 3D printing

As explained before, at the end of the work, all the layers were obtained using the replica molding technique, with the molds being created through 3D printing. In this thesis work, the 3D printer used was the polyjet OBJET30 Stratasys, which utilizes a liquid UV photopolymer resin called VeroWhite® (Stratasys, as shown in figure 3.2.15).

Figure 3.2.15 Polyjet OBJET30 Stratasysw (50).

Before initiating the printing process, the exported .stl file is loaded into the 3D printer computer using the Objet Studio software. This software also allows for the orientation of the elements within the printer's tray. Once everything is set up, the printing process begins. The resin is deposited layer by layer by the inkjet head, and each layer is polymerized using a UV lamp. The printer's tray then moves down along the Z-axis to continue with the deposition of subsequent layers. In addition to the photopolymeric resin, the printer can also deposit a sacrificial supporting material known as SUP705 (42).

The printing process takes less than one hour. Afterward, the molds can be extracted and need to be washed with water and dried with air before undergoing the curing phase. During the curing phase, the molds are placed in an oven overnight at 150°C. This step is crucial to ensure the complete curing of the photoinitiator in the resin, thus avoiding any interference with the subsequent PDMS polymerization process.

At the end of the process, the molds are re-washed in acetone using an ultrasonic bath with the following parameters: 5 minutes duration, 59kHz frequency, 20°C temperature, and 100% power.

3.2.4 Plasma-oxygen treatment

Plasma is an ionized state of matter consisting of ions and electrons. It is formed when a gas is energized, causing electrons to break free from the atoms' nuclei and creating a mixture of charged particles. Plasma can be described as a partially ionized gas, containing neutral atoms, atomic ions, electrons, molecular ions, and excited or ground-state molecules.

The presence of charged particles in plasma gives it high electrical conductivity. It carries internal energy due to the presence of electrons, molecules, ions, and excited gas particles. When plasma interacts with a surface, plasma treatment occurs (51). The specific effects of plasma treatment on a surface can be controlled by selecting the gas mixture, pressure, power, and other parameters, allowing for precise tuning of the treatment process.

After creating a pattern on a PDMS substrate using replica molding, the PDMS undergoes oxidation in air or oxygen plasma. This process involves the removal of organic and hydrocarbon materials through chemical reactions with reactive oxygen radicals and ablation by energetic oxygen ions. As a result, silanol (SiOH) groups are formed on the surface, increasing its hydrophilicity and improving surface wettability (52). Once the PDMS is activated by plasma treatment, it is immediately brought into contact with another oxidized PDMS or glass surface, this process is also called *"Bonding"*. At the interface, a bridging Si-O-Si bond is formed, creating a strong and irreversible seal. This covalent bond ensures that the interface is watertight, making it well-suited for the formation and functioning of microchannels (figure 3.2.16).

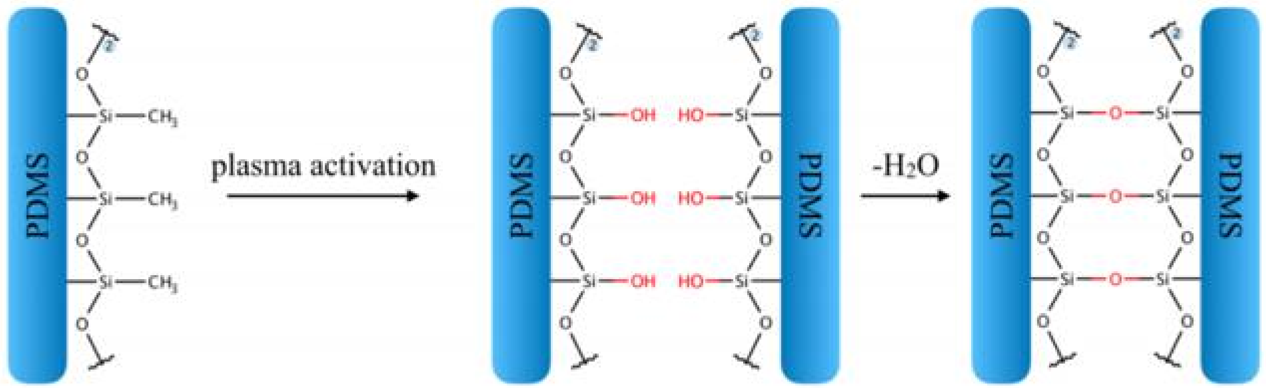

Figure 3.2.16 PDMS-PDMS bonding (53)

For this thesis work, the Electronic Diener Plasma-Surface-Technology (shown in figure 3.2.17) was utilized. The plasma treatment parameters are listed in table 1 (42).

Parameters	
Pumping down pressure	0.3mbar
Gas supply period	1min
O2 flow	100%
Plasma process duration	0.30s
Plasma power	22%
Venting time	1min

Table 1 Parameters used during plasma oxygen treatment (42).

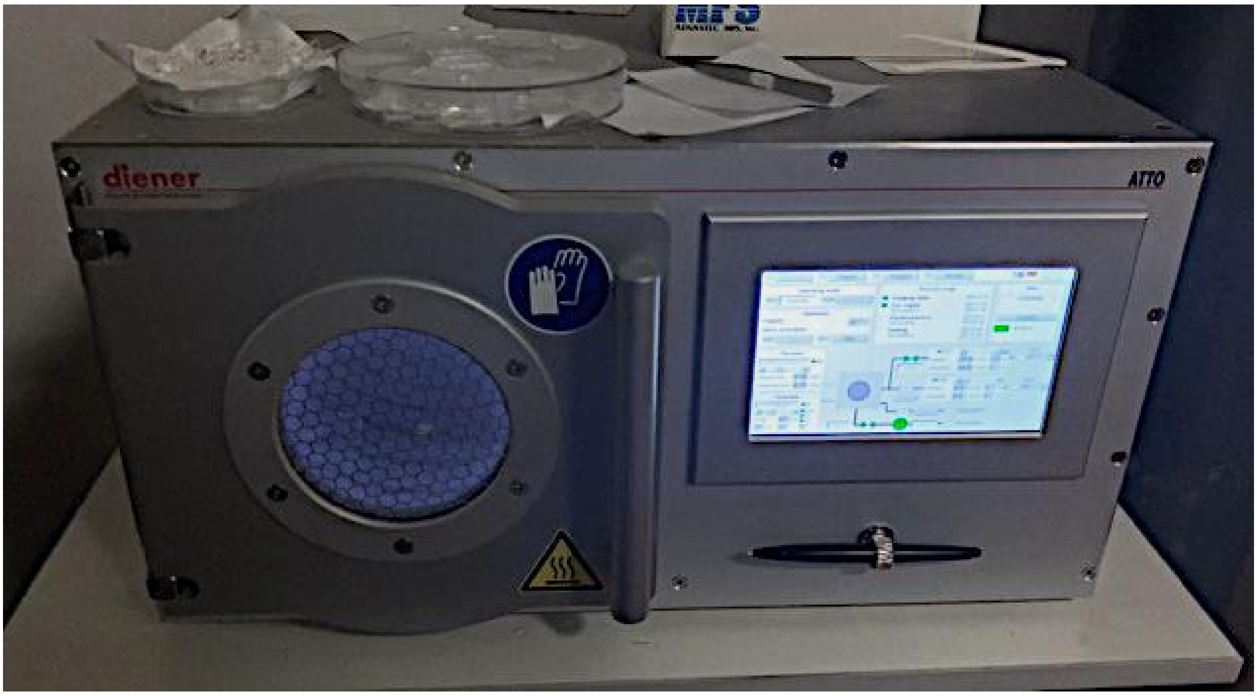

Figure 3.2.17 Electronic Diener Plasma-Surface-Technology at Chilab.

Prior to plasma treatment, PDMS replicas were cleaned in ethanol using an ultrasonic bath. Subsequently, they were dried on a hot plate at 100°C for 5 minutes. After the plasma treatment, a thermal treatment was conducted on the bonded layers. The layers were subjected to a hot plate at 80°C for 60 seconds to enhance the bonding process (52).

3.2.5 Insertion of the membrane

The membrane is cut to size from the electrospun foil sheet, with dimensions of approximately 1x1.5 cm. PDMS is inserted into the two cavities on the sides of the device (figure 3.2.18).

Figure 3.2.18 Electronic Diener Plasma-Surface-Technology at Chilab.

Figure 3.2.19 Device with membrane.

Subsequently, it is placed on a hot plate to cure the PDMS at a temperature of 100ºC for 2-3 minutes. It is removed from the hot plate before it completely crosslinks, leaving it sticky to facilitate the adhesion of the membrane without wetting it (figure 3.2.19).

3.2.6 Electrospinning

Electrospinning is an electrohydrodynamic process used to generate fibers by stretching and elongating a liquid droplet. The basic setup for electrospinning consists of a high-voltage power supply, a syringe pump, a spinneret (typically a blunt-tipped hypodermic needle), and a conductive collector (figure 3.2.20) (54).

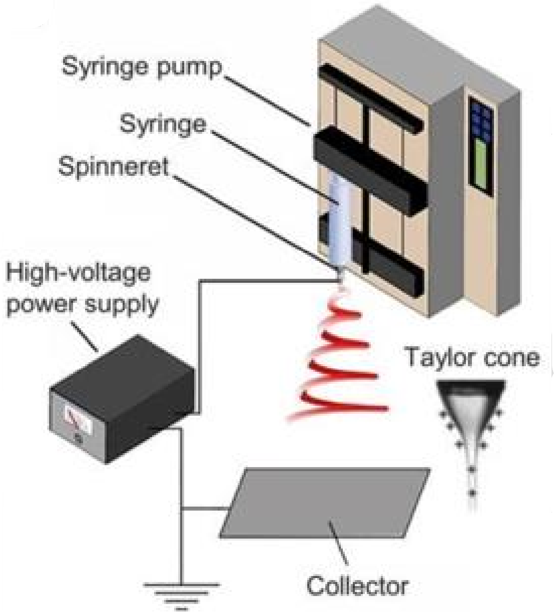

Figure 3.2.20 Setup for electrospinning (54).

The power supply can be either direct current (DC) or alternating current (AC). Initially, the liquid is extruded from the spinneret, forming a pendant droplet due to surface tension. When electrified, the electrostatic repulsion among the like-charged surface charges deforms the droplet into a cone-shaped structure called a Taylor cone, from which a charged jet is emitted. The jet undergoes whipping motions due to bending instabilities as it stretches and solidifies into finer diameters. The solidified jet deposits as solid fiber(s) onto the grounded collector. The electrospinning process can be divided into four main steps:

- charging of the liquid droplet and formation of the Taylor cone or cone-shaped jet,
- extension of the charged jet in a straight line,
- thinning of the jet accompanied by electrical bending instability (whipping instability),
- solidification and collection of the jet as solid fiber(s) on the grounded collector. Further details on these steps are discussed in subsequent subsections.

Figure 3.2.21 Electrospinning process.

PCL/gel	parameters
Voltage (kV)	+ 16/-4
Z distance (mm)	160
Flow rate (µl/h)	500
Volume (ml)	5
Stroke (mm)	measured

Table 2 Electrospinning parameters.

A solution of PCL/gelatin was electrospun to obtain the membrane and the spun fibers were collected on a foil sheet, as shown in Figure 3.2.21. The selected electrospinning parameters for membrane fabrication are summarized in Table 2. The electrospinner used for this work is depicted in figure 3.2.7 and is referred to as the NovaSpider instrument.

3.2.7 Confocal microscopy

The confocal microscope utilizes fluorescence optics, similar to the widefield microscope, but instead of illuminating the entire sample simultaneously, the confocal microscope focuses laser light onto a specific spot at a particular depth within the sample. This precise focusing results in the emission of fluorescent light exclusively at that specific point. To eliminate out-of-focus signals, a pinhole positioned within the optical pathway restricts the entry of such signals, allowing only the fluorescence signals from the illuminated spot to reach the light detector (55).

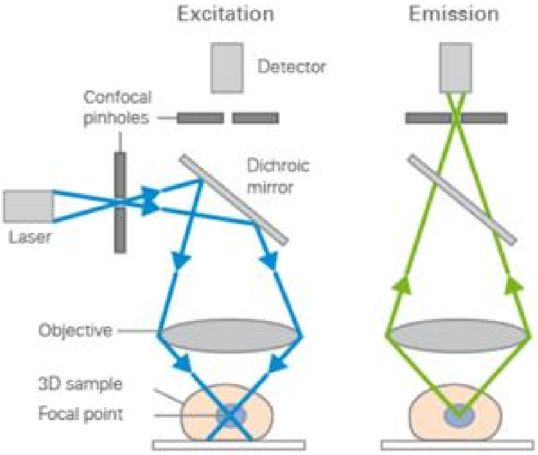

Figure 3.2.22 Excitation and emission light pathways (55).

To generate images of a single optical plane, the specimen is scanned in a raster pattern. By scanning multiple optical planes and stacking them together using advanced microscopy deconvolution software (z-stack), three-dimensional objects can be visualized. Additionally, modern confocal microscopes equipped with multiple lasers and emission/excitation filters enable the analysis of multicolor immunofluorescence stainings (55). The microscope used for biological characterization is the Nikon Eclipse Ti2 at Politecnico di Torino (figure 3.2.23).

Figure 3.2.23 Nikon Eclipse Ti2 at Politecnico di Torino.

3.3 Device materials

3.3.1 PDMS

In this thesis work, PDMS was used to produce the layers of the microfluidic device. Polydimethylsiloxane (PDMS) is a widely used silicone elastomer in various fields, including microfluidics, bioengineering, and soft robotics. PDMS possesses unique properties that make it an ideal material for these applications (Table 3).

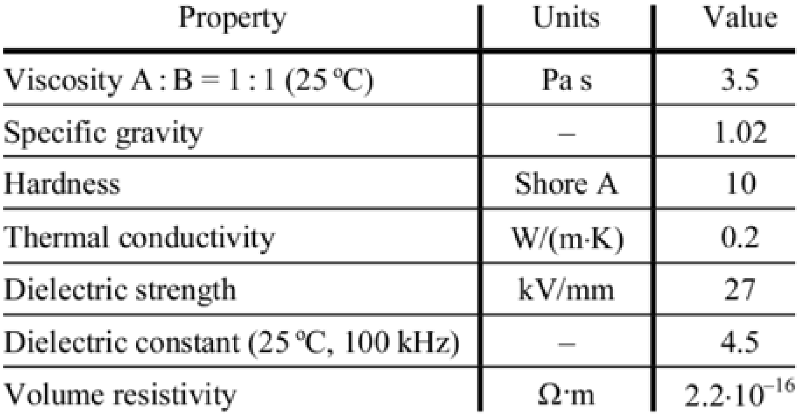

Property	Units	Value
Viscosity A : B = 1 : 1 (25 °C)	Pa s	3.5
Specific gravity	–	1.02
Hardness	Shore A	10
Thermal conductivity	W/(m·K)	0.2
Dielectric strength	kV/mm	27
Dielectric constant (25 °C, 100 kHz)	–	4.5
Volume resistivity	Ω·m	$2.2\cdot10^{-16}$

Table 3 PDMS properties (56)

PDMS is a transparent, flexible, and biocompatible material. It exhibits excellent optical transparency, allowing for easy visualization of samples and cells under a microscope. Its flexibility enables the fabrication of intricate structures and devices, making it suitable for creating microfluidic channels and flexible membranes.

One of the key advantages of PDMS is its permeability to gases, including oxygen and carbon dioxide. This property is crucial in biological applications as it allows for the exchange of gases, supporting cell culture and maintaining physiological conditions within microfluidic systems.

PDMS is also known for its ease of use in fabrication processes. It can be molded or cast into various shapes and sizes, making it highly versatile. Its low surface energy prevents the adhesion of proteins and cells, reducing the risk of unwanted interactions and enabling precise control over the flow of fluids. Polydimethylsiloxane (PDMS) can be chemically functionalized to modify its surface properties and enhance its compatibility with specific applications. Functionalization of PDMS involves introducing various chemical groups or coatings onto the surface of the material (57).

One common method of PDMS functionalization is plasma treatment. Plasma treatment exposes the PDMS surface to a highly reactive plasma, which leads to the formation of new chemical groups on the surface. This process can increase the surface energy of PDMS, making it more hydrophilic and improving its wettability. Plasma treatment can also introduce functional groups, such as carboxylic acids or amino groups, onto the PDMS surface, enabling further modifications or covalent bonding with other molecules. This technique, in particular oxygen-plasma treatment, has been used to realize the interface bonding between layers (52). Other methods of PDMS functionalization include chemical vapor deposition (CVD), where a thin layer of desired material is deposited onto the PDMS surface, and surface grafting, where specific molecules are attached to the PDMS surface through covalent bonds (58).

Functionalization of PDMS allows for a wide range of applications. It can be used to improve cell adhesion and promote cell growth in tissue engineering, enhance protein immobilization and biosensing capabilities in microfluidic devices, and create specific surface properties for drug delivery systems or surface patterning (59).

To achieve a thoroughly crosslinked solid structure (figure 3.3.1), a PDMS solution for replica molding was prepared by combining a polymeric base and a curing agent from the SYLGARDTM 184 Silicone Elastomer kit (figure3.3.2) in a volumetric ratio of 10:1. The solution was mixed vigorously by hand, and any trapped air bubbles were subsequently removed using a vacuum pump (figure 3.3.3).

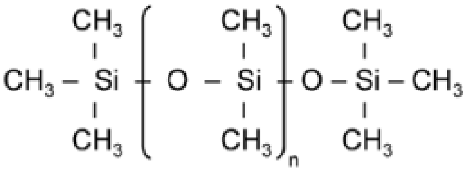

$$CH_3-\underset{CH_3}{\overset{CH_3}{Si}}-\left[O-\underset{CH_3}{\overset{CH_3}{Si}}\right]_n-O-\underset{CH_3}{\overset{CH_3}{Si}}-CH_3$$

Figure 3.3.1 PDMS structure (60).

Figure 3.3.2 SYLGARDTM 184 Silicone Elastomer kit (61).

Figure 3.3.3 Vacuum pump with PDMS replicas.

3.3.2 Collagen

Collagen is a crucial component of the extracellular matrix and widely used in tissue engineering. It has diverse applications, including tissue substitutes, drug delivery systems, and wound dressings. Its biocompatibility and binding capacity make it suitable for multi-purpose bioscaffold designs. The collagen superfamily consists of 28 identified types, mainly classified into fibrillar and non-fibrillar subfamilies (62). Type I collagen, belonging to the fibrillar subfamily, is the most abundant, comprising about 80% of total collagen in the human dermis. Other types, such as IV, VI, and VII, have specific functions in basement membranes and anchoring structures. Collagen, with its diverse types and structures, plays a crucial role in tissue engineering. The molecular structure of collagen consists of triple helices formed by three polypeptide α-chains. These helices can be homotrimers or heterotrimers, depending on the collagen type. Collagen type I, the most abundant in human dermis, is a heterotrimer composed of two alpha-1 (α1) chains and one alpha-2 (α2) chain (figure 3.3.4). Collagen triple helices assemble into microfibrils, which further form fibrils of different diameters in tissues. The arrangement of collagen fibrils contributes to the specific properties and functions of various tissues. For example, in the skin, collagen forms a complex network, while in bone, it combines with hydroxyapatite crystals in an ordered composite. Tendons have parallel bundles of large-diameter collagen fibrils, while the cornea contains smaller-diameter fibrils arranged orthogonally for transparency. Cartilage exhibits zonal architecture with collagen fibres packed differently in each zone. Collagen type I has been extensively studied due to its repetitive structure, self-assembly properties, and relevance to tissue regeneration. Collagens have a distinct molecular structure characterized by a repeated proline-rich amino acid sequence and a glycine (Gly) residue every third position, forming a triple helix (62).

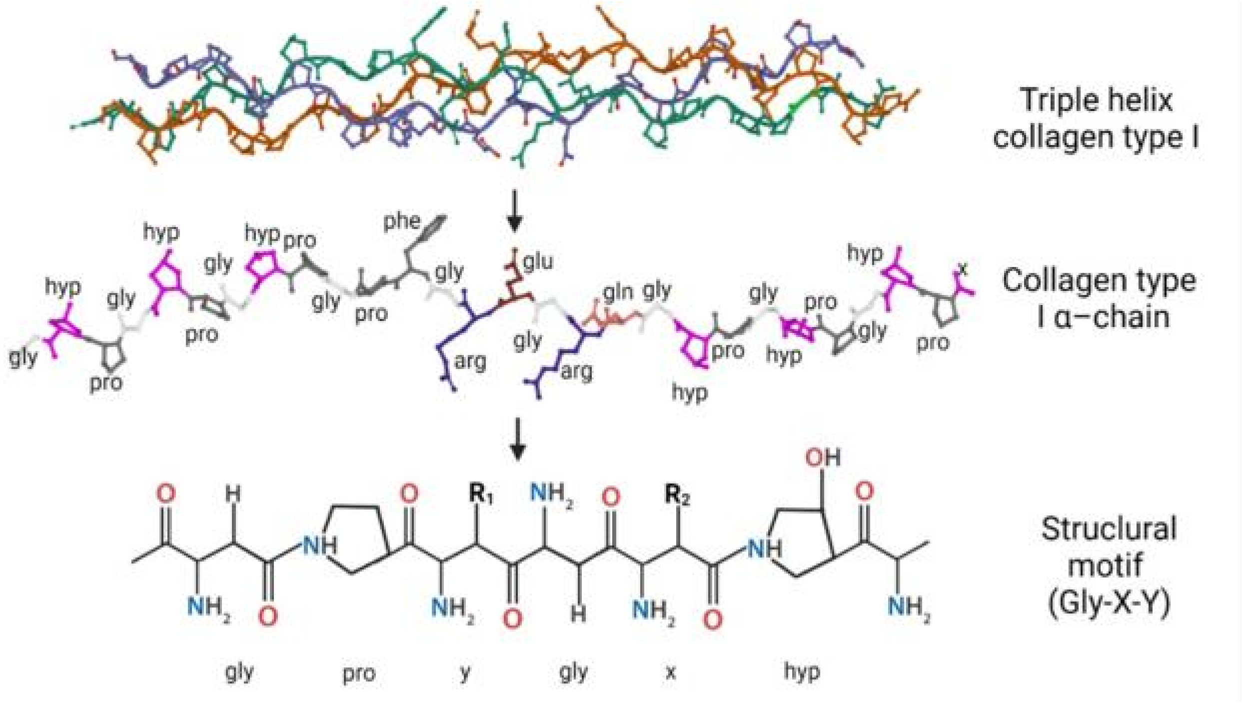

Figure 3.3.4 Collagen structure (62).

The Gly-X-Y motif, with X and Y commonly being proline and 4-hydroxyproline, is essential for collagen's gelling function. The triple helix structure varies in length among collagen types, with approximately 300 nm corresponding to 1000 amino acids. Gly residues form the central axis, while X and Y residues are positioned on the helix's surface for binding interactions crucial in fibril formation. Despite variations in amino acid composition between collagen types, hydroxyproline, glycine, and proline are prevalent in all collagens (62). Different collagen sources exhibit variations in amino acid content, which can impact chemical and physical properties relevant to tissue engineering applications. Understanding the amino acid sequences and their role in collagen assembly is essential for developing suitable biomaterials for tissue engineering.

In this thesis, a hydrogel solution was created using Advanced BioMatrix Fibricol®, a type I collagen solution (figure 3.3.5). The proprieties are snown in the table 4. Fibricol® contains 97% type I collagen and 3% type III collagen, with a collagen concentration of 10mg/mL.

Figure 3.3.5 Collagen solution (63).

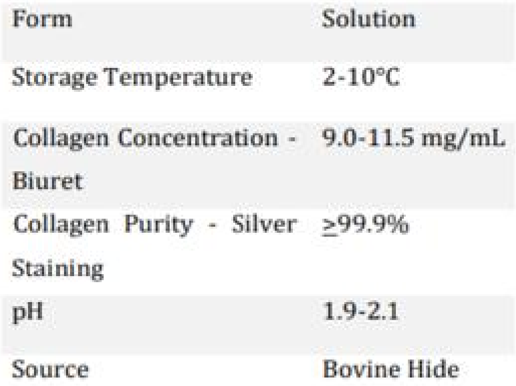

Form	Solution
Storage Temperature	2-10°C
Collagen Concentration - Biuret	9.0-11.5 mg/mL
Collagen Purity - Silver Staining	≥99.9%
pH	1.9-2.1
Source	Bovine Hide

Table 4 Collagen properties (42).

The hydrogel solution was prepared by mixing 1 part of PBS 10X and 8 parts of collagen at low temperature. The mixture was stirred at 230 rpm for a few minutes to ensure homogeneity. The pH of the solution was monitored using pH paper and sterile 0.1M NaOH was added if the pH was too low, followed by additional stirring. An optimal pH is around 7.5/8. Finally, 1 part of sterile distilled water was added. The entire process was carried out in an ice-filled beaker on a stirrer to maintain a low temperature and prevent the gelation of the solution.

3.3.3 PCL

PCL (polycaprolactone) is an aliphatic polyester belonging to the poly-α-hydroxy acid group, along with polylactic and polyglycolic acids. It is a biocompatible, biodegradable, and bioresorbable polymer. It consists of a chain of repeated ε-caprolactone units $(C6H10O2)n$, with the length of the chain (n) determining its degradation time and persistence.

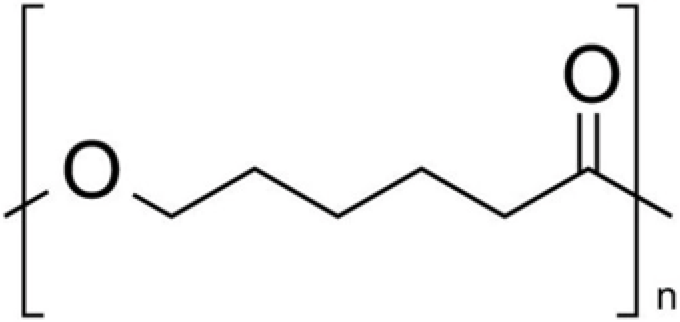

Figure 3.3.6 PCL structure (64).

PCL is a hydrophobic, semi-crystalline polymer with a low glass transition temperature of -60°C and a melting point ranging from 59° to 64°C. It has favorable viscoelastic properties, making it easy to manufacture and manipulate into various structures such as microspheres, fibers, films, and foams. PCL can also be blended with other polymers to create copolymers with different properties and degradation rates (65).

PCL (polycaprolactone) is both biodegradable and bioresorbable. In vitro and in vivo tests conducted according to ISO 10993 standards have demonstrated the safety of PCL when in contact with human tissues and fluids. The biodegradation of PCL occurs through hydrolysis of its ester bonds. This degradation process involves two phases. In the first phase, water penetrates the polymer, causing chain scission. This phase follows a controlled and predictable first-order linear pattern, with the length of the polymer chain decreasing over time. The rate of chain scission is determined by factors such as water permeability and polymer length. In the second phase, which occurs when the polymer is more crystalline, the shorter polymer chains allow small fragments to diffuse through the matrix. Ultimately, the degradation end products, carbon dioxide (CO2) and water (H2O), are completely eliminated from the body (65).

3.3.4 Gelatin

Gelatin is a natural polymer derived from the hydrolytic degradation of collagen protein. It is commonly found in the form of tablets, granules, or powders and is used in various applications. Gelatin is widely studied as a matrix for three-dimensional cell culture and tissue-engineering scaffolds. It is also a high-protein component in nutritionally balanced foods and can serve as a fat and carbohydrate substitute. Collagen, the source protein of gelatin, is naturally abundant in the skin, bones, tendons, and ligaments of humans and animals. There are two main types of gelatin: type A, produced from acid-treated collagen, and type B, produced from alkaline-treated collagen (66). These types differ in their isoelectric points and crosslinking degrees (table 5). Gelatin exhibits amphoteric behavior due to its functional amino acid groups and terminal amino acids, making it versatile in various applications.

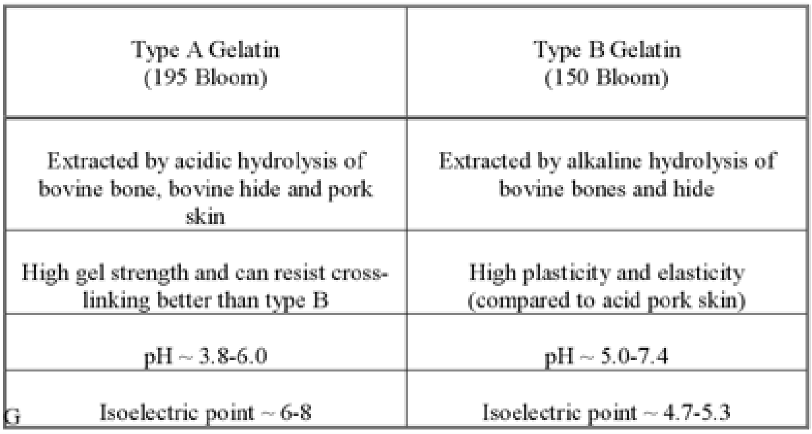

Type A Gelatin (195 Bloom)	Type B Gelatin (150 Bloom)
Extracted by acidic hydrolysis of bovine bone, bovine hide and pork skin	Extracted by alkaline hydrolysis of bovine bones and hide
High gel strength and can resist cross-linking better than type B	High plasticity and elasticity (compared to acid pork skin)
pH ~ 3.8-6.0	pH ~ 5.0-7.4
Isoelectric point ~ 6-8	Isoelectric point ~ 4.7-5.3

Table 5 Differences and properties of Type A and B gelatin (67).

Gelatin is a complex polymer composed of various amino acids, with glycine, proline, and hydroxyproline being the major components. It has a hydrophilic character and consists of different polypeptide chains. Gelatin undergoes a gelatinous state below a certain temperature range, but prolonged boiling leads to irreversible changes in its properties. The viscosity and gel strength of gelatin are influenced by factors such as molecular mass distribution, electrolyte concentration, pH, and temperature. Gelatin gels are thermally reversible and are held together by hydrogen-bonded junction zones. However, they are not stable at physiological temperatures, necessitating chemical or enzymatic crosslinking for stability. Gelatin is derived from the hydrolysis of collagen found in animal tissues, and appropriate pre-treatment is required to solubilize collagen and extract gelatin. Gelatin exhibits favorable physical properties such as jelly force, dispersibility, low viscosity, dispersion stability, and water retention. It is used as a food additive for coating, toughness, reversibility, thickening, foam formation, and emulsification purposes.

3.3.5 Membrane

The membrane was obtained by electrospinning a PCL/gelatin solution, following the protocol outlined below.

PCL and type A gelatin were combined in a weight ratio of 80:20 and dissolved in a mixture of acetic acid and formic acid (1:1 v/v) at a concentration of 15% w/v. The solution was stirred for 24 hours at room temperature to achieve a well-mixed consistency. To prevent gelatin degradation, a gelatin crosslinker called GPTMS was added at a concentration of 3.68% v/v. The solution was further stirred for 30 minutes to promote the formation of tangled chains and ensure a transparent solution. The membrane characterization has been previously carried out by the other thesis students and reaches a thickness of 100 micrometers (41) (42).

3.4 Cellular Components

3.4.1 Human Foreskin Fibroblasts cells

The Human Foreskin Fibroblast (HFF-1) cell line was utilized to simulate the PDAC stroma. These cells were suspended in a collagen hydrogel and seeded in the central channel of the bottom layer. As mentioned in the *"Introduction"* chapter, fibroblasts are a type of connective tissue cells that play a significant role in producing ECM components, making them valuable for studying the function of PDAC stroma.

HFF-1 have been purchased from the American type culture collection (ATCC), and they have been grown into DMEM 1X (Dulbecco's Modified Eagle Medium, Gibco, ThermoFisher scientific).

In this work, DMEM has been enriched with:

- 15% Fetal bovine serum (FBS, Gibco ThermoFisher scientific), used as a supplement for cell growth, it provides nutrients such as growth factors, proteins, vitamins, hormones and trace elements (68).
- 1% Penicillin/streptomycin (P/S, Gibco, ThermoFisher scientific), an antibiotic to avoid gram-positive/gram-negative contamination.
- 2% L-glutamine (Gibco, ThermoFisher scientific), an aminoacid.

3.4.2 Epithelial cell

HPDE

Human Pancreatic Duct Epithelial (HPDE) cells are immortalized cell lines, obtained from normal human pancreatic duct cells, that are used to recreate pancreatic epithelia. In this thesis, they have been seeded into top layer channel. The HPDE-used cells were purchased from the American type culture collection (ATCC). Two cell lines were used for this work. To mimic normal physiological conditions, the wild-type form, the HPDE-WT cells, which does not have gene mutations, was used, While, to recreate the pathological conditions of PDAC, cells from the HPDE-KRAS line that carry a mutation in the KRAS gene were used. These cells have been suspended in RPMI media, Roswell Park Memorial Institute (Gibco, ThermoFisher scientific), which contains glutathione and high concentrations of vitamins (biotin, vitamin B12). It has been supplemented with:

- 10%, fetal bovine serum (FBS, Gibco ThermoFisher scientific), used as a supplement for cell growth, it provides nutrients such as growth factors, proteins, vitamins, hormones and trace elements (68).
- 1%, Penicillin/streptomycin (P/S, Gibco, ThermoFisher scientific), an antibiotic to avoid gram-positive/gram-negative contamination.
- 1%, L-glutamine (Gibco, ThermoFisher scientific), an aminoacid.

show non-mutated gene (HPDE-WT) to mimic healthy microenvironment, and Human Pancreatic Duct Epithelial Cells with oncogene KRAS mutation (HPDE-KRAS) or MIA-PaCa-2 cells for the pathological condition.

MIA-PACA-2

Another cell line used to mimic the cancer condition is the MIA-PACA-2, an epithelial cell line that was derived from tumor tissue of the pancreas obtained from a 65-year-old (69). Unlike HPDE cells, these were cultured using DMEM as the culture medium. Additionally, it was supplemented with:

- 10%, fetal bovine serum (FBS, Gibco ThermoFisher scientific), used as a supplement for cell growth, it provides nutrients such as growth factors, proteins, vitamins, hormones and trace elements (68).
- 1%, Penicillin/streptomycin (P/S, Gibco, ThermoFisher scientific), an antibiotic to avoid gram-positive/gram-negative contamination.
- 2%, L-glutamine (Gibco, ThermoFisher scientific), an aminoacid.

3.4.3 Common Culture Medium

Once fibroblasts were seeded in the bottom layer and epithelial cells in the top layer, a common culture medium for both cell types was introduced through the two inlets of the side channels until the reservoirs were filled.

The culture medium consisted of DMEM/F-12 (Dulbecco's Modified Eagle Medium/Nutrient Mixture F-12, Gibco, ThermoFisher scientific) and:

- 15%, fetal bovine serum (FBS, Gibco ThermoFisher scientific), used as a supplement for cell growth, it provides nutrients such as growth factors, proteins, vitamins, hormones and trace elements (68).
- 1%, Penicillin/streptomycin (P/S, Gibco, ThermoFisher scientific), an antibiotic to avoid gram-positive/gram-negative contamination.
- 2%, L-glutamine (Gibco, ThermoFisher scientific), an aminoacid.

3.4.4 Splitting and Count

To maintain cells in a proliferative state and prevent overconfluence, regular cell passaging at defined intervals is crucial. Cell passaging, also known as cell splitting or subculturing, is performed to sustain cell cultures, scale up cell volume, or initiate experiments. The optimal timing for passaging depends on the proliferation rate and desired cell number. Each cell type requires a specific splitting protocol. Typically, adherent cells are detached from the substrate using proteolytic enzymes like trypsin/EDTA, which break down the protein attachments. After detachment, cells are homogenized, counted, and seeded into a new vessel, incrementing the passage number by one (70).

For cell splitting, a 0.05% trypsin solution was used following the protocol outlined below:

- Remove the culture medium.
- Wash cells with Dulbecco's phosphate-buffered saline (DPBS, Gibco) to prevent trypsin action interference with residual serum.
- Add trypsin and incubate the flask at 37°C for 3 minutes to facilitate the detachment of cells from the substrate by disrupting cell-to-substrate protein interactions.
- Observe cell morphology; if cells appear round-shaped, it indicates successful detachment by trypsin.
- Add culture medium to stop trypsin activity.
- Aspirate the cell suspension and transfer it into a Falcon tube.

Afterward, the cells needed to be seeded into the bottom layer by resuspending them in collagen. To ensure the correct volume of cell suspension to centrifuge and resuspend, cell counting was performed. The desired cell concentration was 7000 cell/μL for each device.

A 10μL aliquot of the cell suspension was placed in a Burker chamber (figure 3.4.1), covered with a microscope glass, and observed under an optical microscope.

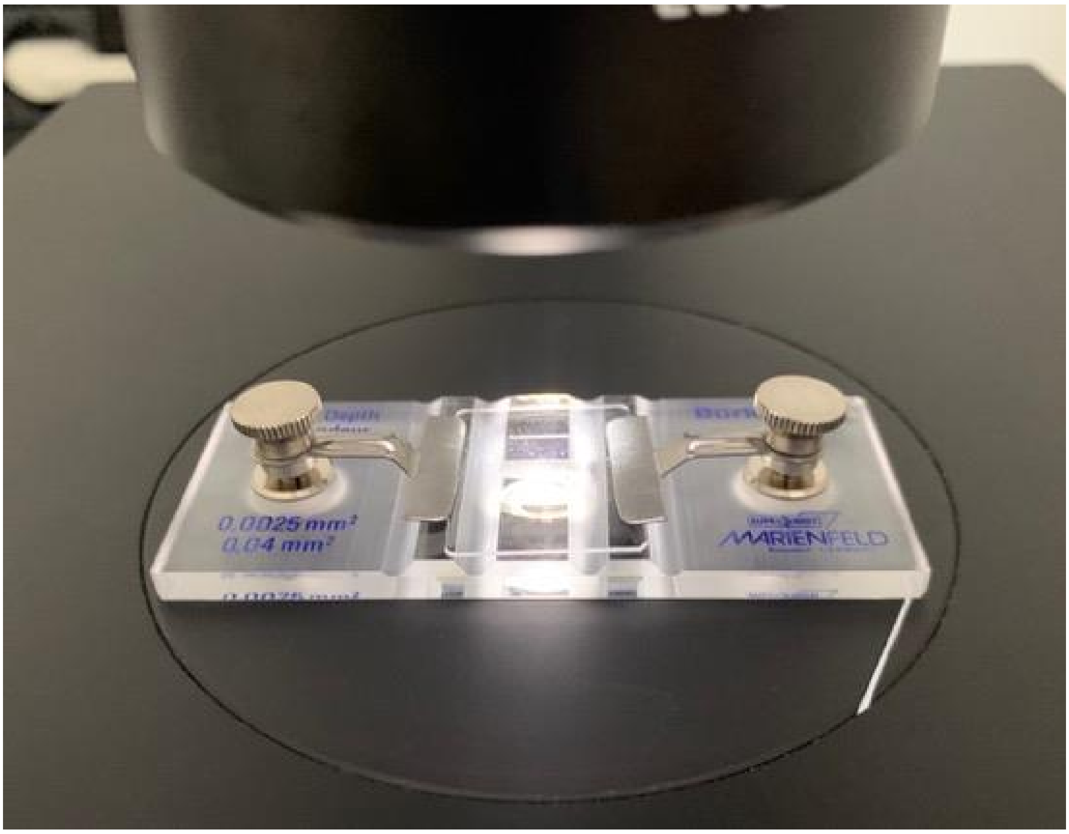

Figure 3.4.1 Burker chamber under the optical microscope.

The Bürker chamber has 9 large squares (1 mm 2 each), divided by double lines (0.05 mm apart) into 16 group squares. The double lines form small 0.0025 mm 2 squares. The Chamber depth is 0.1 mm (71)(figure 3.4.2).

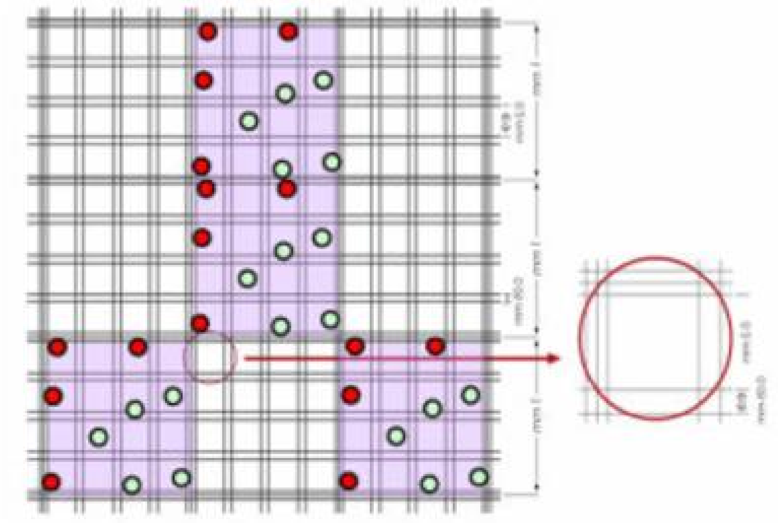

Figure 3.4.2 Burker chamber (71).

Only cells in the four-square grid are considered, and the total number of cells is calculated as follows:

Number of cells = cell count * 10,000 * square factor / 4

The volume to centrifuge was then calculated using the proportion:

Number of cells to seed : seeding volume = Number of cells counted : volume to centrifugate

The obtained volume was centrifuged at 1000rpm for 8 minutes to separate the solid cell pellet from the liquid phase, which was discarded. The cells were resuspended in a small quantity of fresh media to disrupt cellular aggregates. Finally, the calculated volume of this cell suspension was added to each chip. After seeding, the chips were incubated at 37ºC in a humidified atmosphere with 5% CO2 for 30 minutes. Subsequently, the culture medium was added to the two lateral channels through the reservoirs and replaced daily. The microfluidic chips seeded with HFF-1 and HPDE-WT, HFF-1 and HPDE-KRAS, HFF-1 and MIA-PACA-2 cells were analyzed at three different time points (24 hours, 48 hours, and 72 hours). Each cell combination was sampled three times per time point to have reliable results, obtaining a total of 27 samples.

3.4.5 Immunostaining

Immunostaining is a powerful technique used in research laboratories to identify and visualize specific proteins in tissue sections. It involves incubating the tissue sample with antibodies that are specific to the protein of interest, followed by visualization of the bound antibodies using a chromogen (immunohistochemistry or IHC) or fluorescence (immunofluorescence or IF) method.

In contrast to techniques like in situ hybridization, which detect gene transcripts in cells, immunostaining allows the direct identification of the proteins themselves. This provides valuable information about the localization of proteins within cells, such as whether they are found in the nucleus, cytoplasm, cell membrane, or extracellular matrix (72).

For this thesis work, two fluorescent markers were used: DAPI to detect cell nuclei and Phalloidin for cytoskeletons, while E-cadherin was considered for immunostaining as an antigen and marker of epithelial cells (73). This allowed for a clear distinction between the seeding of epithelial cells on the top and fibroblasts on the bottom layer.

Before doing that, each device was treated with paraformaldehyde for 40 minutes to ensure cell fixation and preserve cellular structures effectively and then wash each device three times with PBS. Paraformaldehyde is capable of binding to free amino groups present in the lateral chains of amino acids, thereby providing good conservation of cellular structures (74).

Following the protocol, *Triton X-100* and *Tween-20*, non-ionic detergents, were used to enhance the cell membrane permeability (75) (76) without affecting their biological activity (77). Also, a blocking buffer was used, the *Bovine Serum Solution (BSA)* to saturate excess protein-binding sites on membranes (78).

Each device was incubated with a solution of Triton-X-100 (0.2%) in PBS for 10 minutes at room temperature and then washed three times using PBST (PBS + 0.1%Tween-20). After that, they were treated with a solution of 2% BSA, diluted in PBST for 60 minutes at room temperature, and left overnight at 4°C with a solution of PBST, 1% BSA and Anti-E-Cadherin antibody in 1:2000 concentration. The next day, each chip was washed three times with PBST and incubated for 2 hours at room temperature with the secondary antibodies (PBST + 1% BSA + Cyanine 1:500), washed again three times with PBST and set on with the fluorescence marker solutions: PBST+1%BSA+phalloidin(1:60) for 2 hours, washing with PBS, PBS+DAPI(1:1000) for 5 minutes and final cleaning with PBS.

4 Results and discussion

Membrane Detachment

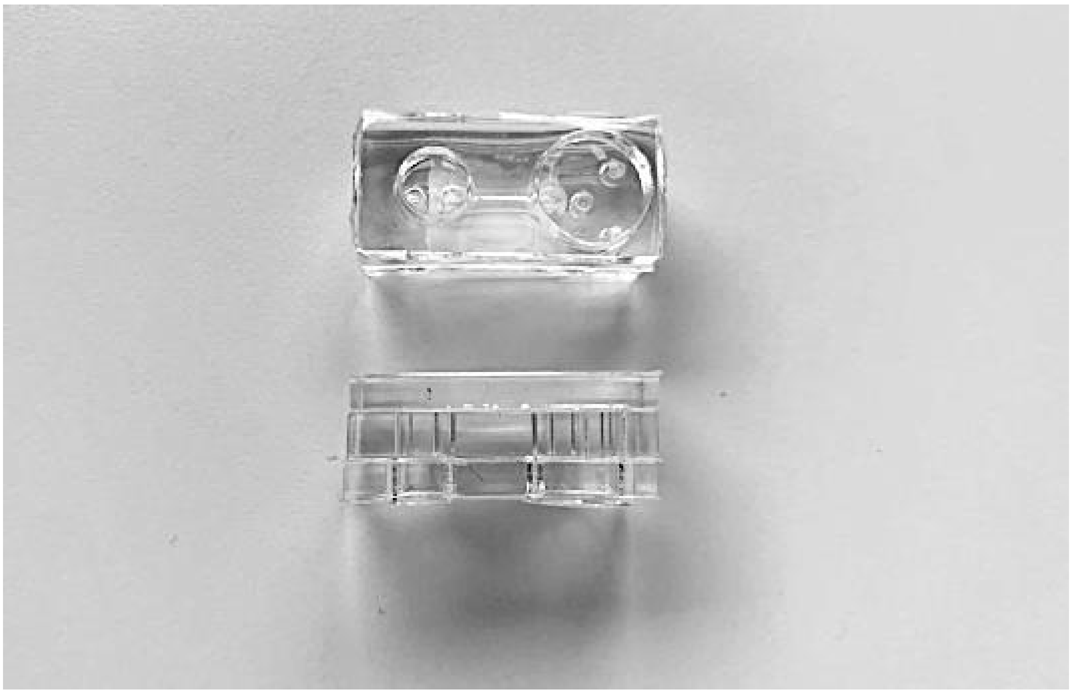

Figure 4.1 Assembled device.

One of the first successes of the new device developed (Figure 4.1) is certainly the ease of removal and disassembly of the device. As mentioned earlier, previous versions of the chip had difficulties in model monitoring, since the membrane remained stuck to the top layer during the debonding phase, and the fibroblast-laden hydrogel in the bottom layer resulted difficult to be isolated and characterized. Furthermore, the membrane also caused problems regarding the filling of the central channel because when the device was assembled, it would collapse and fall into the central channel, obstructing it. So, the idea was to design lateral cavities to be filled with PDMS for the housing and fixation of the membrane.

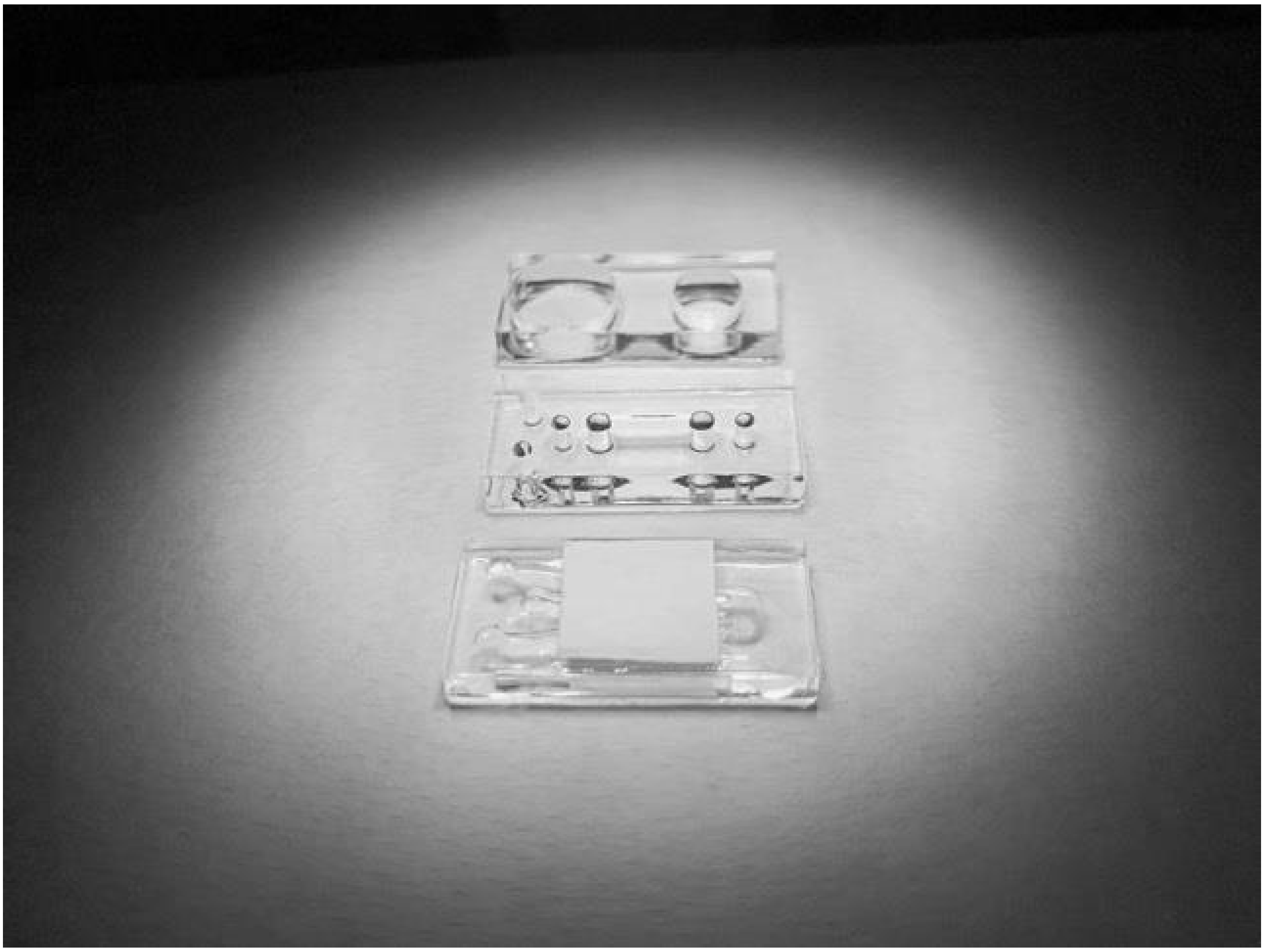

Figure 4.2 Device before the bonding.

From Figures 4.2 and 4.3, we can see respectively the device disassembled before bonding, prior to the oxygen plasma treatment, and after bonding, following the cell seeding and culture.

Figure 4.3 Disassembled device after the bonding.

This provided a significant advantage: the membrane could be directly analyzed under a microscope by placing the bottom layer on the microscope slide (Figure 4.4) or by removing the membrane from the bottom layer and examining it separately (Figure 4.5).

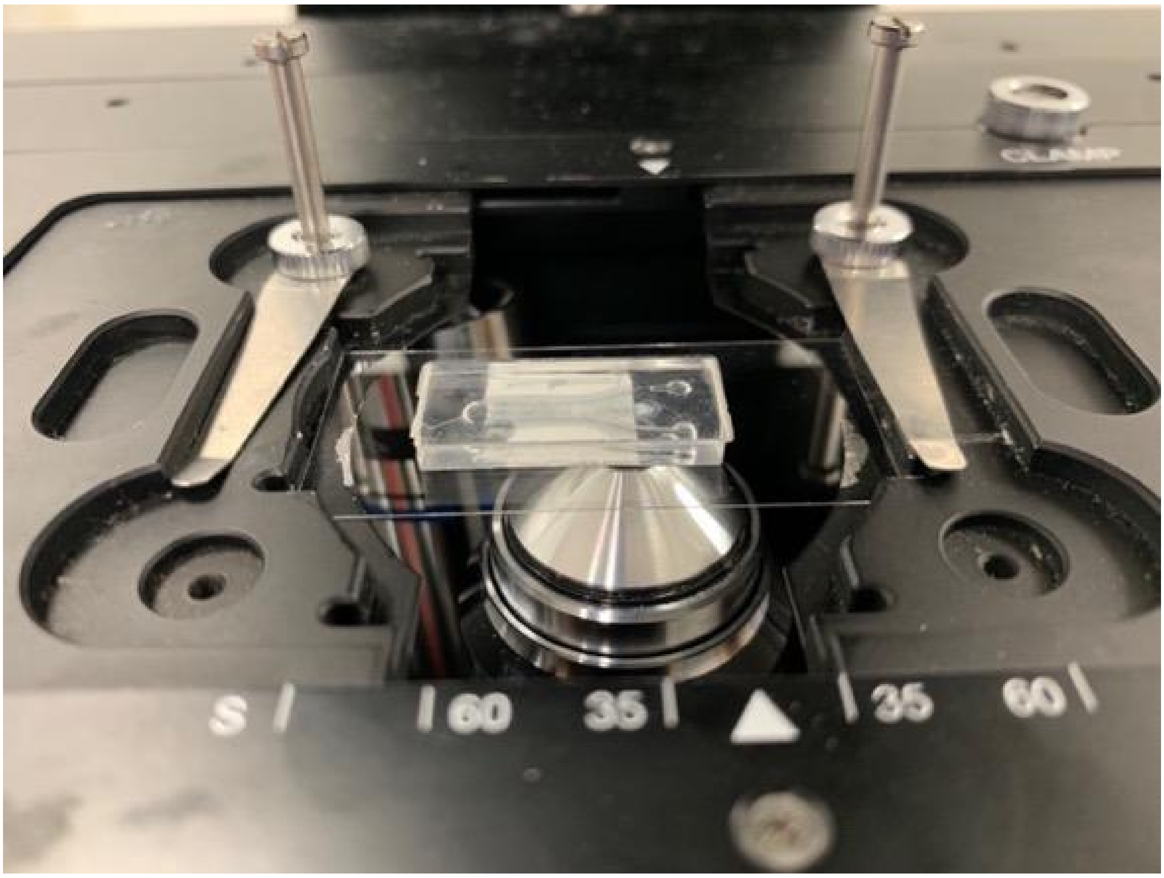

Figure 4.4 Bottom layer with membrane under the microscope.

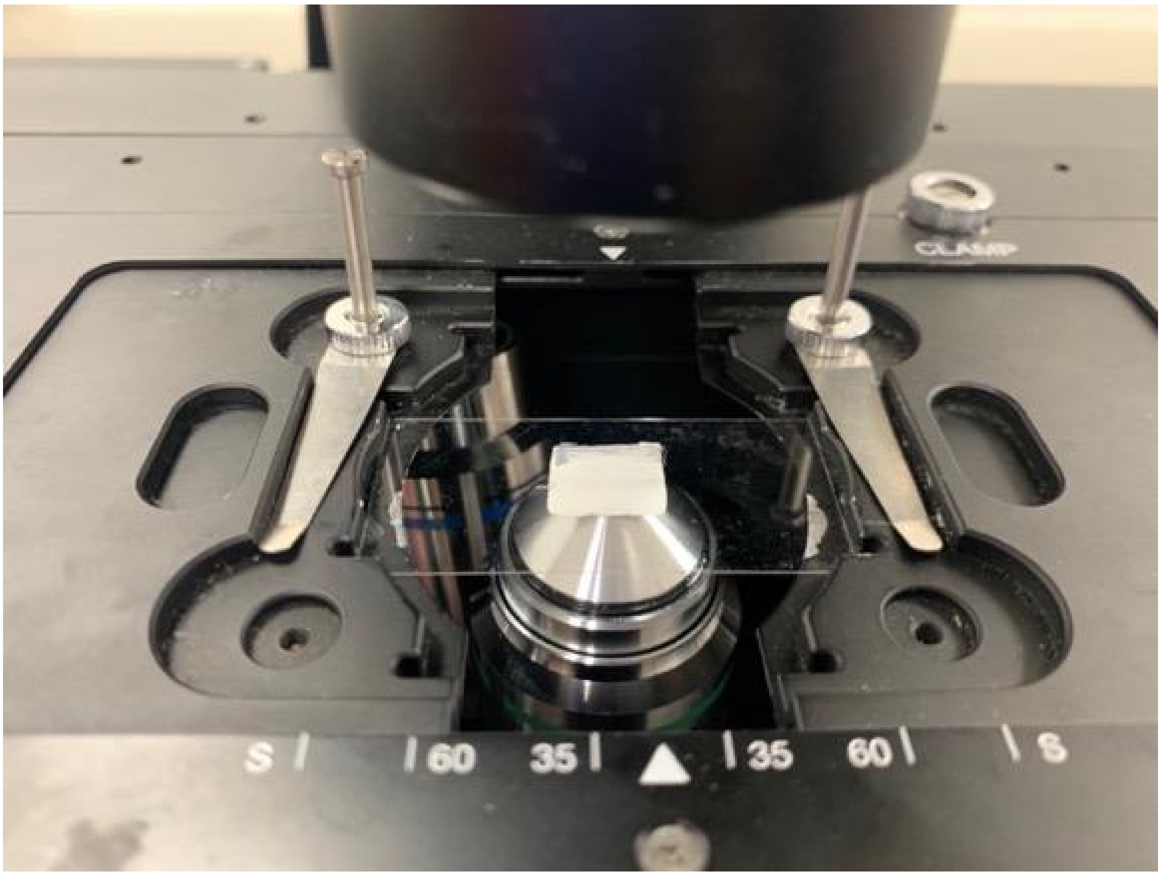

Figure 4.5 Membrane under the microscope.

HPDE-WT

Focusing now on the biological characterization, we will analyze confocal microscope images. A first HFF-1/HPDE-WT sample was taken at 24 hours. From a 10x acquisition of the membrane (Figure 4.6), we can clearly see the cells confined within the channel where they were injected. Therefore, the cell solution inserted in the inlet did not leak out of the channel but remained confined inside, and the cells adhered and proliferated on the membrane, showing the perimeter of the channel. Three different channels were acquired (Figure 4.7):

- The green color emitted by Phalloidin highlights the cytoskeleton, enabling the identification of cell types. HPDE cells exhibit a flat cuboidal shape (79), whereas fibroblasts display a more elongated and expanded, spindle-shaped morphology (80).
- DAPI (4′,6-diamidino-2-phenylindole) is a DNA stain that emits a blue fluorescence. It is commonly employed to label DNA in fixed cells due to its inability to penetrate cell membranes. However, it should be noted that at higher concentrations, DAPI can enter live cells and stain DNA (81).
- Cyanine5 (Cy5) dye is a bright, far-red-fluorescent dye (82). It identifies the e-cadherin expressed by epithelial cells (83). This allows for a proper distinction between epithelial cells and fibroblasts.
- Alexa 555 (AF555) has an excitation peak at 555 nm and an emission peak at 565 nm and shows a red-orange fluorescence (84). It was used to detect the α-SMA protein expressed by CAFs (Cancer-

Associated Fibroblasts), as a marker of their inflammatory status (85), to observe and compare the secretions of fibroblasts associated with the three types of epithelial cells in HPDE-WT, HPDE-KRAS, and MIA-PACA-2 configurations, thereby understanding how epithelial cells influence fibroblasts and their cancer severity level (86).

The membrane is analyzed from the top layer. Firstly, we can see a layer of cuboidal epithelial cells from Phalloidin staining and this is confirmed by the presence of E-cadherin marked with Cyanine. We can observe the successful seeding, culturing, and fixation of HPDE-WT cells in the top layer.

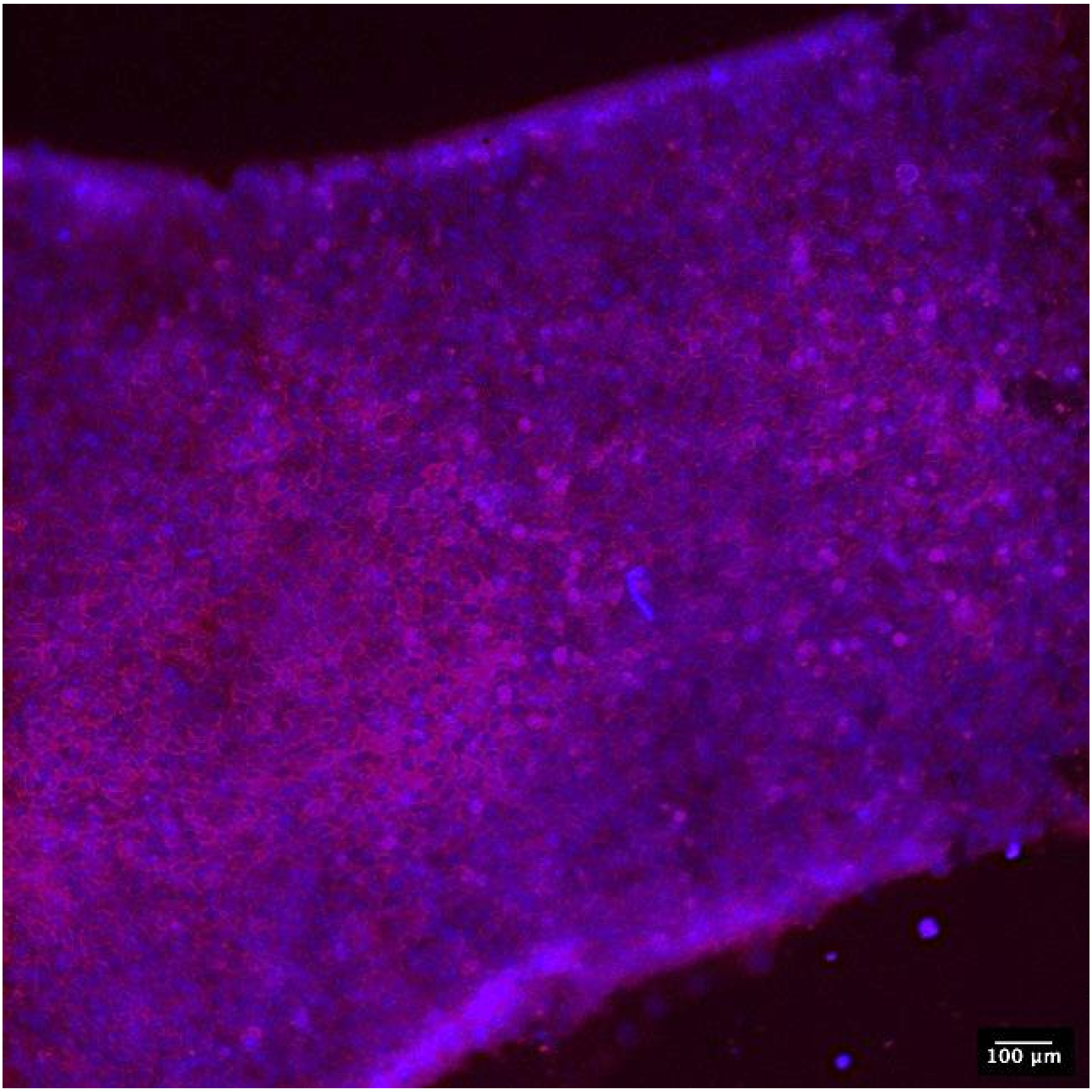

Figure 4.6 HFF-1/HPDE-WT, 24h, 10x – DAPI-Cyanine merged channels

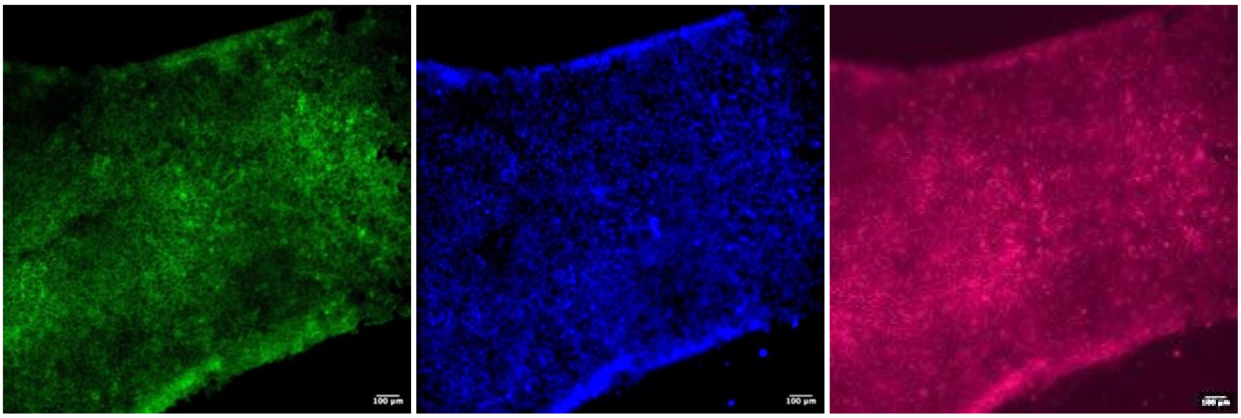

Figure 4.7 Channels from left: Phalloidin, DAPI, Cyanine

From a higher magnification image at 20x, we can better observe the shape of HPDE-WT cells (Figure 4.8.1-4.8.2) and the epithelial layer they have formed with their interconnections.

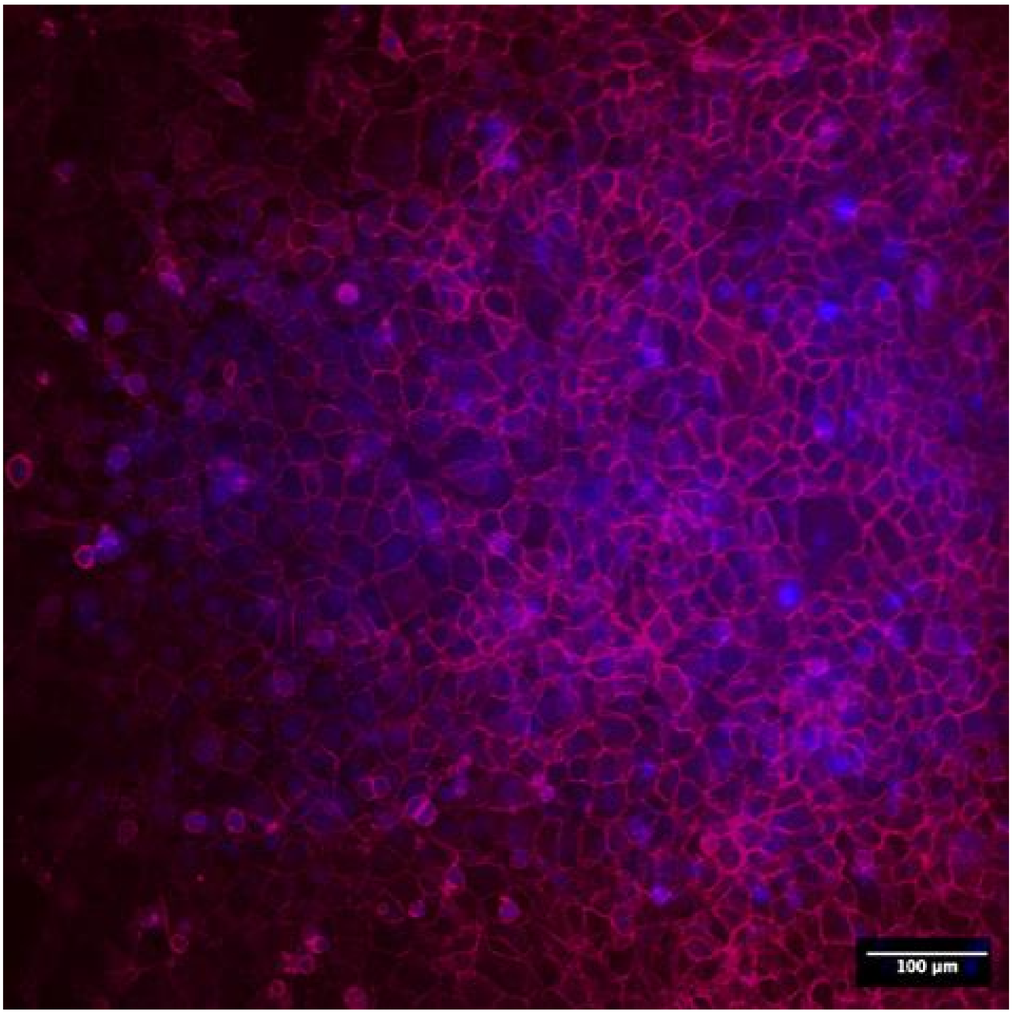

Figure 4.8.1 HPDE-WT, 24h, 20x – DAPI-Cyanine merged channels

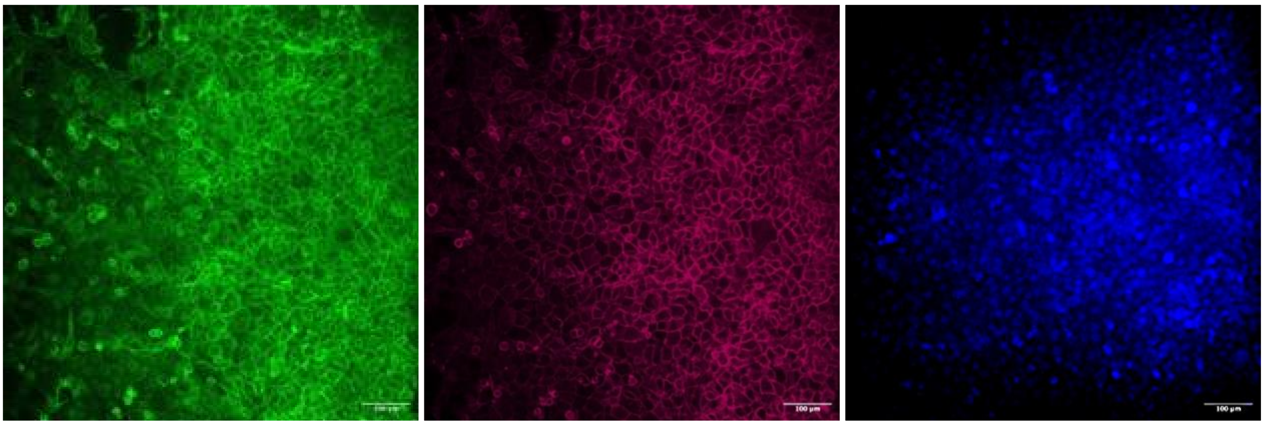

Figure 4.8.2 HPDE-WT, 24h, 20x – Phalloidin, Cyanine,Dapi channels

As for the seeding and cultivation of fibroblasts on the other side of the membrane, this was evaluated by removing the membrane from a chip fixed at 72 and placing it on the microscope slide. (Figure 4.9).

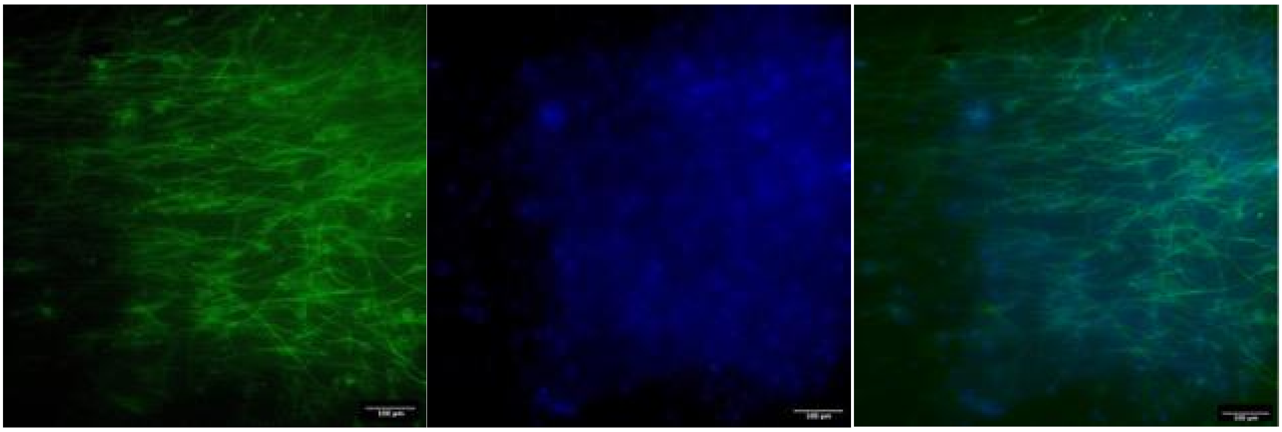

Figure 4.9 HFF-1, 72h, 20x

Fibroblasts exhibit a distinctive star-like shape, and their vitality can be assessed by observing the branching and filamentous connections.

The inflammatory state of fibroblasts was also evaluated using the Alexa 555 channel (figure 4.10), and only a low level of fluorescence is observed in the presence of HFF-1, this indicates that the fibroblasts have not been cultured in an aggressive tumor environment (85) (86).

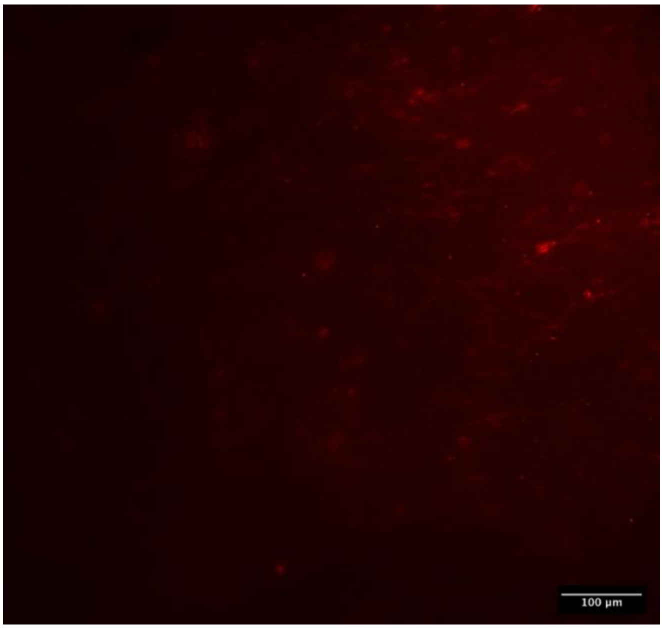

Figure 4.10 Alexa 555 channel, HFF-1, 72h, 20x

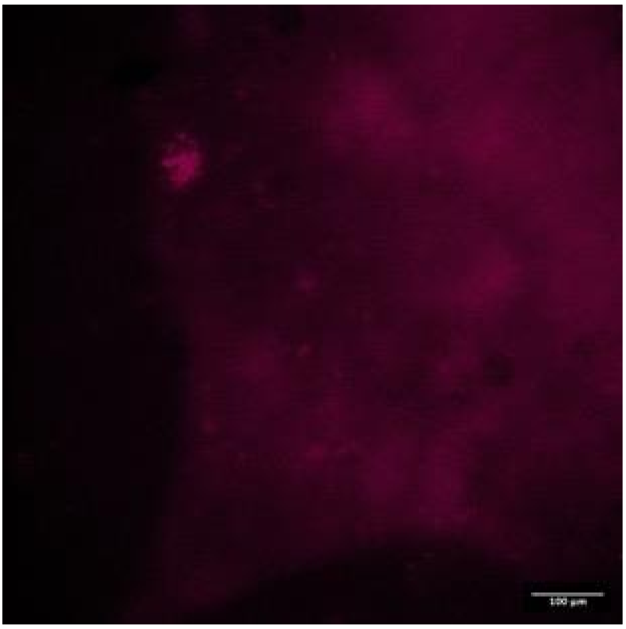

Figure 4.11 Cyanine produced by HPDE-WT.

Instead, analyzing the cyanine dye (Figure 4.11), we observe a hazy fluorescence that it is not expressed by the fibroblast monolayer but from the underlying membrane plane produced by HPDE-WT.

We sought the same exact point, characterized by a triangular shape likely caused by a folding of the membrane, on the opposite side of the membrane to verify the correspondence of the epithelial culture (Figure 4.12).

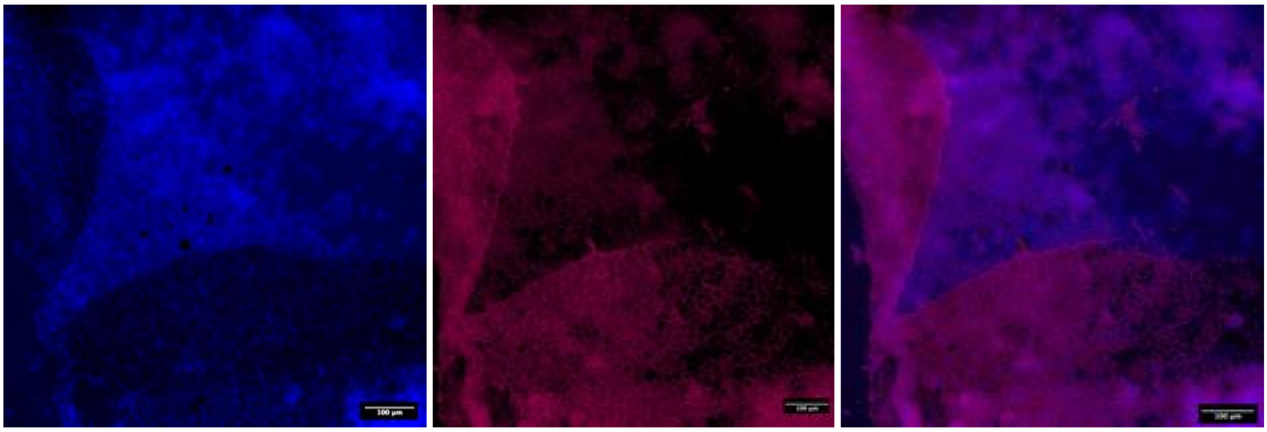

Figure 4.12 HPDE-WT correspondence.

In fact, it can be observed that the weak cyanine signal in Figure 4.8 is not produced by fibroblasts but by the underlying epithelial cells. If it had originated from the HFF-1 layer, knowing that they do not express E-cadherins, it would have meant that a mixing of the two cell lines had occurred and some epithelial cells had entered the bottom layer. This result proves the effectiveness of this model in separating the two cell types and therefore study the crosstalk effect in a specific and controlled way.

From a 4x widefield acquisition at 48h, we can observe the distribution of HFF-1 and HPDE-WT. The Brightfield, Phalloidin, and Cyanine channels were merged (Figure 4.13).

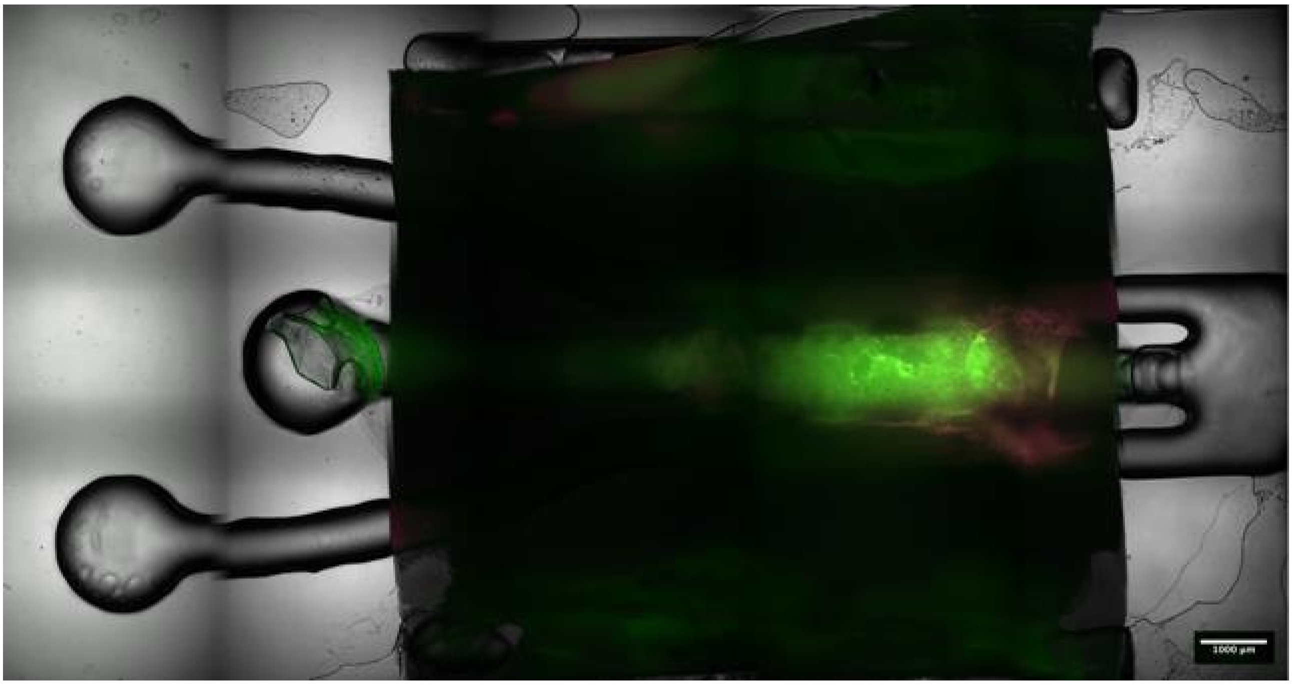

Figure 4.13 HFF-1/ HPDE-WT panoramic view, 48h.

The gel containing fibroblasts remained confined in the central channel without any leakage into the outer channels. Additionally, the presence of epithelial cells on the upper side of the membrane was indicated by the fluorescence from the E-cadherin signal. By capturing a series of 21 slices (Table 3) in a close z-stack near the inlet of the central channel, we can observe, from slice 1 and using phalloidin staining (figure 4.14), the presence of residual collagen gel at the channel entrance and the passage of fibroblasts beneath the membrane.

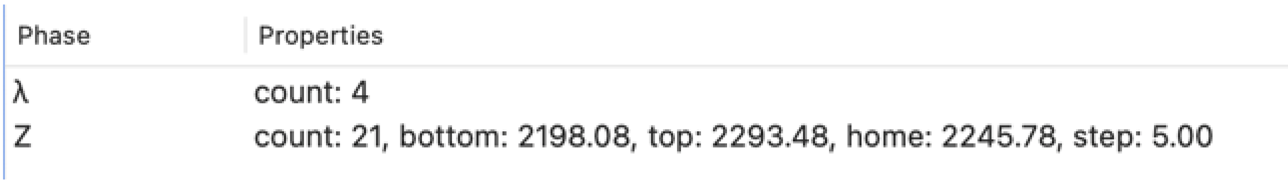

Phase	Properties
λ	count: 4
Z	count: 21, bottom: 2198.08, top: 2293.48, home: 2245.78, step: 5.00

Table 3 z-stack properties acquisition.

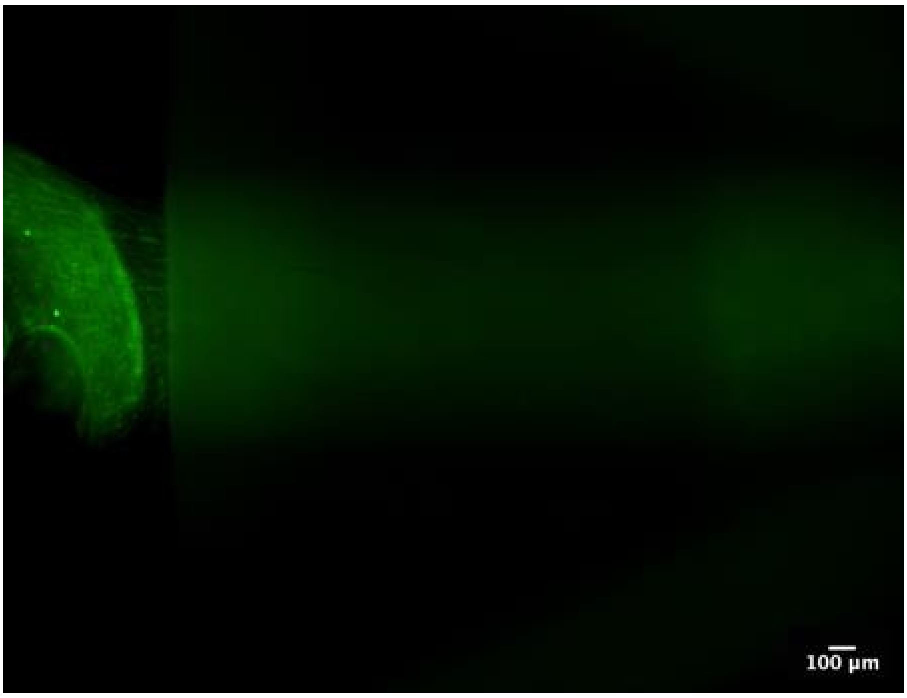

Figure 4.14 HFF-1/collagen at slice 1.

By focusing on the last slice (slice 21) using the cyanine channel, we can instead observe the seeded epithelial cells above the membrane at the inlet, with the collagen/HFF-1 meniscus passing beneath them (Figure 4.15).

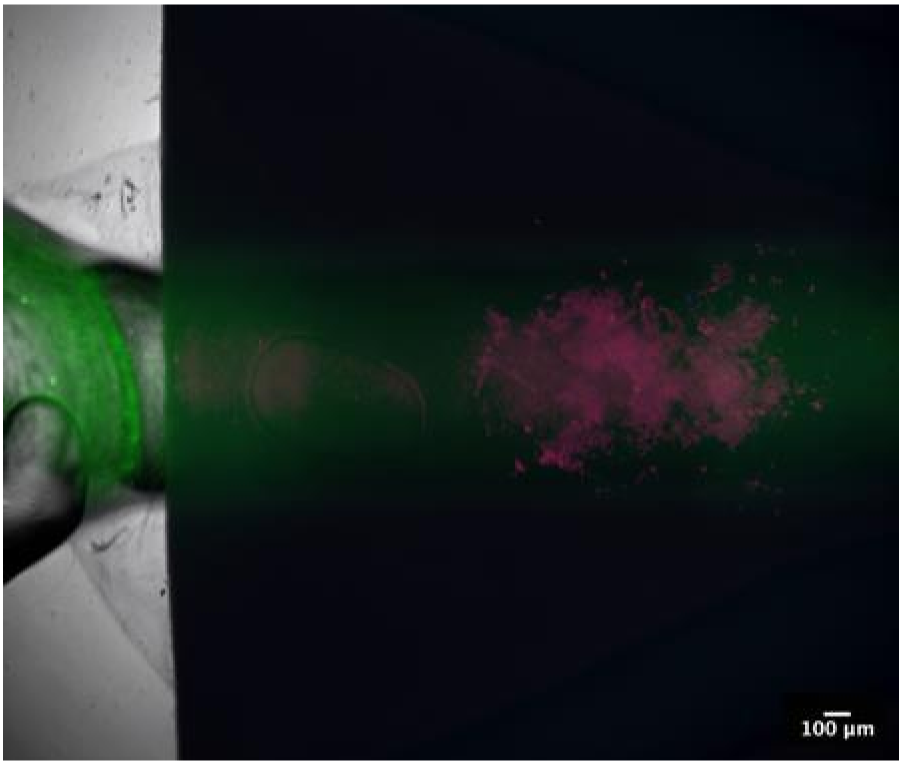

Figure 4.15 HFF-1/HPDE-WT at slice 21.

HPDE-KRAS

Furthermore, analyzing a sample seeded with HFF-1/HPDE-KRAS and fixed at 48 hours, the overlap of epithelial and fibroblast cells can be seen while keeping the device assembled, without having to completely remove the membrane. This is achieved simply by utilizing the z-stack feature of the confocal microscope, which allows movement across multiple slices along the z-axis.

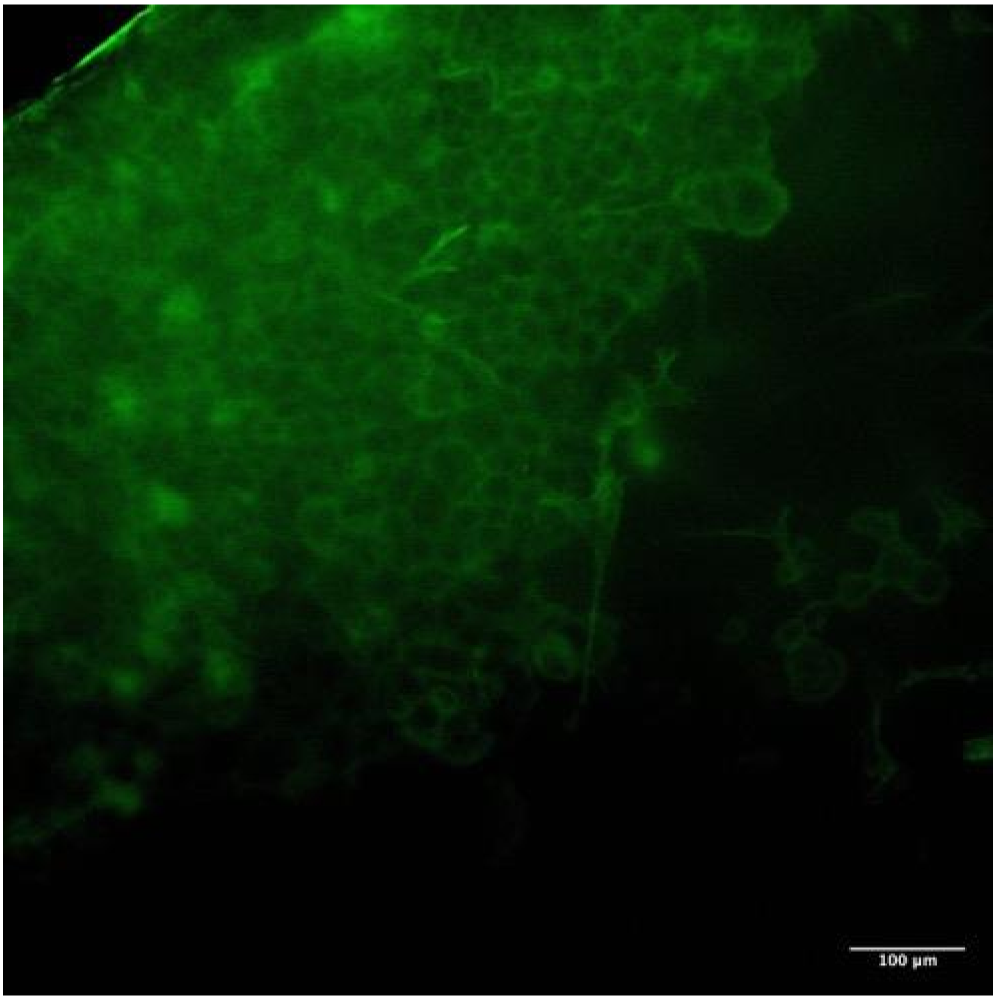

Figure 4.16 HFF-1 at slice number 27, 48h, 20x.

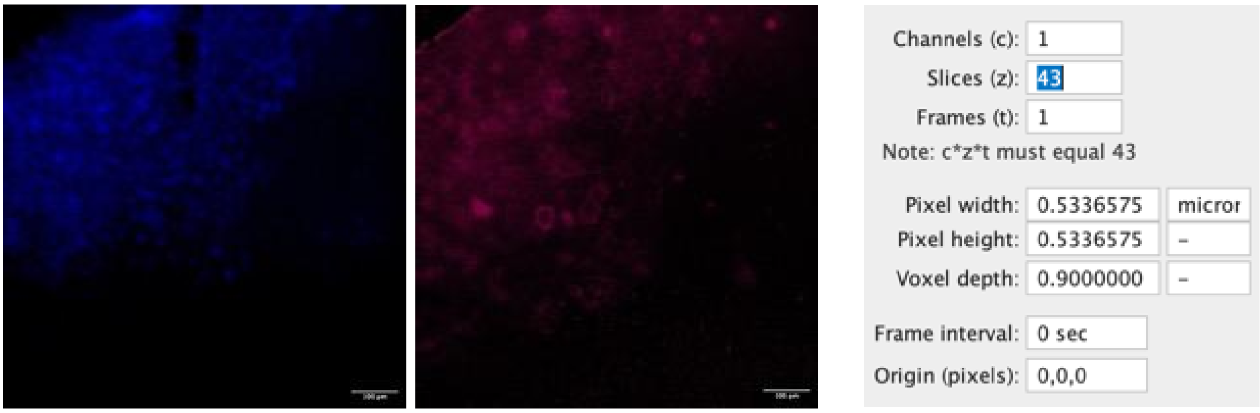

Channels (c): 1
Slices (z): 43
Frames (t): 1
Note: c*z*t must equal 43
Pixel width: 0.5336575 micror
Pixel height: 0.5336575 -
Voxel depth: 0.9000000 -
Frame interval: 0 sec
Origin (pixels): 0,0,0

Figure 4.17 Dapi and Cyanine channel at slice 27 and properties' z-stack.

From the acquisition of the z-stack frame, we can observe on slice 27 the slight presence of fibroblasts (figure 4.16) that the microscope was able to focus on with the assembled device as shown in Figure 4.4. The overall depth reached is 43 slices, and the properties are shown in Figure 4.17. By increasing the number of slices and reaching maximum depth, the microscope instead focused on the layer of epithelial cells, confirming their stratification into different layers (Figure 4.18). The epithelial cells highlighted by phalloidin and cyanine are more focused compared to the previous image, where they emitted a faint halo of fluorescence, and the excellent state of overconfluence in which they were fixed can be observed.

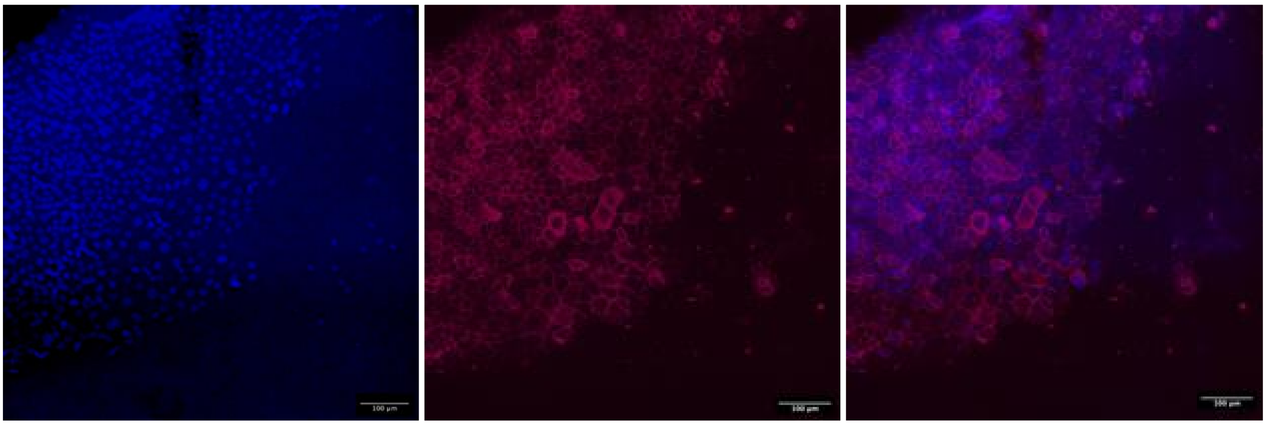

Figure 4.18 HPDE-KRAS at slice number 43, 48h, 20x.

To obtain a more detailed assessment of the vitality and culture proliferation state of fibroblasts, the membrane was removed from the bottom layer and analyzed separately using a 20x acquisition (figure 4.19).

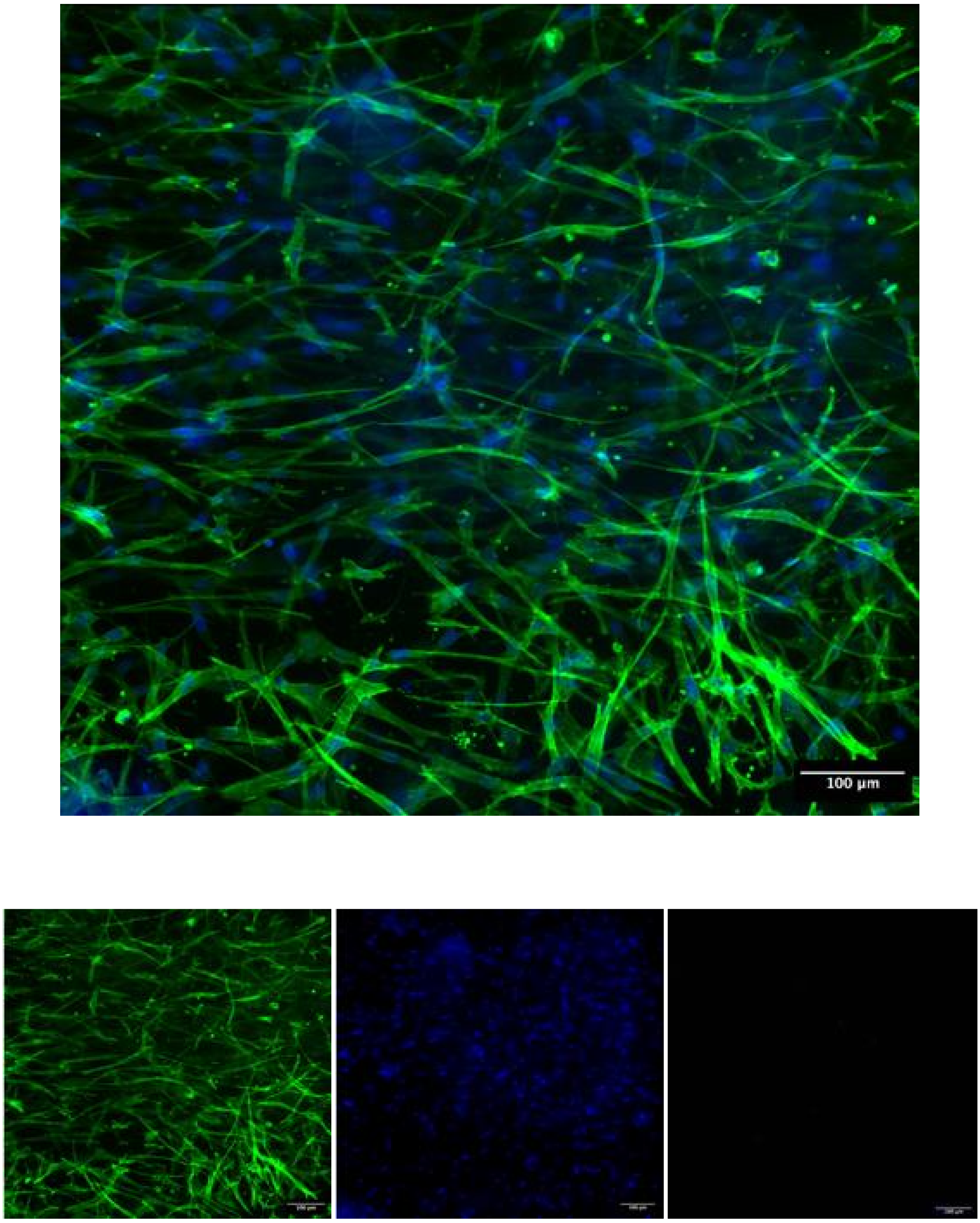

Figure 4.19 Three channels acquisition of HFF-1, 48h, 20x.

The cyanine channel does not detect fluorescence because we are completely in the plane of fibroblasts, so E-cadherin is not expressed. The fibroblasts exhibit excellent signs of adhesion and growth, appearing spindle-shaped, tightly packed, and communicating with each other.

Upon observing the channel corresponding to Alexa 555 (figure 4.20) of a chip fixed at 72h, it is evident that it manifests a higher level of fluorescence in comparison to HPDE-WT. This discrepancy implies an increased concentration of alpha-SMA, thereby indicating that the fibroblasts have been more profoundly influenced by the tumor microenvironment established through the utilization of HPDE-KRAS.

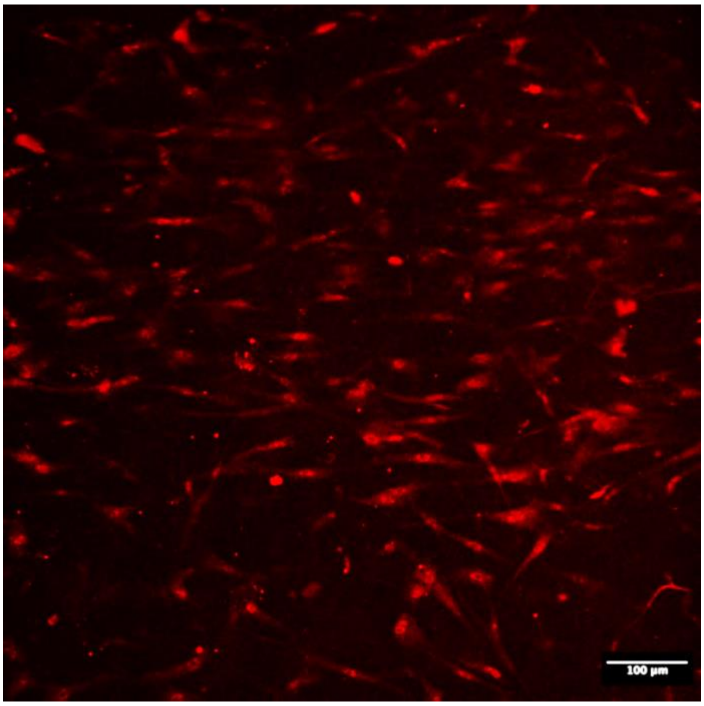

Figure 4.20 Alexa 555 channel, HFF-1, 72h, 20x.

Examining a sample collected at the 48-hour mark, we identified a membrane defect near the inlet channel of the top layer. This defect was likely a result of inadvertent perforation during the injection of epithelial cells. Nevertheless, this observation is significant in shedding light on the co-culturing of cell lines, as depicted in Figure 4.21.

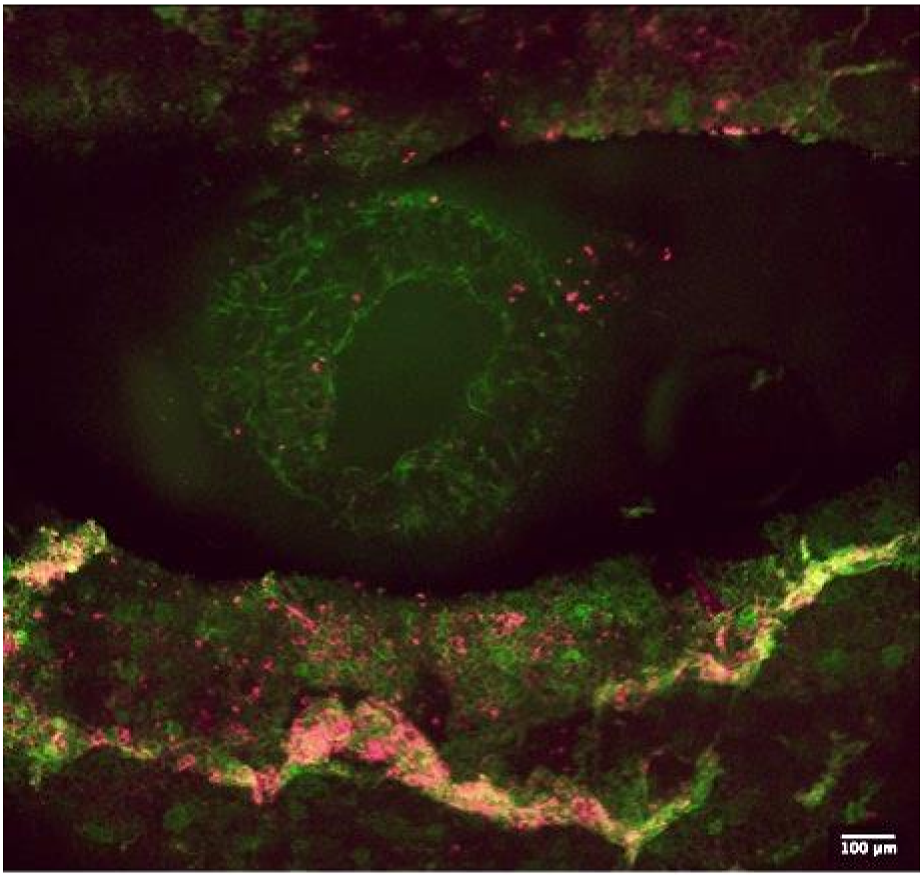

Figure 4.21 HFF-1/HPDE-KRAS on a membrane defect, 48h, 10x.

The epithelial cells are sharply in focus, while the fibroblasts can be observed in the background, located in the bottom layer. This serves as further confirmation that the separation of the two cell cultures has been successfully accomplished.

MIA-PACA-2

Regarding the co-culture of MIA-PACA-2 and HFF-1, we did not achieve satisfactory results, which requires further investigation. Anyway, the size of MIA-PACA-2 cells should be smaller than that of HPDE cells (87), in fact we can see the scaled-down form in Figure 4.22. Additionally, the expression of E-cadherin should be in low quantities (88), as evidenced by the fact that the channel corresponding to cyanine is almost completely obscured.

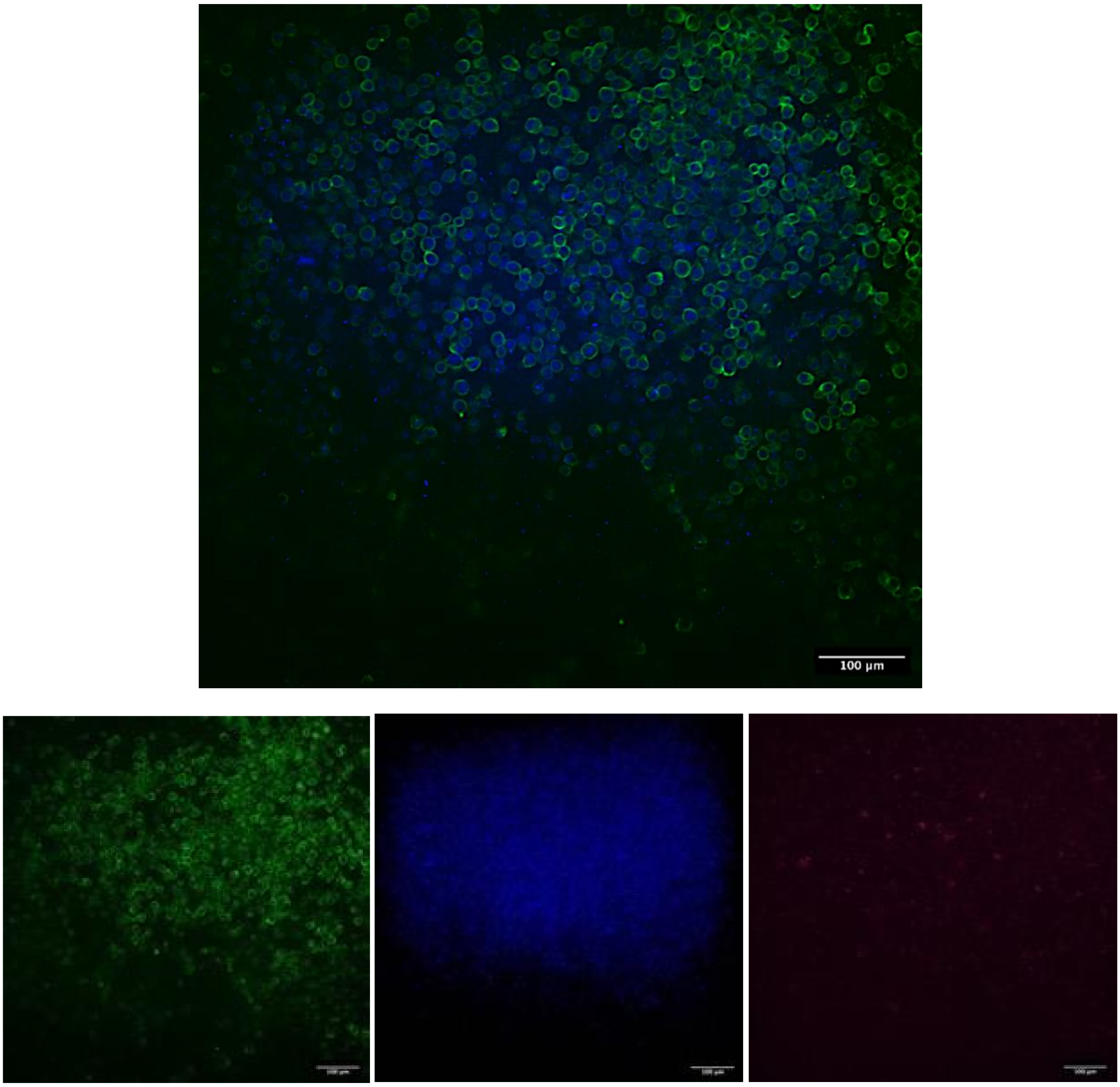

Figure 4.22 Channels acquisition of MIA-PACA-2, 72h, 20x.

The fibroblasts are scarce and do not appear to be in a healthy state, as they are accompanied by the presence of debris and secretions. However, the DAPI staining reveals the presence of numerous nuclei, suggesting that the fibroblasts may be dead. It is advisable to perform a cellular vitality analysis to detect both live and dead cells (figure 4.23).

For this reason, the α-SMA assessment is not evaluable due to the low HFF-1 quantity and their worse condition as well.

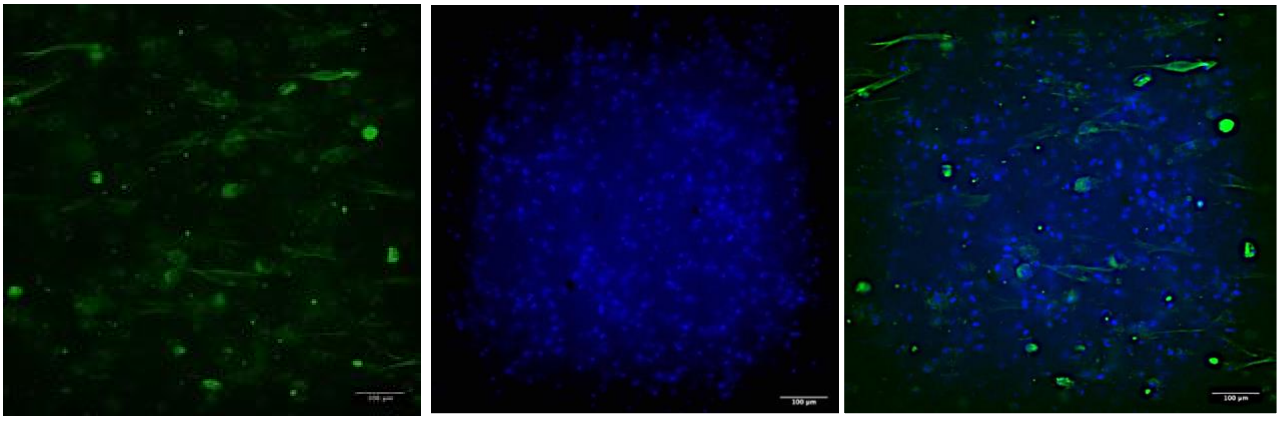

Figure 4.23 Channels acquisition of HFF-1, 72h, 20x.

5 Conclusion

Based on the findings in this thesis work, the device exhibited significant improvements in terms of monitoring and characterization of the assembled chip, improved microfluidics related to the filling of the central channel of the top and bottom layers, and external channels of the bottom layer, as well as appropriate fluid separation between the channels. This was achieved through the redesign of the chip's CAD, abandoning lithography and leveraging the versatility and speed of 3D printing, while analyzing the pros and cons of previous devices.

Regarding potential future developments, it may be considered to conduct faster analysis during biological characterization using confocal microscopy by employing a thinner membrane, thereby enabling visualization of both faces of the membrane through z-stack imaging, with one face seeded with fibroblasts and the other with epithelial cancer cells. This is because one of the limitations of this device was the inability to access the opposite face of the membrane with the current thickness. If both cell lines were analyzable, it would no longer be necessary to remove and examine the membrane separately, thereby avoiding the risk of damage.

Another aspect to evaluate is why the fibroblasts appeared dehydrated and deceased when co-cultured with MIA-PACA-2 cells. A more in-depth analysis and viability test could be conducted to understand the factors contributing to the impaired proliferation of fibroblasts and how they were influenced by MIA-PACA-2 cells. Furthermore, a comparison of different cell cultures could be performed to understand the effects that various cell lines have on fibroblasts, by exploiting α-SMA detection and conducting a qualitative and quantitative analysis in order to better investigate the levels of cancer severity (86) in HPDE-WT, HPDE-KRAS, and MIA-PACA-2 configurations.

Additionally, the effects of newly available drugs on PDAC could be evaluated using this chip as a drug screening tool. During drug screening, specific methods and tests are employed to assess the interaction of a substance with relevant biological targets, such as proteins or enzymes, in order to determine the compound's effects on the biological system. These microfluidic systems are currently subjects of extensive analysis because they allow to mimic and recapitulate the pathological conditions involved in PDAC, which is undoubtedly one of the most challenging tumors to treat. Therefore, making a microfluidic system capable of replicating the true physiological and pathological conditions of the tumor constitutes an essential starting point for the establishment of innovative therapeutic strategies.

Bibliografia

1. Society, American Cancer. Pancreatic Cancer Survival Rates. [Online] 2021. https://www.cancer.org/cancer/pancreatic-cancer/detection-diagnosis-staging/survival-rates.html .
2. Version, Merck Manual Professional. [Online] 2021. https://www.merckmanuals.com/professional/gastrointestinal-disorders/pancreatitis/pancreas .
3. The pancreas. [Online] https://teachmeanatomy.info/abdomen/viscera/pancreas/.
4. Axelsson, Jakob. [Online] https://www.researchgate.net/figure/Morphology-of-the-acini-and-adjacent-ducts-Each-acinus-consists-of-a-cluster-of-acinar_fig5_315564510.
5. Longnecker, D. The Pancreapedia: Exocrine Pancreas Knowledge Base. [Online] 2014. https://www.pancreapedia.org/reviews/anatomy-and-histology-of-pancreas.
6. Pancreas - Chapter 9. [Online] https://obgynkey.com/pancreas/.
7. Jensen, Ole N. *ResearchGate.* [Online] https://www.researchgate.net/figure/The-pancreatic-islets-of-Langerhans-are-small-conglomerates-of-cells-on-average-1-000_fig1_8034185.
8. *Molecular Pathogenesis of Pancreatic Cancer.* Trevor J. Grant, Kevin Hua, and Anurag Singh. s.l. : Prog Mol Biol Transl Sci, 2016. 10.1016/bs.pmbts.2016.09.008.
9. *Desmoplasia in primary tumors and metastatic lesions of pancreatic cancer.* Whatcott CJ, Diep CH, Jiang P, et al. s.l. : Clin Cancer Res, 2015, Vols. 21(15):3561-3568.
10. *Fibroblast heterogeneity in the cancer wound.* Öhlund D, Elyada E, Tuveson D. s.l. : J Exp Med, 2014.
11. *Clinical Strategies Targeting the Tumor Microenvironment of Pancreatic Ductal Adenocarcinoma.* Nebojsa Skorupan, Mayrel Palestino Dominguez, Samuel L. Ricci and Christine Alewine. s.l. : Cancers, 2022.
12. *high M1/M2 ratio of tumor-associated macrophages is associated with extended survival in ovarian cancer patients.* Zhang M, He Y, Sun X, et al. s.l. : J Ovarian Res, 2014.
13. *Oncogenic KRAS regulates tumor cell signaling via stromal reciprocation.* Tape CJ, Ling S, Dimitriadi M, et al. s.l. : Cell, 2016, Vols. 165(4):910-920.
14. *Depletion of carcinoma-associated fibroblasts and fibrosis induces immunosuppression and accelerates pancreas cancer with reduced survival.*

Özdemir BC, Pentcheva-Hoang T, Carstens JL, et al. 25(6):719-734, s.l. : Cancer Cell, 2014.
15. *A starring role for stellate cells in the pancreatic cancer microenvironment.* Apte MV, Wilson JS, Lugea A, Pandol SJ. s.l. : Gastroenterology, 2013, Vols. 144(6):1210-1219.
16. *Identification, culture, and characterization of pancreatic stellate cells in rats and humans.* Bachem MG, Schneider E, Gross H, et al. s.l. : Gastroenterology, 1998, Vols. 115(2):421-432.
17. *Inhibition of the hedgehog pathway targets the tumor-associated stroma in pancreatic cancer.* Hwang RF, Moore TT, Hattersley MM, et al. s.l. : Mol Cancer Res, 2012, Vols. 10(9):1147-1157.
18. *Pancreatic stellate cells: partners in crime with pancreatic cancer cells.* Vonlaufen A, Joshi S, Qu C, et al. s.l. : Cancer Res, 2008, Vols. 68(7):2085-2093.
19. *Organoid models of human and mouse ductal pancreatic cancer.* Boj SF, Hwang CI, Baker LA, et al. s.l. : Cell, 2015, Vols. 160(1-2):324-338.
20. *Distinct populations of inflammatory fibroblasts and myofibroblasts in pancreatic cancer.* Öhlund D, Handly-Santana A, Biffi G, Elyada E, Almeida AS, Ponz-Sarvise M, et al. s.l. : J Exp Med, 2017, Vols. 214(3):579-596.
21. *Bioengineered 3D models to unravel pancreatic ductal adenocarcinoma progression and therapy response.* Duarte Campos DF, Bonnin Marquez A, Marques AP, Reis RL, Oliveira JM, Levato R. s.l. : Acta Biomater, 2020.
22. *Bone grafts and biomaterials substitutes for bone defect repair: A review. .* Wang W, Yeung KWK. s.l. : Bioact Mater, 2017.
23. *Large Animal Models in Regenerative Medicine and Tissue Engineering: To Do or Not to Do .* Iris Ribitsch, Pedro M. Baptista, Anna Lange-Consiglio, Luca Melotti, Marco Patruno, Florien Jenner, Eva Schnabl-Feichter, Luke C. Dutton6, David J. Connolly, Frank G. van Steenbeek, Jayesh Dudhia and Louis C. Penning. s.l. : Front. Bioeng. Biotechnol, 2020.
24. *Multimodality imaging techniques for evaluation of tissue-engineered constructs.* Chang R, Emami K, Wu H, Sun W. s.l. : Tissue Eng Part B Rev, 2014.
25. *2D and 3D cell cultures – a comparison of different types of cancer cell cultures.* Marta Kapałczyńska, Tomasz Kolenda, Weronika Przybyła, Maria Zajączkowska, Anna Teresiak, Violetta Filas, Matthew Ibbs, Renata Bliźniak, Łukasz Łuczewski and Katarzyna Lamperska. s.l. : Arch Med Sci, 2018, Vols. 14(4): 910–919.
26. Benjamin D. Gastfriend, Sean P. Palecek, and Eric V. Shusta. *Modeling the blood-brain barrier: Beyond the endothelial cells.* [Online] https://par.nsf.gov/servlets/purl/10098050#:~:text=Transwell%20models,well%20plate%20(Figure%201B)..

27. *Geometric control of cell life and death. .* Chen CS, Mrksich M, Huang S, Whitesides GM, Ingber DE. 276(5317):1425-1428., s.l. : Science, 1997.
28. *Tubeless microfluidic angiogenesis assay with three-dimensional endothelial-lined microvessels.* Bischel LL, Young EW, Mader BR, Beebe DJ. s.l. : Biomaterials, 2013, Vols. 34(6):1471-1477.
29. *Pancreatic cancer genomes reveal aberrations in axon guidance pathway genes.* Biankin AV, et al. s.l. : Nature, 2012, Vols. 491(7424):399-405.
30. *Patient-Derived Organoids in Precision Medicine: Drug Screening, Organoid-on-a-Chip and Living Organoid Biobank.* Zilong Zhou, Lele Cong and Xianling Cong. s.l. : Sec. Molecular and Cellular Oncology , 2021, Vol. 11.
31. *Microtechnology-based methods for organoid model.* Vanessa Velasco, S. Ali Shariati & Rahim Esfandyarpour. s.l. : microsystems & nanoengineering, 2020.
32. Microfluidics: A general overview of microfluidics. *elveflow.* [Online] https://www.elveflow.com/microfluidic-reviews/general-microfluidics/a-general-overview-of-microfluidics/#:~:text=Microfluidics%20have%20diverse%20assets%3A%20faster,on%2Da%2Dchip)..
33. *A microfluidic device for label-free, physical capture of circulating tumor cell clusters.* Yu M, et al. s.l. : Nat Methods, 2014, Vols. 12(7):685-691).
34. *3D Bioprinting as a Powerful Technique for Recreating the Tumor Microenvironment.* Ilaria Parodi, Donatella Di Lisa, Laura Pastorino, Silvia Scaglione and Marco Massimo Fato. s.l. : Weimin Li, 2023.
35. *A Microfluidic Hanging-Drop-Based Islet Perifusion System for Studying Glucose-Stimulated Insulin Secretion From Multiple Individual Pancreatic Islets.* Patricia Wu Jin, Nassim Rousset, Andreas Hierlemann and Patrick M. Misun. s.l. : Front. Bioeng. Biotechnol, 2021, Vol. 9.
36. *Microfluidic technologies for circulating tumor cell isolation.* Hyungseok Cho, Jinho Kim, Hanjung Song, Keun Yong Sohn, MinHyon Jeon, Ki-H. s.l. : pubmed., 2018. 10.1039/c7an01979c.
37. *A microfluidic-based PDAC organoid system reveals the impact of hypoxia in response to treatment.* Marlene Geyer, Daniel Schreyer, Lisa-Marie Gaul, Susanne Pfeffer, Christian Pilarsky & Karla Queiroz. s.l. : Cell Death Discovery volume, 2023.
38. Lithography. *mems and nanotechnology exchange.* [Online] https://www.mems-exchange.org/MEMS/processes/lithography.html.
39. Soft Lithography. *ScienceDirect.* [Online] https://www.sciencedirect.com/topics/materials-science/soft-lithography.
40. POLYJET 3D PRINTING – THE ULTIMATE GUIDE. *all3dp.* [Online] https://all3dp.com/2/polyjet-3d-printing-technologies-simply-explained/.

41. *In vitro microfluidic 3D platform as a pathological model of the pancreatic acino-ductal unit.* Minervini, Beatrice. 2021.
42. *Development of an organ-on-chip model to mimic exocrine pancreas.* Aronne, Matilde. 2022.
43. STRATASYS, THE. OBJET30 SERIES. [Online] https://proto3000.com/product/objet30-series/.
44. *A bioengineered heterotypic stroma-cancer microenvironment model to study pancreatic ductal adenocarcinoma.* Cole R. Drifka, Kevin W. Eliceiri, Sharon M. Weber, and W. John Kao. s.l. : Lab Chip, 2013.
45. Selsman, Adam. *Replica molding (REM).* [Online] https://openwetware.org/wiki/Replica_molding_(REM)_-_Adam_Selsman.
46. *microtechweb.* [Online] https://microtechweb.com/2d/2d.htm.
47. *SU-8 nanocomposite photoresist with low stress properties for microfabrication applications.* Sébastien Jiguet, Arnaud Bertsch, Moshe Judelewicz, Heinrich Hofmann, Philippe Renaud. 2006. https://doi.org/10.1016/j.mee.2006.02.004.
48. *SU-8: a photoresist for high-aspect-ratio and 3D submicron lithography.* Greiner, A del Campo and C. 2006. stacks.iop.org/JMM/17/R81.
49. DataSheet, MicroChem -. SU-8 2000 Permanent Epoxy Negative Photoresist.
50. Stratasys. Objet30. [Online] https://www.aniwaa.com/product/3d-printers/stratasys-objet30/.
51. *tantec.* [Online] https://tantec.com/the-basics-of-plasma-treatment/.
52. Plasma, Harrick. PDMS BONDING (MICROFLUIDICS). [Online] https://harrickplasma.com/pdms-bonding/.
53. Vasireddi, Ramakrishna. Fabrication of Novel Microfluidic Devices for Investigating Ultrafast Structural Dynamics. [Online] https://www.researchgate.net/figure/Schematic-mechanism-of-the-PDMS-PDMS-bonding-due-to-oxygen-plasma-activation-The-plasma_fig19_343696248.
54. *Electrospinning and Electrospun Nanofibers: Methods, Materials, and Applications.* Jiajia Xue, Tong Wu, Yunqian Dai, and Younan Xia. s.l. : Chem Rev, 2019.
55. [Online] https://ibidi.com/content/216-confocal-microscopy.
56. [Online] https://www.researchgate.net/figure/Main-properties-of-used-PDMS_tbl1_274653893.
57. *Poly(dimethylsiloxane) as a material for fabricating microfluidic devices.* J Cooper McDonald, George M Whitesides. s.l. : PubMed, 2002. 10.1021/ar010110q.

58. Zhou, Jinwen. Surface Modification of Poly(dimethylsiloxane) (PDMS) for Microfluidic Devices. [Online] https://flex.flinders.edu.au/file/d86de87e-5ff9-45bd-b003-f83fc4b7379b/1/Thesis-Zhou-2012.pdf.

59. *Simple surface engineering of polydimethylsiloxane with polydopamine for stabilized mesenchymal stem cell adhesion and multipotency .* Yon Jin Chuah, Yi Ting Koh, Kaiyang Lim, Nishanth V. Menon, Yingnan Wu & Yuejun Kang. s.l. : Scientific Reports , 2016, Vol. 5.

60. [Online] https://www.researchgate.net/figure/Molecular-structures-of-PDMS-For-the-high-purity-silicon-oil-SILFAR-R-1000-the-molecular_fig1_242271474.

61. [Online] https://www.mavom.nl/kernassortiment/elektronica-bescherming/ingietharsen/sylgard-184.

62. *A Comprehensive Review on Collagen Type I Development of Biomaterials for Tissue Engineering: From Biosynthesis to Bioscaffold.* Ibrahim N. Amirrah, Yogeswaran Lokanathan, Izzat Zulkiflee, M. F. Mohd Razip Wee, Antonella Motta and Mh Busra Fauzi. s.l. : Biomedicines, 2022.

63. [Online] https://advancedbiomatrix.com/fibricol.html.

64. *polysciences.* [Online] https://www.polysciences.com/india/polycaprolactone-powdered-40895.

65. *Polycaprolactone: How a Well-Known and Futuristic Polymer Has Become an Innovative Collagen-Stimulator in Esthetics.* Vercesi, Marie-Odile Christen and Franco. s.l. : Clin Cosmet Investig Dermatol, 2020. 10.2147/CCID.S229054.

66. *A review of gelatin: Properties, sources, process, applications, andcommercialisation.* J. Alipala, N.A.S. Mohd Pu'adb, T.C. Leeb, N.H.M Nayana, N. Saharia, H. Basric, M.I. Idrisd, H.Z. Abdullah. s.l. : Elsevier, 2020.

67. [Online] https://www.semanticscholar.org/paper/Characterization-and-correlation-analysis-of-Felix/111c135736f4ff552846f477ba071581fc0a5716.

68. sigmaaldrich. [Online] https://www.sigmaaldrich.com/IT/en/products/cell-culture-and-analysis/cell-culture-supplements-and-reagents/fbs.

69. atcc. *MIA PaCa-2.* [Online] https://www.atcc.org/products/crl-1420.

70. Cell Culture: General Cell Handling. *ibidi.* [Online] https://ibidi.com/content/434-cell-handling.

71. Ferrero, Ivana. *researchgate.* [Online] https://www.researchgate.net/figure/Buerker-chamber-and-Fast-Read-102-W-cell-count-method-The-Buerker-chamber-has-9-large_fig8_225084954#:~:text=The%20Bürker%20chamber%20has%209,Chamber%20depth%20is%200.1%20mm..

72. *Immunostaining of Skeletal Tissues.* Crystal Idleburg, Madelyn R. Lorenz, Elizabeth N. DeLassus, Erica L. Scheller, and Deborah J. Veis. s.l. : Methods Mol Bio, 2021. 10.1007/978-1-0716-0989-7_15.
73. *E-cadherin: a marker for differentiation and invasiveness in prostatic carcinoma.* T. Otto, K. Rembrink, M. Goepel, M. Meyer-Schwickerath & H. Rübben. s.l. : Urological Research, 1993, Vol. 21.
74. Rodig, Scott J. Fixing Attached Cells for Staining. [Online] https://cshprotocols.cshlp.org/content/2020/8/pdb.prot099689.abstract.
75. [Online] https://it.vwr.com/store/product/en/2342303/tritontm-x-100-per-analisi-per-biochimica?languageChanged=en.
76. *Tween-20 Induces the Structural Remodeling of Single Lipid Vesicles.* Lara Dresser, Sarah P. Graham, Lisa M. Miller, Charley Schaefer, Donato Conteduca, Steven Johnson, Mark C. Leake,and Steven D. Quinn. 2022.
77. *Triton X-100 concentration effects on membrane permeability of a single HeLa cell by scanning electrochemical microscopy (SECM).* Bard, Dipankar Koley and Allen J. 2010.
78. [Online] https://www.sigmaaldrich.com/IT/en/support/calculators-and-apps/bsa-blocking-buffer.
79. [Online] https://my.clevelandclinic.org/health/articles/22062-epithelium#:~:text=Cuboidal%20epithelium%3A%20Cuboidal%20epithelial%20cells,taller%20than%20they%20are%20wide..
80. *Heterogenecity of fibroblasts.* Manyam Ravikanth, P Soujanya, K Manjunath, TR Saraswathi, and CR Ramachandran. s.l. : J Oral Maxillofac Pathol, 2011.
81. [Online] https://www.thermofisher.com/it/en/home/life-science/cell-analysis/fluorophores/dapi-stain.html.
82. [Online] https://www.thermofisher.com/it/en/home/life-science/cell-analysis/fluorophores/cy5-dye.html#:~:text=Invitrogen%20Cyanine5%20(Cy5)%20dye%20is,or%20647%20nm%20laser%20lines..
83. *Significance of E-cadherin and Vimentin as epithelial-mesenchymal transition markers in colorectal carcinoma prognosis.* Zohreh Niknami, Ahad Muhammadnejad, Alireza Ebrahimi, Zahra Harsani, and Reza Shirkoohi. s.l. : EXCLI J, 2020.
84. [Online] https://app.fluorofinder.com/dyes/161-alexa-fluor-555-ex-max-555-nm-em-max-565-nm.
85. *In search of definitions: Cancer-associated fibroblasts and their markers.* Martin Nurmik, Pit Ullmann, Fabien Rodriguez, Serge Haan and Elisabeth Letellier. s.l. : International Journal of Cancer, 2018.

86. *High stromal expression of α-smooth-muscle actin correlates with aggressive pancreatic cancer biology.* Nanda, Shreeya. s.l. : Nature Reviews Gastroenterology & Hepatology , 2010.
87. *Stiffness of pancreatic cancer cells is associated with increased invasive potential.* Angelyn V. Nguyen, a Kendra D. Nyberg et al. s.l. : Integr Biol, 2016.
88. *Enhanced morphological and functional differences of pancreatic cancer with epithelial or mesenchymal characteristics in 3D culture.* Yuuki Shichi, Norihiko Sasaki et al. s.l. : Sci Rep, 2019.
89. *Application of Patient-Derived Cancer Organoids to Personalized Medicine.* Masahiro Shiihara, Toru Furukawa. s.l. : Yuki Yoshimatsu, Academic Editor and Tadashi Kondo, Academic Editor, 2022, Vol. 12(5): 789.
90. *advancedbiomatrix.* [Online] https://advancedbiomatrix.com/fibricol.html.
91. *Alpha-smooth muscle actin-positive cancer-associated fibroblasts secreting osteopontin promote growth of luminal breast cancer.* Anna Muchlińska, Anna Nagel, Marta Popęda, Jolanta Szade, Magdalena Niemira, Jacek Zieliński, Jarosław Skokowski, Natalia Bednarz-Knoll & Anna J. Żaczek. 2022.
92. [Online] http://www.vivo.colostate.edu/hbooks/pathphys/digestion/pancreas/histo_exo.html.
93. [Online] https://www.britannica.com/science/fibroblast.